Universidade de Aveiro
2019

Departamento de Eletrónica,
Telecomunicações e Informática

Pedro Alexandre Tavares Rodrigues

Plataforma de testes para posicionamento por luz visível

Test platform for Visible Light Positioning

Universidade de Aveiro
2019

Departamento de Eletrónica,
Telecomunicações e Informática

Pedro Alexandre Tavares Rodrigues

Plataforma de testes para posicionamento por luz visível

Test platform for Visible Light Positioning

Dissertação apresentada à Universidade de Aveiro para cumprimento dos requisitos necessários à obtenção do grau de Mestre em Engenharia Eletrónica e Telecomunicações, realizada sob a orientação científica do Doutor Pedro Nicolau Faria da Fonseca, Professor auxiliar do Departamento de Eletrónica, Telecomunicações e Informática da Universidade de Aveiro, e do Doutor Luís Filipe Mesquita Nero Moreira Alves , Professor auxiliar do Departamento de Eletrónica, Telecomunicações e Informática da Universidade de Aveiro.

Dedico este trabalho principalmente aos meus pais, Álvaro Ferreira Rodrigues e Maria Margarida Tavares de Oliveira Rodrigues por nunca terem desistido de mim. O meu muito Obrigado por tudo.
Agradeço também à minha família por todo o apoio que me foi oferecido ao longo destes anos. Agradeço à Magda Oliveira pela longa paciência em me aturar seja nos bons ou nos maus momentos.
Agradeço aos meus colegas de curso por ajudarem aqui o velhote baguette, o meu muito obrigado a todos os que me acompanharam de mais próximo.

o júri / the jury

presidente / president

Professor Doutor António José Ribeiro Neves
Professor Auxiliar do Departamento de Eletrónica, Telecomunicações e Informática da Universidade de Aveiro

vogais / examiners committee

Doutor Paulo Jorge de Campos Bartolomeu
Investigador Doutorado (nível 2) da Universidade de Aveiro

Professor Doutor Pedro Nicolau Faria da Fonseca
Professor auxiliar do Departamento de Eletrónica, Telecomunicações e Informática da Universidade de Aveiro

agradecimentos /
acknowledgements

Agradeço toda a ajuda recebida pelo meu orientador, Professor Pedro Nicolau Faria da Fonseca, assim como ao meu co-orientador Professor Luís Filipe Mesquita Nero Moreira Alves, pelo apoio dado ao longo da realização desta dissertação. Agradeço aos meus colegas de laboratório de Circuitos e Sistemas Integrados por todos os momentos de apoio. O meu especial agradecimento ao Luís Rodrigues, aluno de Doutoramento, e ao Miguel Rêgo, também finalista de curso, por todos os momentos de brainstorming independentemente da hora ou local. Quero também agradecer a todos os funcionários do Instituto de Telecomunicações - polo de Aveiro, assim como à própria instituição, por me terem também ajudado a desenvolver este projecto. Agradeço por fim, à Universidade de Aveiro por me ter oferecido as condições necessárias para a aquisição de uma formação superior.

Palavras Chave

posicionamento por luz visível, comunicação por luz visível, projeto luminotécnico, diodo emissor de luz , sensor de imagem, foto-díodo.

Resumo

Esta dissertação aborda os sistemas de localização em espaços interiores com recurso à iluminação artificial baseada em díodos emissores de luz comerciais e comunicação por luz visível, dando principal ênfase ao estudo do comportamento da luz no espaço e de um driver de corrente apto para modular a intensidade da luz e suportar a transmissão de informação. Atualmente, a maior parte dos sistemas de iluminação tradicionais estão a ser a substituídos por iluminação LED, tendo em conta a alta eficiência energética destes. Deste modo, é realizado um estudo sobre as características de fontes luminosas artificiais, especialmente do aprofundamento de conhecimentos em fotometria e suas propriedades optoelectrónicas. De seguida, procedeu-se à elaboração de um projeto luminotécnico de adaptação de uma sala para a plataforma em questão de acordo com os requisitos dos sistemas de iluminação, em conformidade com a regulação europeia. Desenvolveu-se também um regulador linear de corrente para a polarização das luminárias led em modo contínuo e pulsado, que permite a redução do fluxo luminoso. Foram ainda analisadas modulações de sinal para realização de comunicação por luz visível de baixo débito para implementação através de um microcontrolador de modo a atuar sobre a corrente que atravessa o LED. O sistema de iluminação desenvolvido permite, no modo de comunicação, a modulação do identificador de cada luminária através de luz visível permitindo ao mesmo tempo iluminação necessária para desenvolver tarefas no espaço em questão. Os sinais modulados são recebidos por fotossensores, foto-díodos ou sensores de imagem (camaras), responsáveis por capturar o sinal, necessitam, no entanto, de um sistema capaz de extrair a informação transmitida, assim como de medir a distância relativa, seja ela utilizando a potência do sinal (foto-díodos) ou por deformação de imagem (sensores de imagem). A adaptação de uma sala escura no laboratório de Sistemas de Circuitos Integrados do Instituto de Telecomunicações de Aveiro reúne assim as condições necessárias para implementar sistemas de localização por luz visível em ambientes reais e permitindo a sua validação.

Keywords

visible light positioning, visible light communication, lighting project, light-emitting diode, image sensor, photodiode.

Abstract

This dissertation is addressed to location systems in indoor environments using artificial light source, based in off-the-shelf light emitting diodes, and visible light communication. It emphasizes the study of the light behaviour travelling through space and the design of a current LED driver capable of producing pulsed light. Nowadays, most of the traditional lighting systems are being replaced by LED lighting due to their energy efficiency. A study over artificial light sources is performed, specially photometry measures and their optoelectronic properties. A lighting project has been developed to adapt a dark room with the European lighting standards regulation, that follows a traditional lighting project. A linear LED current driver has been designed for regulation of LED current, continuous or pulsed mode, which allows dimming of light intensity. Light modulations have been studied for low bandwidth visible light communication system to be implemented with a microcontroller acting directly on the current that passes through the LED. The built lighting system allows, when communicating, modulation of each LED identification number through light, while performing the basic need of illumination. The modulated signals are received by photo detectors, photo diodes or image sensor (camera), which receives the signal, extracts the ID, and have the ability to measure a relative distance to the emitters, using power reception (photo diodes) or image deformation of image sensors. The adaptation of a dark room in Integrated Circuit Systems laboratory of Instituto de Telecomunicações in Aveiro, meets the necessary requirements for implementation and validation of VLP in real environments.

Contents

List of Figures

List of Tables

Acronyms

AC	Alternating Current
DC	Direct Current
AoA	Angle of Arrival
HPA	Half Power Angle
GPS	Global Positioning System
IPS	Indoor Positioning System
OWC	Optical Wireless Communication
VLC	Visible Light Communication
VLP	Visible Light Positioning
LoS	Line of Sight
OOK	On-Off Keying
PPM	Pulse Position Modulation
VPPM	Variable Pulse Modulation
PAM	Pulse Amplitude Modulation
PWM	Pulse Width Modulation
OFDM	Orthogonal Frequency-Division Multiplexing
FSK	Frequency Shift Keying
RF	Radio-Frequency
RFID	Radio Frequency Identification
UWB	Utra Wide Band
GSM	Global System for Mobile Communications
GPIO	General Purpose Input/Output
IR	Infra-Red
UV	Ultra-Violet
LED	Light Emitting Diode
PD	Photo-Diode
FOV	Field-of-View
OCC	Optical Camera Communication
CCD	Charged Coupled Devices
CMOS	Complementary Metal-Oxide Semiconductor
GS	Global Shutter
RS	Rolling Shutter
TIA	Transimpedance Amplifier
CCT	Correlated Color Temperature
CRI	Color Rendering Index
SOTA	State Of The Art
ISO	International Organization for Standardization
ICS	Integrated Circuits and Systems
SPI	Serial Peripheral Interface
SI	Systeme Internationale
SOA	Safe Operating Area
Op-Amp	Operational Amplifier
MOSFET	Metal–Oxide–Semiconductor Field-Effect Transistor
uC	Microcontroller
RSS	Received Signal Strength
TDOA	Time Difference of Arrival
FPGA	Field Programmable Gate Array
IS	Image Sensor
ISR	Interruption Service Routine
SoF	Start of Frame
EoF	End of Frame
UART	Universal Asynchronous Receiver/Transmitter

CHAPTER 1

Introduction

With the lightning speed of technological evolution where location is a primordial necessity, mankind developed in the early 70's a global positioning system Global Positioning System (GPS) to overcome previous navigation systems. Since this system is Radio-Frequency (RF) based, due to signal attenuation caused by construction materials it loses significant power in an indoor environment (houses, towers, parking, underground parks) causing the need to develop alternatives for positioning systems in an indoor scenario. In the context of Indoor Positioning Systems (IPSs), among other solutions comes up Visible Light Positioning (VLP) as a result of promulgation of Light Emitting Diodes (LEDs). This chapter introduces the actual State Of The Art of VLP.

1.1 Motivation

Indoor positioning is a very complex subject since common outdoor technologies have a poor performance inside buildings. On one hand, construction materials have a very important role in terms of comfort and protection from outside weather, on the other hand, they are the main reason why RF signals are attenuated resulting in an important loss of accuracy. Moreover, since the GPS gives the relationship between sea level and your estimated position, it is unable for the user to determine exactly where he is, for instance which floor he is inside a building. Based on that, there is an expanding interest window on the IPSs representing a market value that was evaluated by $2.642 billion in 2017 and is projected to grow to $43.51 billion in 2025 [1].

Since the inventor Thomas Alva Edison announced in 1879 an electric light that could be used in homes, offices and schools [2], the indoor lighting systems have being evolving from incandescent to the so much popular LEDs, which are driving a revolution in lighting systems due to their superior energy efficiency. Since artificial indoor lighting is an undeniable need, LEDs are in constant evolution in terms of construction of the package increasing the Luminous Efficiency. With this evolution appears an alternative to RF based communication systems, VLC which makes use of a particular portion of the electromagnetic spectrum that corresponds to visible light between Infra-Red (IR) and Ultra-Violet (UV) [390;750] nm (Figure 1.1) allowing the use of the optical channel for lighting and communication [3], [4]. This technology features a non-licensed channel, is harmless to human, and has high bandwidth [3]. For the demand of IPS problem, VLP is a recent technique that accommodates the use of Visible Light Communication (VLC) to infer the position of the luminaries used as reference anchors to estimate the position of an object or person in a room or building. These lighting fixtures can have individual fingerprint that can be explored for further positioning techniques [3]. These systems have the advantage of using the lighting infrastructure with minor changes adding the advantage of being installed in environments that are sensitive to electromagnetic waves where RF signals may create electromagnetic interference (EMI) to machinery [3], [4].

The construction of a laboratory with off-the-shelf LED luminaries that respects the European Union regulation for indoor lighting purposes is the first step to demonstrate the fully and commercial concept of VLP.

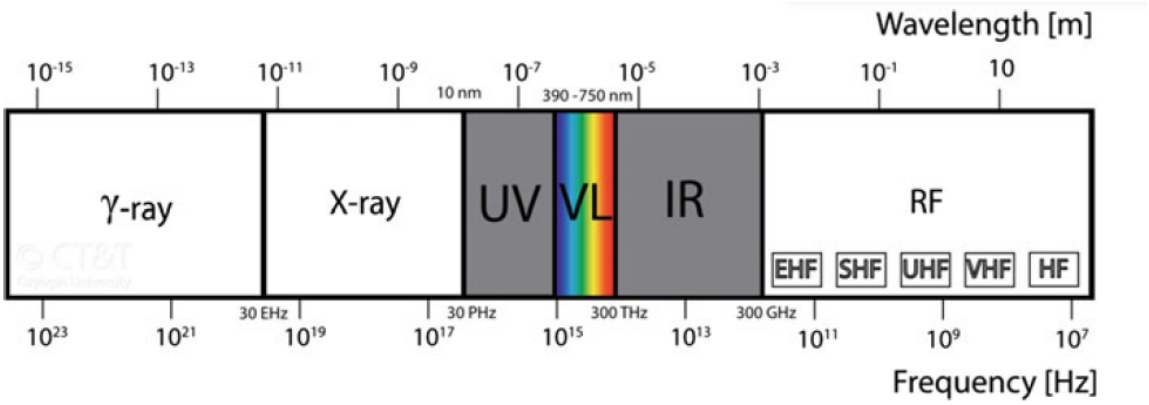

Figure 1.1: The electromagnetic spectrum [5].

1.2 Objectives

The main objectives of this dissertation are determined by the study of the requirements for the development of a suitable environment for the validation and assessment of VLP algorithms. This task can be detailed in the following order:

- Study of indoor lighting systems
- Study and selection of luminaries
- Simulation of the lighting project for the experimental room
- Development of a lighting system designed for VLP
- Development of remote platform for remote control of the system

1.3 Framework

This work is based on the past works developed at Instituto de Telecomunicações on the topic of VLP, [6]–[8]. The group of Integrated Circuits and Systems (ICS) is also in close connection with the European project VisIoN financed by the European Union's Horizon 2020 research and innovation programme under the Marie Skłodowska-Curie grant agreement, in which the subject of VLP is also a crucial topic of development.

1.4 Structure of dissertation

This document is divided in the following chapters:

- Chapter 2 presents a introduction to the theme of lighting, where the evolution of lighting is briefly described, followed by presenting the most recent technologies in illumination. The introduction to the main theme, VLP, is described along with its requirements.
- Chapter 3 presents a lighting project to be implemented in a dark room. This Project should follow the lighting standards which are described.
- Chapter 4 describes the design and simulation of the system that is implemented to achieve the goal of this dissertation.

- Chapter 5 describes and discuss results achieved in the experimental setup.
- Chapter 6 ends with some conclusions relatively to the work developed and some guidelines for the future are suggested.

CHAPTER 2

Visible Light Positioning Systems

This chapter will introduce topics of interest relatively to positioning, illumination, photometry, artificial light sources, complemented with the State Of The Art of VLC and VLP.

Positioning system is a method that enables the computation of location coordinates of a receiver with the purpose of providing location in space. Since ever, the mankind had the necessity to locate itself in land or sea. The use of celestial navigation, or with the auxiliary of the earth magnetism, by the use of a compass, allows a user to navigate from point A to point B. Positioning techniques are based in mathematic models to determine the unknown coordinates of a point P relative to other known coordinates. The most popular techniques used are Triangulation, Trilateration and Multilateration, observable in Figure 2.1.

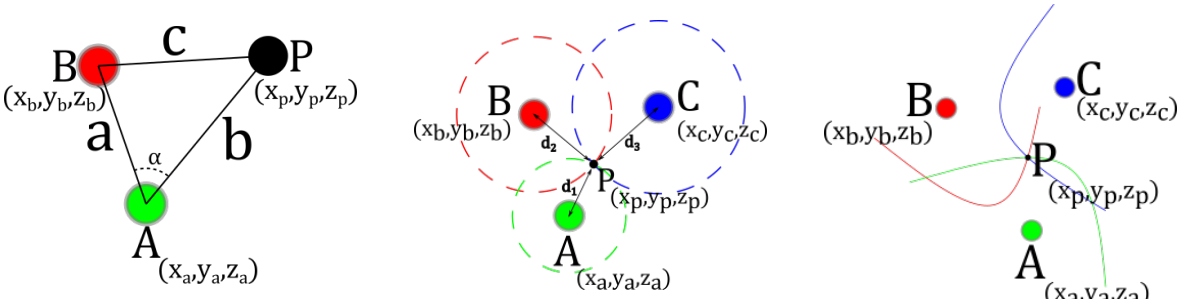

(a) Triangulation. **(b)** Trilateration. **(c)** Multilateration.

Figure 2.1: Positioning techniques

Triangulation makes use of known angles and known distances. In Figure 2.1a A, B and C represents points in space, whereas a, b and c represent the distances between those points, the angle α represents the angle between side a and b. Using the law of cosines,

$$c^2 = a^2 + b^2 - 2abcos(\alpha) \tag{2.1}$$

where the length of side c is easily found and using basic geometric the coordinates of P (x_p, y_p, z_p) can be obtained.

For Trilateration, the coordinates of an unknown point P makes use of the know distances between three known points A, B and C. By intersecting three spheres with diameter d1, d2 and d3 respectively, the solution gives two solutions aligned in a line. Depending on the application, the solution should be selected according to a defined criteria. For simplicity, Figure 2.1b represents one intersection point between three circles. For determination of the intersection of the three spheres, we can use, the equation of a sphere and create a system of equation,

$$\begin{cases} (x_p - x_a)^2 + (y_p - y_a)^2 + (z_p - z_a)^2 = d_1^2 \\ (x_p - x_b)^2 + (y_p - y_b)^2 + (z_p - z_b)^2 = d_2^2 \\ (x_p - x_c)^2 + (y_p - y_c)^2 + (z_p - z_c)^2 = d_3^2 \end{cases} \tag{2.2}$$

where the coordinates of an unknown point P(x_p, y_p, z_p), are obtained from the point coordinates A, B and C and the distances between point P and each center of the spheres.

The last most common technique is Multilaterarion, it relies on the time difference of signal arrival from multiple anchors A, B and C. The difference in the time of arrival is the basis to estimate distance, hence the calculation of position P. The principle of Multilateriation

is similar to Trilateration, but instead of using spheres it makes use of hyperbolas (2-D) or hyperboloids (3-D), Figure 2.1c represents intersection of three hyperbolas.

Mankind evolution requires today, systems that provide accurate positioning system to determine position for large number of applications such as: military and transportation navigation; etc. The accuracy of location systems has been greatly aided by the evolution of electronics, in specially, the radio-frequency. The Global Positioning System, a satellite-based system, has been the most used systems over the world that provides outdoor geolocation. Since this system relies in RF waves, its accuracy decreases in indoor environments due to the lack of Line of Sight (LoS). In those conditions, IPSs have become a true necessity to estimate position of people or objects inside building with a good accuracy. Some of the most common and commercial technologies, that provide IPS, are RF-based such as IR, Radio Frequency Identification (RFID), Bluetooth, ZigBee, Wi-Fi, Utra Wide Band (UWB) where others have emerged making use of acoustic waves or visible light. Each one of these technologies have different properties in terms of maximum range or maximum throughput which can be observed in Table 2.1.

Technology	Maximum Range	Maximum throughput	Power Consumption
RFID	200 m	1.67 Gbps	Low
Bluetooth	100 m	24.0 Mbps	Low
Wi-Fi IEEE802.11n	250m outdoor	600 Mbps	Moderate
Wi-Fi IEEE802.11ac	35m indoor	1.30 Gbps	Moderate
Wi-Fi IEEE802.11ad	short distances	4.60 Gbps	Moderate
UWB	10-20 m	460 Mbps	Moderate
Ultrasound	Couple-tens of meters	30.0 Mbps	Low-Moderate
Audible Sound	Couple of meters	N.A.	Low-Moderate
VLC	1.4 km	10 Gbps	Relatively Higher

Table 2.1: Summary of main wireless technologies for positioning. Adapted from [9]

The choice of the technology is largely dependent of the use-case. The application of IPS can be applied in manufacturing units for keeping track of every asset, or in shopping malls where navigation is important for customers to find products or paths to and endpoint, and tracking for shops to track customers movements or to advertise specific products depending on the target audience. Accuracy in positioning, which roughly refers to the difference between the estimated position and the actual one, may differ depending on the technology used for tracking, an overview of the average accuracies achieved for each technology can be observed in Table 2.2 where installation and maintenance cost (IC) and the cost for each end user (UC) is also included.

In order to enable IPS signal metrics should be used. The three main techniques for positioning are Received Signal Strength (RSS), Time Difference of Arrival (TDOA) and Angle of Arrival (AoA) [11].

Technology	Approx. accuracy (m)	Cost	
		IC	UC
IR	0.57-2.30	H	L
RFID	1.00-5.00	H	L
Bluetooth	0.30-meters	L	L
ZigBee	0.25	L	H
Wi-Fi	1.50	L	L
UWB	0.15	H	H
Ultrasound	0.01-2.00	H	H
Audible Sound	meters	L	L
VLC	0.10	H	L

Table 2.2: Comparison of main indoor positioning technologies. Adapted from [10]

2.2 Illumination

Light can be defined as an electromagnetic wave, defined by Maxwell equations, as a fluctuation of electric and magnetic fields which can transport energy. As for visible light, it has the same properties with the particularity of being possible to be perceived by the human eye. Historically, the study of light as been an important matter for several scientists. But it was in 1905 in a paper on the photoelectric effect, wrote by the famous scientist Albert Einstein, that the duality of light was introduced with the modern concept of the photon. The photon, a massless particle, describes the fundamental excitations of the electric field as a energy carrier. Since Einstein described light as discrete packages, as photons, the energy contained in a single photon is described as,

$$E_{photon} = h \times \nu = h \times \frac{c}{\lambda} \tag{2.3}$$

where E_{photon} is the energy of photon [J], h is the Planck's Constant $= 6.63 \times 10^{-34}$ [J s], ν the frequency of light related to its wavelength [Hz], c is the speed of light in vacuum equals to 2.998×10^{8} [m/s], and λ is the wavelength given in metres.

As energy carrier, photons can be absorbed or emitted. As mentioned before, light energy travels in space in the form of electromagnetic waves. For visible light, the frequency of those waves as to be constrained in the specific frequency range [390;750] nm defined by the human eye. Nevertheless, it is important to refer that human eyes does not perceive different wavelengths with the same sensitivity. The Figure 2.2 represents the spectral sensitivity of the human eye for photopic vision ($V(\lambda)$) and scotopic vision ($V'(\lambda)$), the daylight and the nocturne vision, denoting the maximum sensibility at approximately 555 nm (blue-green color) for daylight vision.

It is known that any hot body will emit electromagnetic radiation which depend exclusively on the temperature of the body, known as thermal radiation. A black-body, is an idealized body that absorbs all incident electromagnetic radiation but it can also emit radiation, known as black-body radiation. Wien described that if a black-body is held in thermal equilibrium (constant temperature), it will radiate a wavelength in function of its temperature (see Equation 2.4). When the temperature increases, the wavelength of maximum emission

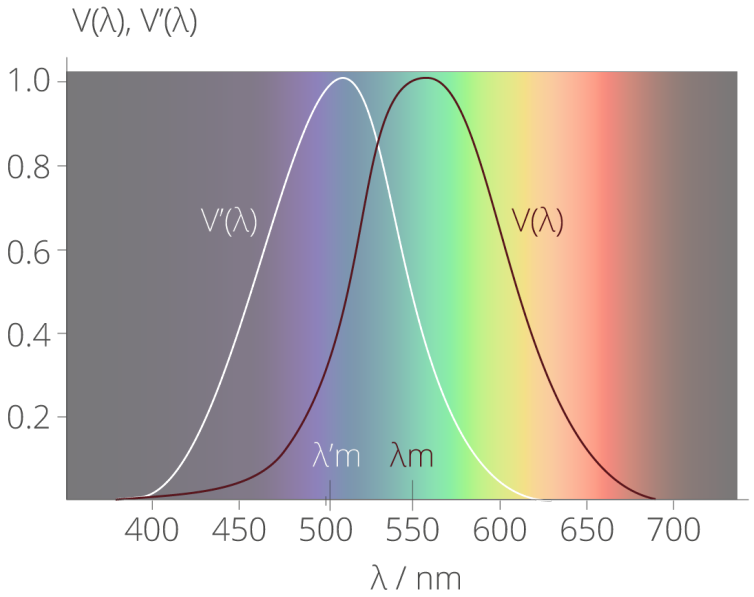

Figure 2.2: Spectral sensitivity of human eye.

radiation shifts from long to short, corresponding in the visible spectrum to a shift from red to blue. The Stefan-Boltzmann law also describes the black-body radiation but related to the total power radiated by a black-body in one square meter as a function of temperature (see Equation 2.5). It is the result from integrating the spectral radiance of a black-body over all wavelengths, and is directly proportional to the fourth power of temperature.

$$\lambda_{max} = b/T \tag{2.4}$$

where:

λ_{max} : the wavelength, in meters, at which the maximum energy of the black-body is emitted;
b : Wien's displacement constant $= 2.898 \times 10^{-3}$ m K;
T : black-body temperature in Kelvins.

$$M(T) = \sigma \times T^4 \tag{2.5}$$

where: M : total amount of radiation emitted per square meter $\mathrm{W/m^2}$;
σ : Stefan-Boltzman constant $= 5.67 \times 10^{-8}$ $\mathrm{W/(m^2\,K^4)}$;
T : black-body temperature in Kelvins.

Wien's and Steffan-Boltzman's laws exposes that the radiation of a black-body radiator is fully determined by its own temperature only, either for the wavelengths where the radiation is at its maximum, either as regards to its maximum power output, respectively. It is therefore possible to determine a specific color, regarding to visible light spectrum, for each temperature of the black-body radiator. This temperature for a light source is called the Correlated Color Temperature (CCT) of the source and is expressed in Kelvin degrees [12]. It is a general term used to describe the color appearance of any light source when compared to a the color of

the black-body radiator [13]. CCT for commercially light sources usually range from 2700 K to 6500 K and are intended by lighting industry to give general indications of the apparent "warmth" or "coolness" of the light emitted by the source. The term "warm" represents values from 2700 K to 3000 K, while the therm "cool" represents values from 4000 K to 6500 K.

There is one more factor for color that contribute to illuminating engineering studies, the Color Rendering Index (CRI). It is a qualitative measure that compares the ability of a light source to reproduce the colors of objects faithfully in comparison with natural light source, such as sun. It is graded in a scale from 0 , to 100 , where 0 means poor match and 100 means excellent match. The criteria for the CRI value of a light source depends from application to application, for instance, it is critical to have a high value in museums and photography studios, nevertheless if a light source with a CRI inferior to 80 is used, it has to be ensured that safety colours can be recognised without problems [12].

2.2.1 Basic photometric concepts

The study of photometric properties is essential for visual science and in lighting engineering. The Systeme Internationale (SI) photometric base unit is the candela [cd], and it is defined as "the luminous intensity, in a given direction, of a source that emits monochromatic radiation of frequency 540×10^{12} Hz and that has a radiant intensity in that direction of (1/683) watt per steradian" [14].

One of the key concepts to understand the relationships between measurements of geometries is that of the solid angle, or steradian. It is defined as the solid angle which cuts off a spherical surface area equal to the square of the radius of the sphere (see Figure 2.3). A unit radius sphere contains $4 \times \pi$ steradians easily verified using the definition of solid angle as,

$$\Omega = \int_0^{2\pi} \int_0^{\theta} sin(\theta')\, d\theta'\, d\phi = \int_0^{2\pi} [-cos(\theta')]_0^{\theta}\, d\phi = 2\pi \times (1 - cos(\theta)) \tag{2.6}$$

where Ω represents the solid angle, r is the radius of the sphere, and θ is the half-angle of a cone.

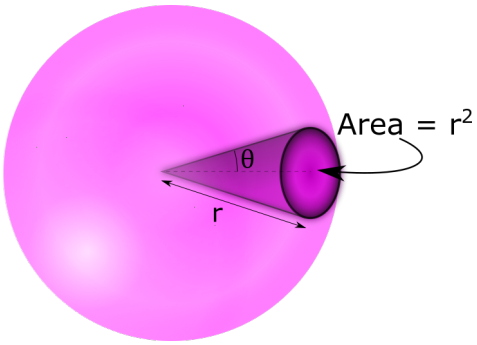

Figure 2.3: One steradian.

The luminous flux F is the quantity or the amount of the light perceived by the human eye [13], [15]. The SI unit is lumen [lm] represented by the symbol Φ and it is defined by the maximum efficacy of the eye response, as 1 W of light at 555 nm gives a luminous flux of 683 lm [13]. Since the luminous flux under normal lighting conditions proceeds a velocity of

about 300 000 km/h, the quantity of the light, therefore, is a rate of the stream flow of the light per second [13]. The relationship between candela and lumen units is defined as 1 cd equals 1 lm/sr [12], [16].

In a general perspective, all light sources, both natural and artificial, emit light at different rates and different directions. Even the sun, which approaches an ideal emitter of light, shines differently in different directions. Given those facts, it is important to distinguish the action of the source into different directions. This gives rise to the concept of luminous intensity [13]. As described earlier, the International Organization for Standardization (ISO) uses the unit of luminous intensity (cd) as the basic unit for all photometry. In conclusion, we can interpret the luminous intensity as the luminous flux in a certain direction [12] and is mathematically defined as $I = \frac{\partial \Phi}{\partial \Omega}$ where Φ is the luminous flux emitted within the solid angle Ω. Thus, an isotropically emitting light with an intensity of 1 cd (lm/sr) has a luminous flux of $4 \times \pi = 12.57$ lm.

When light strikes a surface steadily, an amount of luminous flux is incident on the surface. If the surface is uniformly lit, the illuminance is defined as a density of the luminous flux incident on the surface. The illuminance E is the luminous flux incident per unit area $E = \frac{\partial \Phi}{\partial A}$ and the SI unit is lx (lx = lm/m^2) [12]. It is possible to define E as a mathematical plane through which the light shines [13], [15]. The most common illuminance studies relies on the horizontal, vertical and cylindrical (or semi-cylindrical). If the surface is located horizontally, the illuminance is called the horizontal illuminance (E_h). If it is located vertically, the illuminance is called the vertical illuminance (E_v). Most of standards and recommendations applied in lighting engineering are related to the quality or quantity of light, that is on the horizontal illuminance. For non-flat surfaces, the illuminance is not suitable to express the brightness of spherical or cylindrical objects. In those cases the semi-cylindrical illuminance (E_{sc}) is used, being defined as the average value of illuminances on the surface of a cylinder. Although it is mathematically simple to calculate the illuminance for a single light source, common lighting installations depends on multiple light sources and sometimes from different types. For the characterization of many aspects of lighting installations, the average illuminance is often a crucial parameter. When the illuminance is not uniform, the average illuminance is generally an important characteristic. It can be assessed as $E_{avg} = \frac{\partial \Phi_{tot}}{\partial A}$, where Φ_{tot} is the total luminous flux (in lm) incident in the area and A is the surface area (in m^2) on which the luminous flux is shining.

In most of the practical cases, the distribution of the illuminance is not uniform at all. This implies that the average illuminance usually is not sufficient to characterize the lighting installation. Therefore, almost all indoor and outdoor standards or recommendations on lighting installation, include requirements for the average illuminance, and the acceptable degree of non-uniformity. These requirements are usually given as a relationship between the minimum by the average (E_{min}/E_{avg}) illuminance [12], or as the minimum divided by the maximum (E_{min}/E_{max}) illuminance. This is actually very convenient for calculations since it is independent to the value of illuminance.

An important remark for practical measurements of illuminance must be mentioned, since

the procedure to achieve better results is the correct placement of the illuminance meter — the luxmeter — at a fixed position, parallel to the measuring surface (horizontal/vertical), to avoid disturbances. If the average illumance must be assessed, point measurements must be repeated in different locations in a well-defined grid, if not, severe errors may result, particularly if illuminance is unevenly distributed. If average illuminance is taken into account, point measurements are needed as well to assess the non-uniformity of the lighting installation.

Various studies of light observed that illuminance decreases with the square of the distance between the light source and the receiving plane, calling to this relationship the inverse square law and it is defined by the following equation,

$$E = k \times (I/r^2) \tag{2.7}$$

where E is the illuminance, I is the luminous intensity of the source, r the distance from the source to the measuring point, and k is a constant that depends on the units used. Basically, it states that the illuminance (E) at any point on a plane, that is normal to the light direction, is inversely proportional to the square of the distance (r) between source and plane ($E \propto 1/r^2$) (see Figure 2.4).

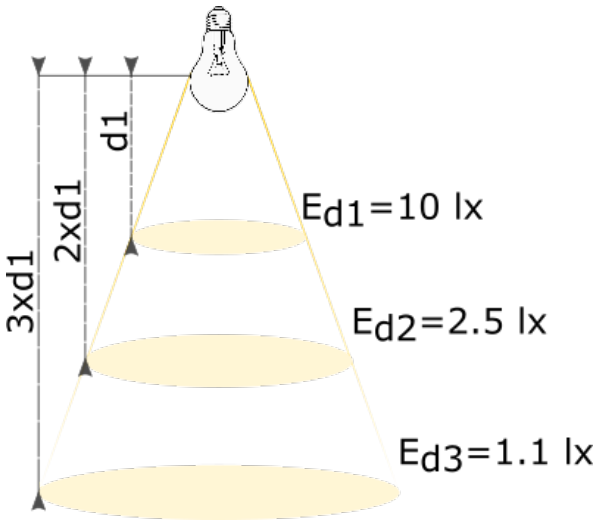

Figure 2.4: Illuminance as a function of distance r.

Additionally, if we measure the illuminance in a certain point it is possible, without knowing the luminous intensity of the source, to determine the illuminance at any distance in the same direction.

If the surface on which the incident light falls is tilted, the illuminance decreases, by the Lambert's Cosine Law (see Figure 2.5). This law, in combination with the inverse square law,

$$E = \frac{I}{r^2} \times \cos\theta \tag{2.8}$$

where it states that the illuminance, E, is inversely proportional to the square of the distance, r, but also it decreases in proportion with the cosine of the incident angle, θ (see Equation 2.8).

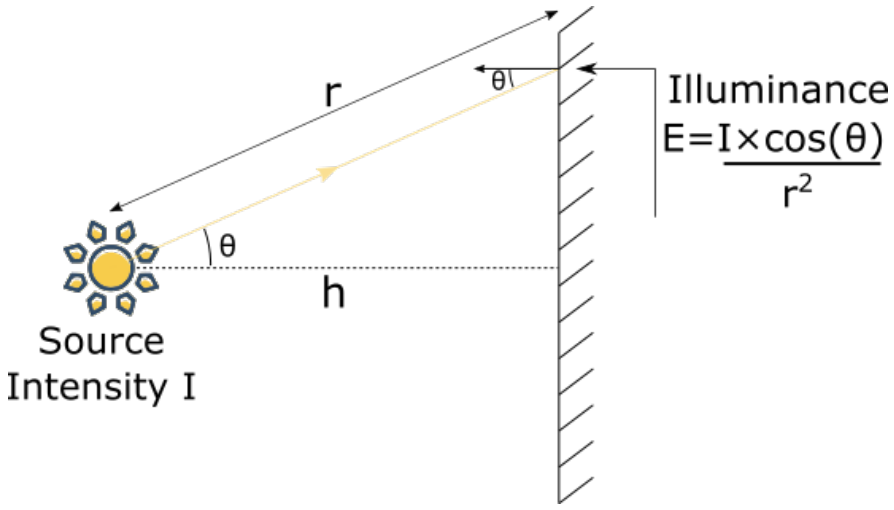

Figure 2.5: Illuminance as a function of the incident angle θ and distance r.

To define the illuminance at diferent points in a horizontal plane relative to the plane where the luminaires are installed, a trigonometric identity is applied to Equation 2.8 deriving: the cosine to the third law. It describes the illuminance, E, in a plane with a fixed height, h, in function of the incident angle, θ defined by,

$$E = \frac{I}{h^2} \times \cos^3 \theta \tag{2.9}$$

where the distance from source to point is a function of height. It has many applications for indoor lighting calculations particularly when the plane in consideration is flat and horizontal, for eg: floor, tables, etc.

2.2.2 Artificial light sources

Artificial lighting has been a fundamental human need, representing in 2018 15 % to 20 % of electricity in developed countries reflecting the high dependency for multiple purposes such as private individual house, palaces or temples, streets, lighthouses, among others [15].

Artificial lighting goes back to the 19th century with different approaches to electrical illumination with a unsustainable electrical grid system. In 1879, Thomas Edison invented a practical gasless incandescent lamp and in 1880 conceived a small-scale system at Menlo Park (New York) with a successful demonstration of a functional lighting system with more than 50 lamps [2]. Those developments lead to a major technological achievement in the 20th century. In name of evolution the 24/7 economy was born, powered by this artificial lighting meaning that the presence of light could be felt 24 hours a day, 7 days a week. Although its importance, it requires energy and causes light pollution. Lighting requirements are quite high as regards lighting level and colour to ensure an amenable surrounding in the running days since amenity and comfort are the ultimate good insuring human safety and well-being [13]. As regards to generation of light, there are several sources of light based on electricity being the most important:

- Incandescence - basis of incandescent lamps;

- Recombination of electrons and ions in a plasma - the basis for gas-discharge lamps;
- Recombination of electrons and holes in a semiconductor - the basis for semiconductors lamps like LED.

The main types of artificial light sources are represented in Figure 2.6.

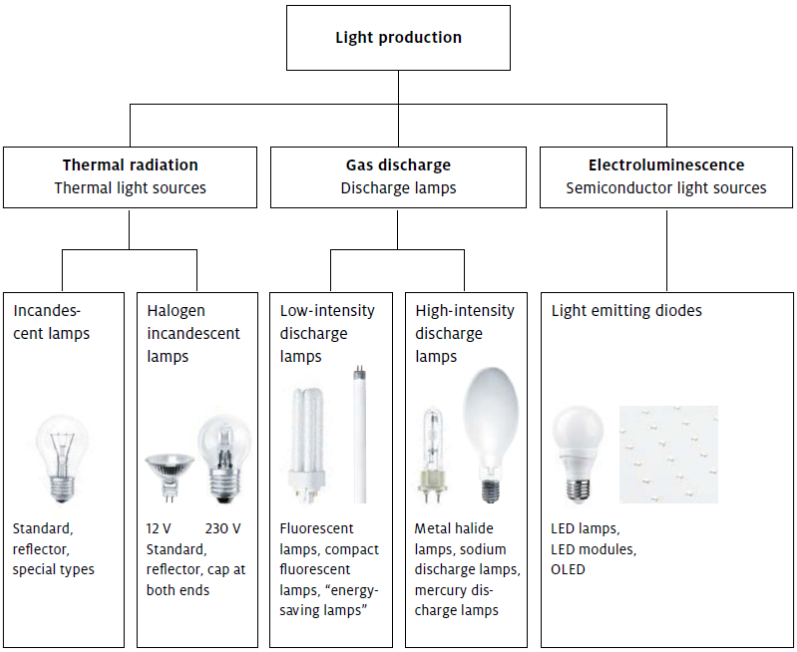

Figure 2.6: Main groups of artificial light sources [12].

Lighting sources have evolve since 1880 till today due to their properties. The incandescent lamps consists in a filament enclosed in a glass that when excited by a flowing current produces heat and therefore light [13]. However it is limited by two main factors: their black-body emission concept, which leads to a large fraction of the emitted spectrum in the IR; the limited filament temperature. The average life-span of an incandescent lamp is about 1000 hours with average efficiency of 20 lm/W. A revolutionary progress of this lighting bulb has reached in the 60s-70s with the advent of the quartz halogen lamp, relying on a self-repair process to operate at 200 °C hotter temperatures than the usual incandescent lamps. These lamps are indicated for residential lighting since it has a Color Rendering Index of 100, they can be installed in any position and have a warm temperature.

Gas discharge lamps (so-called fluorescent lamps) appeared in the 30s rely on the UV light, generated by excited atoms, which are down-converted (in terms of frequency) to visible light by a phosphor coating placed on the interior of the glass casing. Those lamps have average efficiencies in the order of 35 lm/W. Later, appeared the sodium low and high-pressure discharge lamps, with an efficiency of 150 and 80 lm/W respectively [15].

A recent technology suitable for indoor and outdoor lighting is, the LED. This technology is a solid-state light source that emits light when current flows through it. Although LEDs were commonly known for years when applied in low power applications, for example televisions have an LED to indicate its power status (ON/OFF), these devices are not used for lighting

purposes due to their low light output [12]. Recent researches developed high-power white LED for illumination purposes that are mounted on printed circuit boards, since they have a reduced size they have an easy fitting in terms of space required for mounting [12]. The luminous efficacy of LEDs is located in hundreds of lm/W. If grouped in matrices, they can achieve a powerful luminous flux with less power required for the same amount of luminous flux from an incandescent lamp. High-power white LEDs are expected to become a major candidate for future illumination due to their potential for energy conservation, high efficiency, long lifetime, and low cost [4], [11], [12], [17]–[19].

2.2.3 LEDs luminaires

The LEDs are solid state lighting (SSL) devices. They are a replacement for conventional incandescent and fluorescent lamps used for general lighting purposes.

This device is composed by two electrodes: anode and cathode. Except for the lighting phenomenon, the behaviour of an LED is equal to a common diode: it conducts current only in one direction (positive polarity), and blocks the current flow in the reverse direction (reverse polarity). The LED is composed by two types of semiconductor: type P which have a deficit of electrons (or excess of holes) in the valence band so it can attract free electrons and give rise to hole currents; type N which have an excess of electrons, which are not bound to covalent bonds, are free to conduct current. When N-type and P-type semiconductors materials are brought together in contact, they form a P-N junction. At equilibrium condition (thermal condition), the excess of electrons in the N side are attached together with the excess of holes from the P side, in a process called recombination. The result is a region near the junction of the two materials that repels mobile charges due to the electric field created in that region — this is the formation of the depletion region. At thermal equilibrium, there is no current passing through the junction. There is in total, three possible biasing conditions: thermal equilibrium; positive polarity; reverse polarity (see Figure 2.7). Under thermal equilibrium the Fermi level (E_f) of the junction is aligned on both sides of the junction. The energy required to produce this alignment is given by $q\Phi_0$, where q is the charge of the electron and Φ_0 is the built-in potential. The separation between valence and conduction bands is the gap energy, E_g. When positive polarity is applied, the external voltage, V_D, reduces the effect of the built-in potential allowing the flow of current (electrons from the N side travels to the P side as for holes for the opposite direction). For reverse polarity, V_R will add more energy to the built-in potential, thus contributing to a larger energy separation between the conduction bands. As stated before, LEDs are constituted by a P-N junction and operate in the forward polarization condition with an external source providing the necessary voltage for current conduction. When the excess of electron-holes pairs in the material recombine in such a way that an electron in the conduction band recombines with a hole in the valence band, a photon is emitted. Recombination occurs when an electron loses energy and passes from the conduction band to the valence band. The wavelength of the light is determined by the energy required for the electrons to cross the band gap, corresponding to the energy of the photons by 2.3. The color that is emitted by an LED depends on the semiconductor material

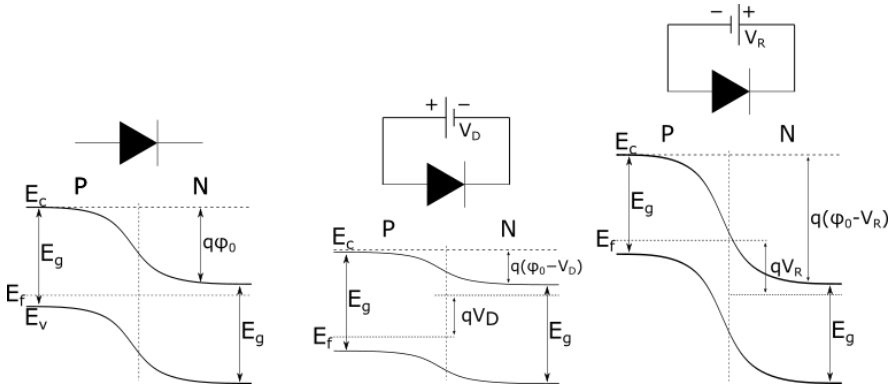

Figure 2.7: Energy band diagrams. From left to right: thermal equilibrium; positive polarization; reverse polarization. Adapted from [16]

of the substrate and on the doping materials [12]. Most common LEDs are based on Gallium Phosphide (GaP) and Gallium Arsenide Phosphide (GaAsP) which may produce, depending on the doping materials, the wavelength from green to red. The Gallium Nitride (GaN) may produce purple and blue light.

For LED lighting purposes, it is preferable to achieve a color wavelength similar to the one produced by the incandescent light bulb, by other words, white light. There are several ways to make white, or near-white, light with LEDs. The more commonly used are:

1. If three LEDs of different colors are combined, such as, red, green and blue, closely together, they can be clustered in packages of one color each. The combination of those LEDs can achieve any combination on the RGB color model by modifying the intensity of each individual LED.
2. Blue-emitting GaN-based LEDs combined with a phosphor layer, convert part of blue light into light with longer wavelength ($465nm \mapsto [500; 700]nm$). The phosphor absorbs photons with a given energy and re-emits them with a lower energy and larger wavelength in the yellow region. Thus, the combination of blue and yellow photons produces the white light.

White light production from RGB LEDs is not the best approach for lighting purposes. The efficacity of the combined colors as well as the color rendering promoted by those LEDs are not good enough. The second approach to the problem, using blue-emitting GaN-based LEDs combined with a phospor coating, was studied by Shuji Nakamura in 1994 with the first demonstration of a high brightness blue LED. The white LED quick followed this important landmark. In 2014, Shuji Nakamura received the Nobel Prize in Physics together with Professor Isamu Akasaki and Professor Hiroshi Amano for the invention of blue light-emitting diodes. This type of phosphorescent white LEDs are found in most of the white LED bulbs available in the market [17].

In what concerns LED electric driving requirements, there are some constraints. The Shockley diode equation gives the characteristic curve I-V (current-voltage) of an ideal diode as for forward or reverse polarization defined as,

$$I(V_D) = I_0 \left(e^{\frac{qV_D}{nkT}} - 1 \right) \tag{2.10}$$

where I is the diode current, I_0 is the saturation current, q is the electron charge equal to 1.602×10^{-19}C, V_D is the applied voltage across the diode, n represents the ideality factor typically $1 \leq n \leq 2$, k is the Boltzmann's constant equal to 1.381×10^{-23}J/K, and T is the temperature in Kelvin degrees. This equation follows an exponential model that can be break apart for the different polarizations. As V_D is positive and increases, the diode is directly polarized and the exponential term becomes so high that the forward current (I) becomes much larger that I_0, hence — $I(V_D) \approx I_0 e^{\frac{qV_D}{nkT}}$. When V_D is negative and decreases, the diode is inversely polarized and the exponential term becomes zero, hence — $I(V_D) = -I_0$. Despite the accuracy of this model, it does not contemplate the reverse polarization breakdown where the diode is reverse biased and there is a dramatic increase in current.

For the requirements of lighting purposes, LED luminaries are composed by multiple elements in order to achieve a considerable luminous flux. The association of multiple LEDs is imperative. LED devices can be arranged in series, parallel or in a mixed solution that form a matrix (see Figure 2.8). The topology chosen depends on the number of LEDs and its properties such as nominal current, and maximum forward voltage.

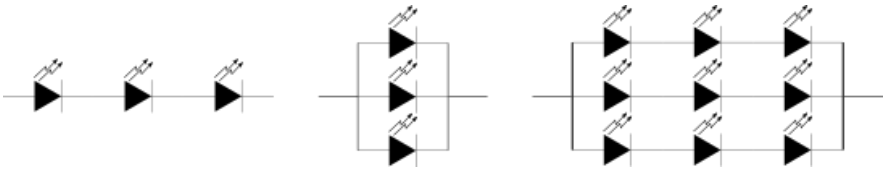

Figure 2.8: LED configuration topologies. From left to right: series; parallel; parallel of series

Due to the exponential relationship between diode forward current and voltage, a small change in voltage across the diode will generate a significant increase of current (intrinsically non-linear). For that reason, its preferable to drive the LED with current bias instead of voltage bias in order to improve lighting control. It is also important to remark that the conversion between electrical current and the luminous flux (optical power) generated by the luminary is approximately linear. In conclusion, LEDs need to be driven at a steady constant current in order to create a steady luminous flux for lighting.

In actual lighting systems, it may be important to include dimming control for energy savings or emotional lighting. For current driven LEDs, dimming can be achieved by two ways (see figure 2.9) [20]:

1. Modifying the value of the current amplitude applied to the LED;
2. Using Pulse Width Modulation (PWM) to set an average value of current.

The dimming of light with PWM can be achieved [19], [20] keeping a constant maximum value of current, (I_{max}), and varying the time of conduction in a fixed period, thus, $I_{pwm}(t)$ can be defined as,

$$I_{pwm}(t) = \begin{cases} I_{max} & 0 < t < \delta T \\ 0 & \delta T < t < T \end{cases} \tag{2.11}$$

for a period of time T and $0 < \delta < 1$, where δ is commonly named as Duty-Cycle and defined

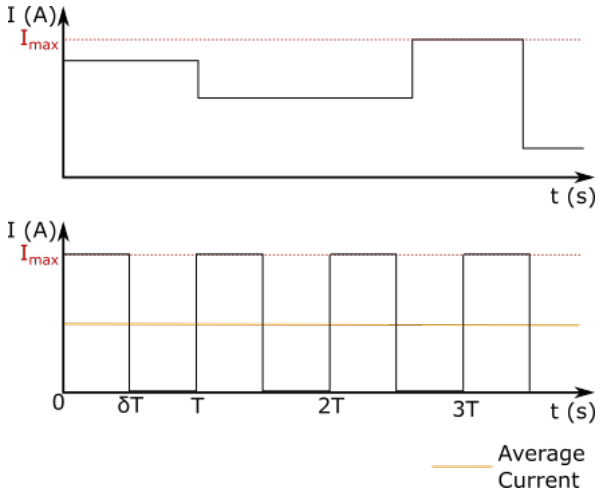

Figure 2.9: LED current driving modes. From top to bottom: constant current; pulsed current (PWM). Adapted from [16]

as $\frac{t_{on}}{T}$. The average current of PWM signal is defined as,

$$I_{avg} = \frac{1}{T}\int_0^T I_{pwm}(t)\,dt = \frac{1}{T}\left[\int_0^{\delta T} I_{max}\,dt + \int_{\delta T}^{T} 0\,dt\right] = \delta I \tag{2.12}$$

However, it has been verified that the use of PWM can lead to color temperature variations.

2.3 Visible Light Communication/OCC

The need of communication appeared in the early civilizations. Messages were mainly transmitted through fire, smoke or sunlight reflection over great distances for communication purposes. The era of electronics in the 19th century revolutionize this field and with the introduction of telecommunications through wire appeared the telegraph and telephone. Over the years a new revolutionary way of communication is invented, without the need of wired infrastructure by Guglielmo Marconi, an Italian inventor, conducting experiments in long-distance radio waves [21]. His work inspired the research to explore wireless systems that society uses till today such as, Wi-Fi, Bluetooth, GPS, among others. With the increasing demand of bandwidth, the evolution of mobile phone technology is the example with the evolution of early Global System for Mobile Communications (GSM) networks like second-generation (2G) to the most recent fifth-generation (5G). Those society high demands are strangling the RF spectrum [22] rapidly requiring the need for alternatives [4]. In the last past years, researchers focused their work in the study of Optical Wireless Communications (OWCs) which makes use of IR, visible, and UV subbands [4], [11], [19], [23]. There are several advantages in the progress of OWCs research, such as, no requirement of RF spectrum licensing, is immune to RF interference, offers ultra-high bandwidth (in order of the THz). OWCs systems in the visible band spectrum, are commonly referred as VLCs that use LEDs technology for lighting purposes and communication at the same time [4], [17], [18]. Actual lighting fixtures that uses LEDs are evolving from an alternative to a standard, the use of VLC for communication purposes is less expensive because it is oriented to make use of the

existent lighting infrastructure [4], [24]. There are numerous applications where it can provide alternative solutions to wireless local area, heterogeneous networks, indoor localization and navigation, vehicular networks, among others. Thus, VLC is a potential candidate for next generation communication networks, additionally, it enables secure data transmission in zones where RF is substantially attenuated or forbidden, such as hospitals, aircrafts, hazardous environments, etc [24].

The increasing presence of LED luminaries for purposes of general lighting is getting attention for VLC applications [22]. They achieve multiple interesting characteristics such as longer lifetime, better controllability, and energy efficiency, points to a bright future for the implementation of VLC systems. Although all positive characteristics for common lighting, there are also problems that need urgent attention for communication, essentially, the slow response and the bandwidth of power LEDs since information is transmitted by subtle changes of light intensity, unnoticeable to human eye [4], [11], [22]. Modulation process for communication with low frequency may cause flicker that is perceived to the human eye. This effect is caused by the fluctuation of the brightness of light, hence, a frequency greater than some hundreds of Hertz is considered safe (eg: 200 Hz) [16], [25]. White light based in LED is commonly created using blue LEDs with phosphor coating, driven with high forward currents. The blue LED has an intrinsic capacitance that slows down the device response, with the photons recombination in the phosphor coating, the response of the device is even more affected. These properties affect the bandwidth of the LEDs used to transmit information. Another important aspect is that VLC operates preferably with LoS configurations [4].

2.3.1 Modulation techniques

Modulation techniques used for VLC are characterized into two types: single carrier modulation and multi carrier modulation, Figure 2.10 shows the different modulation schemes commonly used in VLC. It is important to denote that the low bandwidth of an LED (only a few MHz) [4], [17], [18] implies that information should be concentrated in baseband. VLC systems use intensity modulation, hence, the optical intensity must be a non-negative real value [16], [24].

Since the modulation schemes used in this dissertation are single carrier modulation schemes, only these will be briefly described. Schematic diagrams of this type of modulations can be observed in Figure 2.11.

The OOK scheme, is one the most used signal modulations in VLC [19] because of its simplicity in implementation [4]. A binary "one" is represented by an optical pulse that occupies the bit duration (T_b), and a binary "zero" is represented by the absence of an optical pulse.

The PAM modulation scheme is a variation of OOK that can transmit symbols instead of bits based in multiple pulse amplitudes. Depending on the number of levels (L), the L-PAM scheme can transmit M bits per symbol, being M a positive integer, where $M = log_2(L)$. We can conclude that OOK modulation is defined as 2-PAM scheme as $M = log_2(2) = 1$, it transmits one bit per pulse duration.

The last commonly used scheme is PPM scheme, where the information is encoded in the

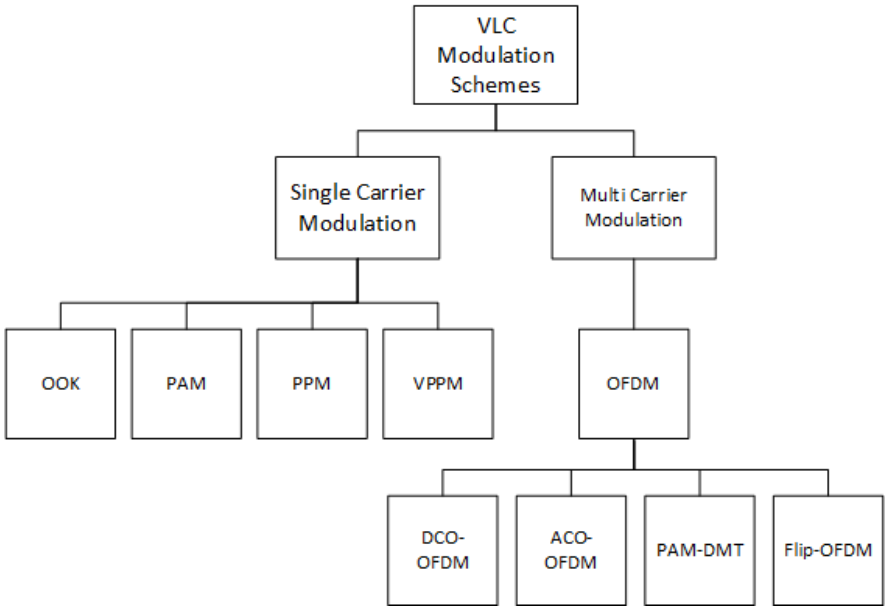

Figure 2.10: Single and multi carrier modulation schemes.

position of a pulse within a symbol duration. A symbol duration can be divided in L time slots of equal duration. The time slot containing a pulse, represents the symbol transmitted where all others slots are empty. The L-PPM scheme transmit M bits per symbol, likewise the L-PAM, where $M = log_2(L)$.

An interesting modulation scheme derived from PPM [4] is, the Variable Pulse Modulation (VPPM). It is a modulation scheme that increase power gain when compared to PPM. This is the scheme recommended for VLC as outlined in IEEE 802.15.7 Section 8.2. VPPM supports simultaneously communication and lighting with dimming [4], it uses binary PPM (2-PPM) for transmitting information and pulse width for dimming [20]. Similar to the PWM technique, the average intensity of the light source will be adjusted with the width of the pulse, with the particularity that the position of the pulse that represents a binary "zero" is aligned to the left of the symbol period and a binary "one" is aligned to the right of the symbol period (see Figure 2.12). This approach is very important in what regards the duality between lighting and communication since for a specific dimming, the mean value of intensity of light, between VPPM symbols, is equal. This property produces the desired flicker-free effect [19]. VPPM can be observed as a OOK scheme applied to a Manchester code line (bit represented by a levels transition) with variable duty-cycle.

Multi carrier modulation can be achieved in VLC with Orthogonal Frequency-Division Multiplexing (OFDM) technique which make use of orthogonal sub-carriers to transmit data. However, OFDM cannot be used in VLC as it is in RF systems since VLC signals must be real and positive. By those terms, Hermitian symmetry is employed to convert RF OFDM into optical OFDM.

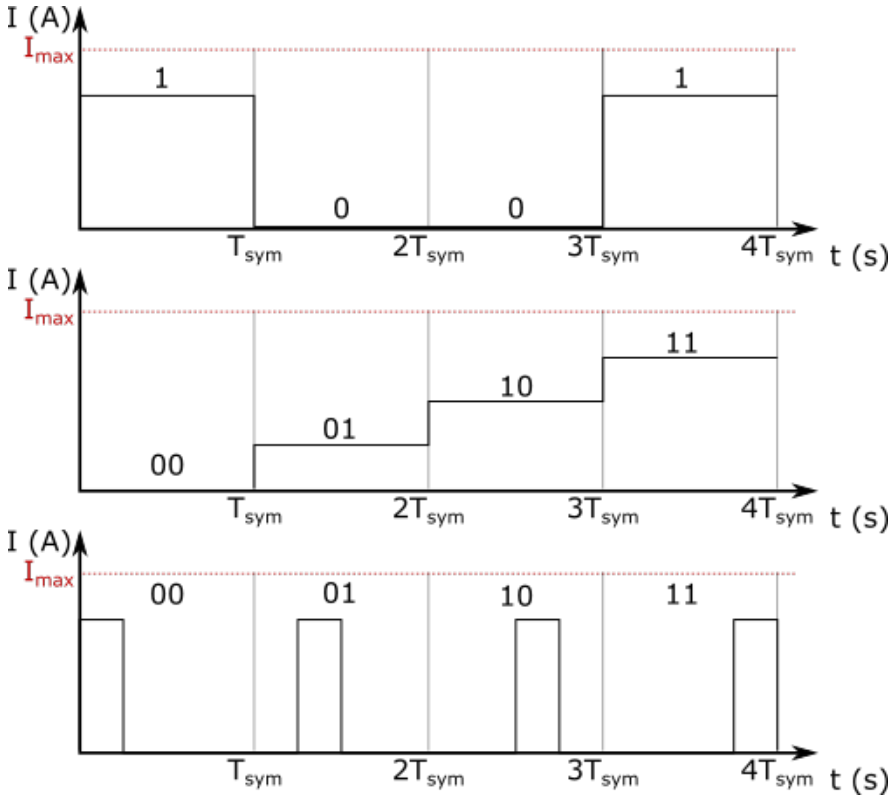

Figure 2.11: Schematic diagrams of Single carrier modulation schemes. From top to bottom: On-Off Keying (OOK); Pulse Amplitude Modulation (PAM); Pulse Position Modulation (PPM).

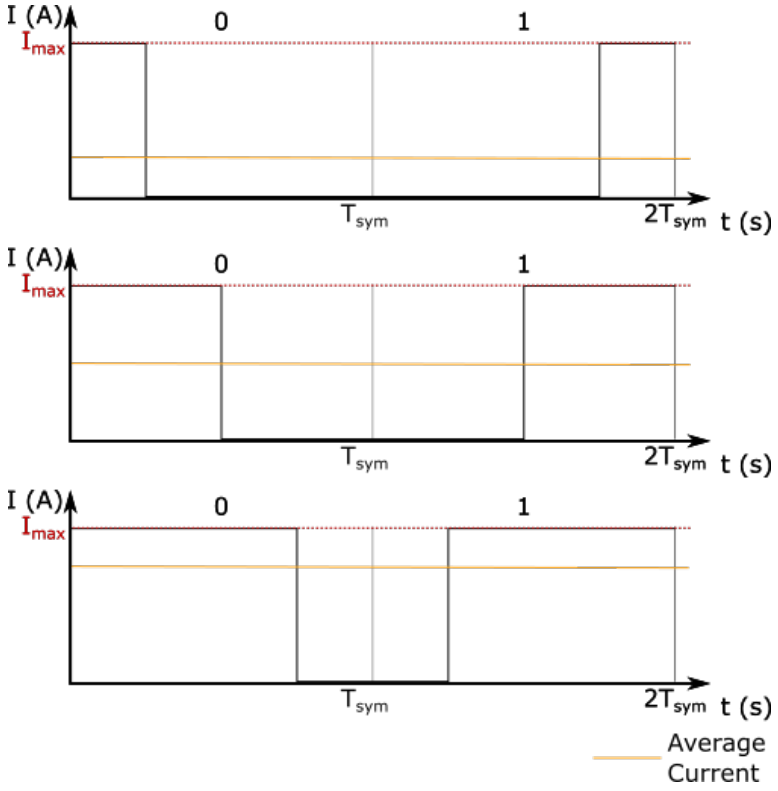

Figure 2.12: VPPM pulse width variation. From top to bottom: 25%; 50%; 75%.

2.3.2 VLC current drivers

One of the main challenges in VLC is the ability to drive high-power LED luminaries. LEDs for the simple purpose of steady lighting offers reasonable turn-ON times, and drivers are designed to regulate a steady DC current. However, for AC signal, LEDs have an intrinsic capacitance that slows down the response of the light to the input signal. As so, drivers for VLC purposes should respond as fast as possible in transient regions.

A VLC signal corresponds to a AC signal added to a DC current bias, this can be achieved using a Bias-T (see Figure 2.13). A capacitor is a open circuit for DC signal and an inductor is a open circuit for AC signal, hence, DC and AC will be added. This circuit is employed in many RF circuits and VLC systems also takes advantage of its properties to test different modulation schemes and verify them experimentally [17].

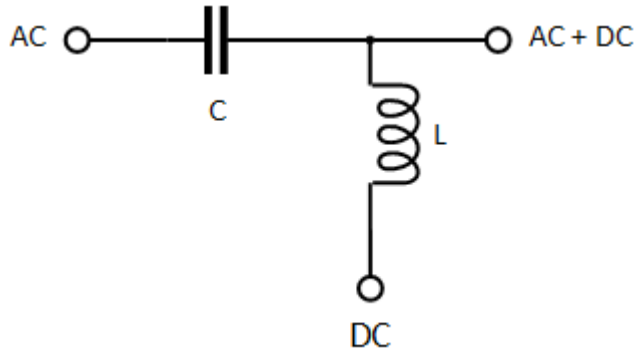

Figure 2.13: Bias-T circuit.

An alternative to the Bias-T, which commercial models are expensive [17], can be seen in Figure 2.14. It is a voltage-to-current converter with current regulation. In this circuit, the first component adds the signal voltage to the DC bias voltage. The sum of those signals is then converted into current by the sensing resistor R_s. Nevertheless, it is important to denote that this configuration has a MOSFET in common-drain configuration, with unit gain. This device is in series with the lighting device, thus, the current that flows through them is equal. The channel width of the MOSFET, controlled by the gate voltage will then control the current flow. Using negative feedback to read the current that passes through the resistor, the second Operational Amplifier (Op-Amp) will drive the MOSFET according with the signal at its non-inverting input. In sum, we can define the current flowing in the LED as $I_{led} = (V_{in} + V_{bias})/R_s$.

The circuit in the Figure 2.14 has some disadvantages, the regulation of the current by the MOSFET will dissipate a considerable amount of heat depending in the forward voltage of LEDs and the voltage of the power supply that should be considered by the circuit designer.

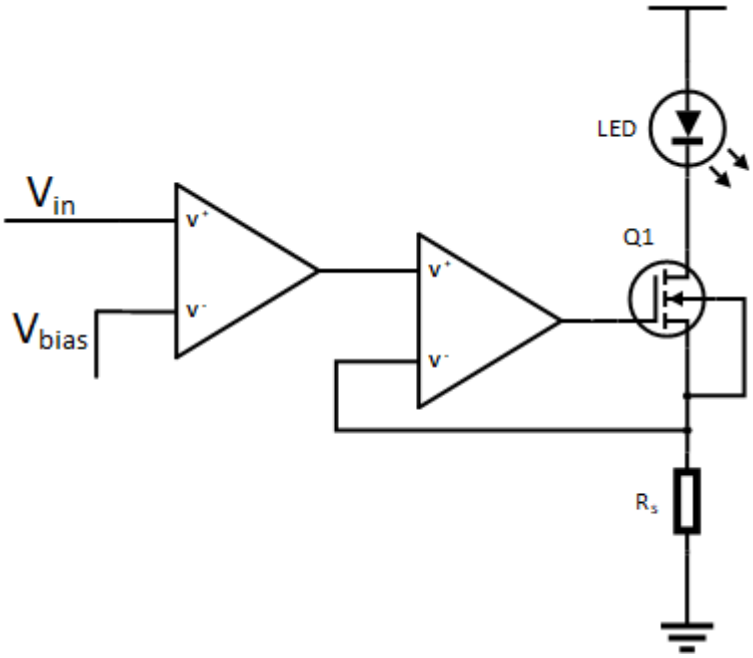

Figure 2.14: Voltage-Current regulator driving LED with DC bias and AC signal. Adapted from [16]

2.3.3 LED bandwidth

The bandwidth of an LED driver is usually limited by the LED itself. The optical LED bandwidth is characterized as a pole in the frequency response, acting like a 1st order RC low pass filter. The circuit of a filter is implemented as in Figure 2.15 and its transfer function is defined by,

$$H(s) = \frac{1}{1 + s/\omega_0} \tag{2.13}$$

where: ω_0 : the frequency cut-off of filter defined by $\omega_0 = 1/(RC)$.

Electrical bandwidth of this circuit is defined as $f_{3dB} \approx 0.35/t_r$, where t_r represents the rising time of the signal to a step-response. Applying a current step input to an LED, the output power is similar to the response of a RC low pass filter, hence,

$$H_{LED}(s) = \frac{1}{1 + s/\omega_0} \tag{2.14}$$

where: ω_0 : the frequency cut-off of an LED defined by $\omega_0 = 1/\tau$.

represents the power transfer function of an LED. The relationship between power gain is $10 \log P_{out}/P_{in}\,(dB)$, therefore, $-3dB$ corresponds to $P_{out}/P_{in} = 0.5$. The optical frequency cut of an LED (based on the model of the RC circuit) can be obtained using the rising and falling time of the signal obtained for an input step-response as,

$$\begin{cases} t_r \approx 2.2\,\tau \\ |H_{LED}(\omega)| = \frac{1}{\sqrt{1+\omega^2\tau^2}} = \frac{1}{2} \end{cases} \therefore\ f_{3dB} \approx \frac{2.2\sqrt{3}}{2\pi t_r} \approx \frac{2.2\sqrt{3}}{\pi(t_r + t_f)} \tag{2.15}$$

where t_r represents the rising-time, t_f the falling-time, τ is the time-constant and ω is the cut-off frequency of the LED defined by $\omega_0 = 1/\tau$.

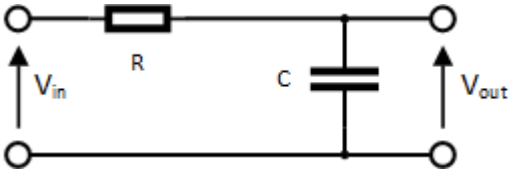

Figure 2.15: 1st order RC low pass filter.

2.3.4 VLC receivers

Light can be detected using semiconductors as well. State-solid lighting is the type of lighting achieved by the use semiconductor LED, the recombination of electrons and holes releases energy in the form of photons with a specified wavelength. The reversal process is also achievable, meaning, for incident photons in a semiconductor, current can be induced over the semiconductor device. This happens because travelling photons may provide electrons in the valence band that creates a conduction path. We call to these devices, photodetectors. It is a device that converts light energy into electrical energy, hence, it can detect the presence of light. Common VLC receivers are listed in Figure 2.16.

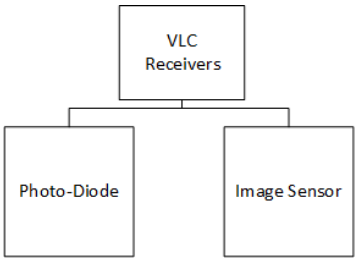

Figure 2.16: Common VLC receivers

One of the most common used devices is the Photo-Diode (PD) [4]. The device is similar to a common LED composed by a P-N junction defined by Equation 2.10, with the addition that the current suffers the influence of the incident light energy defined by,

$$I(V_D) = I_0 \left(e^{\frac{qV_D}{nkT}} - 1 \right) + I_{ph} \tag{2.16}$$

where I_{ph} represents the current imposed by the incident light. The incident energy of the photon must be higher than the energy gap of the device so electrons can flow. This device is normally reverse polarized, in this condition, the power of incident light that falls on the junction of the PD, is directly proportional to the current flowing through it[4], [16] as,

$$I_{ph} = P_0 \frac{q\lambda}{hc}(1-r)(1-e^{\alpha(\lambda)d}) \tag{2.17}$$

where P_0 is the incident optical power, r the reflection coefficient (air-semiconductor), $lambda$ the wavelength, h is the Planck's Constant, c is the speed of light in vacuum, $\alpha(\lambda)$ represents the absorption coefficient and d is the length of the sample.

In order to maximize the VLC signal reception, PDs should be chosen with large surface area. However, it is important to define that the reception of signal from a light source to

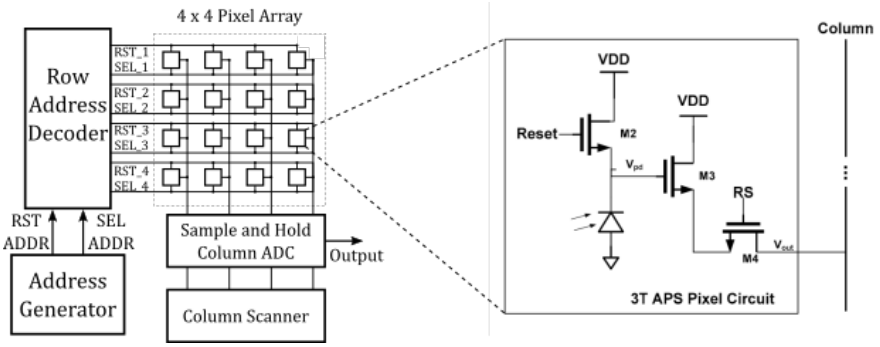

Figure 2.17: CMOS image sensor typical circuitry. From left to right: image sensor architecture adapted from [26]; 3 Transistors Active Pixel model adapted from [27]

a PD is limited by its Field-of-View (FOV). Conversion of the current produced by the PD into voltage, is normally achieved with the use of a TIA [4]. The circuit designer must be aware that other light sources introduce a DC level that will influence the electrical current of the PD.

A recent technology that offers low-cost and simple communication is the Optical Camera Communication (OCC) [11]. Common digital cameras are composed by a lens, a color filter, a 2-D array of photodetectors and post-processing unit [11]. The Image Sensors (ISs) can be either Charged Coupled Devices (CCD) or Complementary Metal-Oxide Semiconductor (CMOS), their main application is the conversion of light into electrons (see Figure 2.17). CMOS ISs operate with two capture schemes: Global Shutter (GS) or Rolling Shutter (RS). GS IS scan the entire image simultaneously, all pixels are exposed to light at the same time, while RS scan the image row-by-row, with a inherent time delay between rows (sequential read-out) (see Figure 2.18) [26]. Since in the RS technique each row of pixels is exposed at once, the captured image of an LED that produces pulsed light will be composed by white and dark stripes, an example of the resulting image can be observed in Figure 2.19 considering that the read-out time is ignored. The width of the stripes in the image will depend of the frequency of the blinking light, and the number of stripes will depend of the distance between sensor and LED. By those conditions, when a RS-based IS receives square waves of different frequencies, the captured stripes widths will be proportional to the inverse of the signal frequency (higher frequency, lower width), enabling the possibility to transmit data symbols modulated in frequency, also known as Frequency Shift Keying (FSK). ISs may severely differ from each others since the Analog-to-Digital conversion (light conversion to 2D image) time is dependent of manufacturer, thus, different cameras can capture different stripes widths for a fixed-frequency light source. Additionally, the frame rate of a camera is not fixed, hence, different cameras can produce images with repeated or lost symbols. Nevertheless, in a multi-user VLC area, the transmitter is not able to tune the transmitting frequency for every device in the LoS.

Nowadays, it is very common that mobile phones possess CMOS camera sensors [26], [27], since OCC technology implies the use of a CMOS IS with RS to receive information from an LED light source, at higher frequency than the maximum frames per second of the device, it

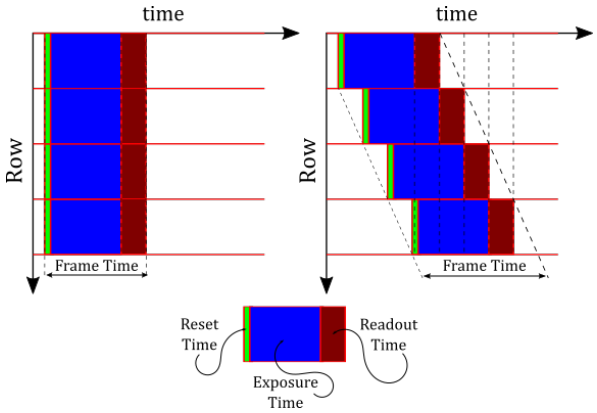

Figure 2.18: Image sensor mechanism acquisition timing. From left to right: Global Shutter; Rolling Shutter. Adapted from [26].

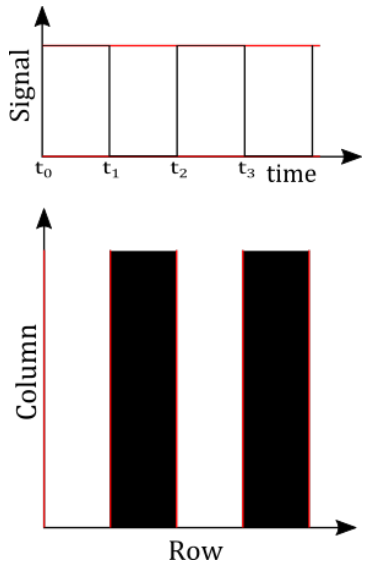

Figure 2.19: Received Image produced with RS mechanism and square wave light signal. From top to bottom: light signal; received image.

is a good alternative to PDs. When compared to PDs, camera offers many features, such as, a larger FOV, spatial separation of light and can process different wavelengths provided by the color filter [11]. Nevertheless, cameras are commonly present in smartphones, thus, in close contact with users. However, CMOS RS-based cameras are limited to low frame rates (from 30 to 60 frames per second), being the data rate of OCC in the range of 0.01 kbit/s to 100 kbit/s [28].

2.4 Indoor Positioning using artificial light

Positioning systems used for the purpose of estimating user, equipment or other object location, are the base for navigation-based services. For that purpose, the popular localization system GPS is widely used in vehicles, portable devices, marine, military for the purpose of real-time location, navigation, tracking and timing. In some environments, specially indoor environments, GPS positioning can be inaccurate and discontinuous since signals suffers from

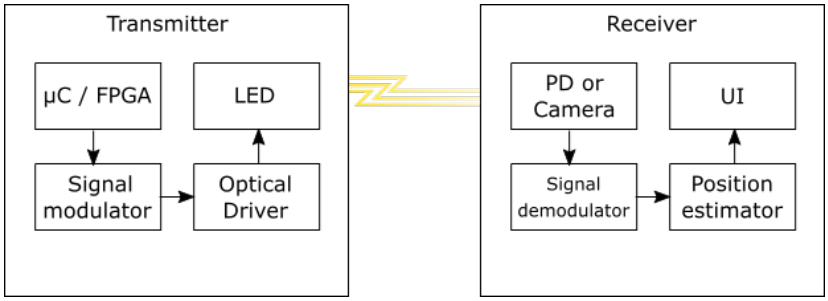

Figure 2.20: Base architecture for VLP. Adapted from [31].

signal attenuation by RF path obstruction, for instance, walls, ceilings or clouds [11]. IPSs determine the position of an object, within physical space continuously and in real-time. Due to the increasing demand for accurate indoor positioning, it has become an active research area [29]. IPSs may offer a variety of applications in the area of navigation such as help blind people navigation, locating devices inside buildings, aiding tourists in museums, promoting discounts to shoppers, among others [4], [22], [24]. With the development of automation in industry, IPSs are critical for robots, robotic guidance and robot cooperation [30]. Alternatives to the GPS system have surged in the matter of indoor localization, such as systems based on wireless signals, Wi-Fi, Bluetooth, RFID, ZigBee [30]. Since these systems are RF-based, they all suffer from interference and bandwidth restrictions [30]. As an alternative, VLP, exploiting the existing LED illumination, has given a huge contribution to IPSs achieving a positioning error in the range of 0.1 m to 0.35 m, when compared to Wi-Fi (1 m to 7 m), Bluetooth (2 m to 5 m), and other technologies. Furthermore, some related work, have achieved millimetre-level position accuracy. Although the accuracy of VLP systems, this positioning technology is still under development and subject to trials, while RF-based systems have been commercially deployed.

The base architecture of a VLP system can be observed in Figure 2.20. Usually, the individuals LED light sources transmit their unique-ID [24] or any other information that allows the extraction of their spatial coordinates in a Cartesian coordinate system. Since the information sent by the light source is repeated through time, a simple uC or a Field Programmable Gate Array (FPGA) can be programmed to modulate the signal to be transmitted [19], [24]. This modulated light is received by an optical sensor, Photo-Diode or Image Sensor, demodulated and processed to allow the estimation of the receiver's position within a room. Using this system, Figure 2.21 represents a self-located robot within a room where four LED luminaries deployed on the ceiling, for lighting purposes and communication, are used to determine its position.

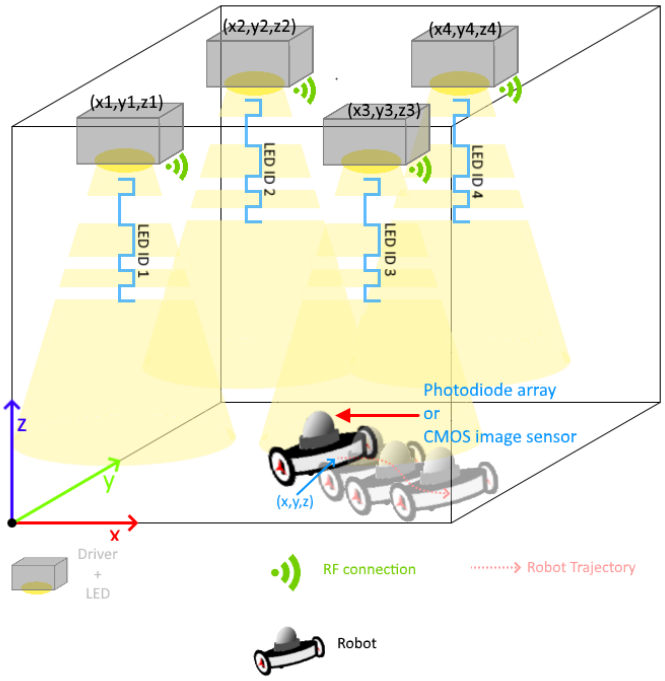

Figure 2.21: Example of a self-located robot in a room using VLP

2.4.1 Positioning techniques using photo-diodes

Depending on the sensor that is used to receive VLC, multiple different techniques are used to estimate position. In the case of PDs, those techniques can be classified using characteristics of received optical signal, which are:

- AoA
- RSS
- TDOA

As LED transmitter radiates visible light, the intensity of light degrades while it propagates through the optical channel. An LED-based light source pattern radiation is defined in literature usually as Lambertian. By those terms, the Lambertian radiant intensity in function of the angle ϕ, $I(\phi)$, is given by

$$I(\phi) = I_0 \times cos^m(\phi),\ |\phi| \leq \frac{\pi}{2} \tag{2.18}$$

where I_0 is the center luminous intensity of an LED and the order of the Lambertian radiation pattern, m, is defined as

$$m = \frac{-ln(2)}{ln(cos(\phi_{1/2}))} \tag{2.19}$$

that depends on the semi-angle at half power of the LED $\phi_{1/2}$ also known as the Half Power Angle (HPA) (see Figures 2.22 and 2.23). Thus, the horizontal illuminance, E_h, at a specific coordinate within the illuminated area is given by

$$E_h = \frac{I(\phi)}{d^2} \times cos(\psi) \tag{2.20}$$

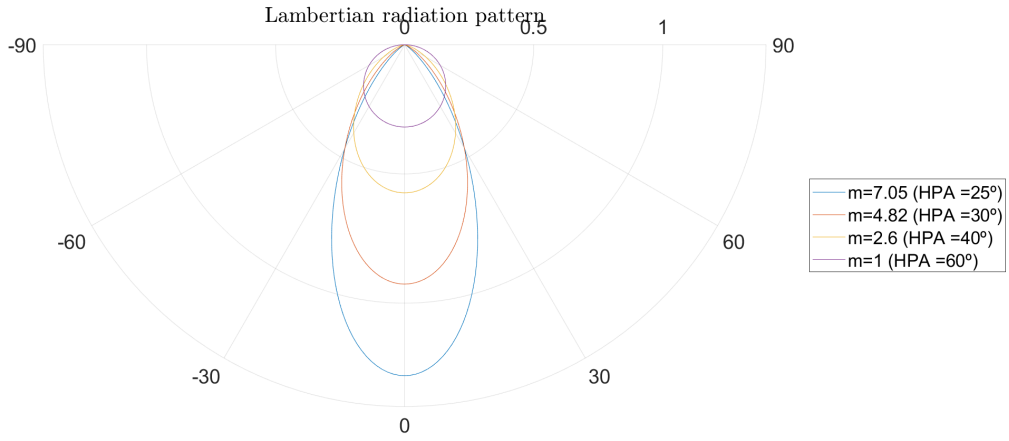

Figure 2.22: LED-based light source radiation pattern.

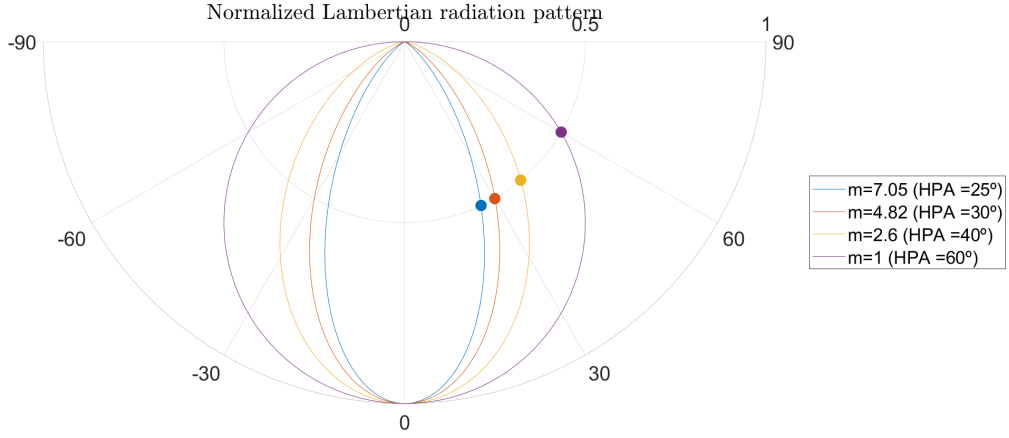

Figure 2.23: LED-based light source normalized radiation pattern

that depends from the luminous intensity at angle ϕ given by $I(\phi)$, d represents the distance between light source and surface, and ψ is the angle of incidence.

The photocurrent generated by a PD is proportional to the optical power received, hence, the relationship between power emitted and received is defined by the Equation 2.21 as a function of channel DC gain, $H(0)$, provided by

$$P_r = H(0)\, P_t \tag{2.21}$$

where the received optical power is fined by P_r, the channel DC gain by H_0 and the transmitted

optical power by P_t. It is important to denote that coating and filter have an effect on the received light on the PD, where the coating will produce a different refractive index modifying light propagation direction in relation the one outside. The channel DC gain H_0 is defined as,

$$H(0) = \begin{cases} \frac{(m+1)A}{2\pi d^2} cos^m(\phi) T_s(\psi) g(\psi) cos(\psi), & 0 \leq \psi \leq \Psi_c \\ 0, & \psi > \Psi_c \end{cases} \tag{2.22}$$

where A denotes the physical area of the PD, d the distance between emitter and receiver, ϕ and ψ is the angle of irradiance and incidence respectively, Ψ_c is the semi-angle of the receiver FOV, influenced by the PD coating factor that defines the gain of an optical concentrator $g(\psi)$,

$$g(\psi) = \begin{cases} \frac{n^2}{sin^2(\Psi_c)}, & 0 \leq \psi \leq \Psi_c \\ 0, & \psi > \Psi_c \end{cases} \tag{2.23}$$

dependant from n, the refractive index, whereas $T_s(\psi)$ defines the optical filter gain.

It is important to denote from Equation 2.21 in conjunction with Equation 2.22 that the received power by a PD will be highly attenuated as distance d, angle of irradiance ϕ and angle of incidence ψ increases until it drops to zero. Figure 2.24 represents a VLC LoS transmitter-receiver system. These are the main factors in VLP that contribute to the estimation of position within a lighted area.

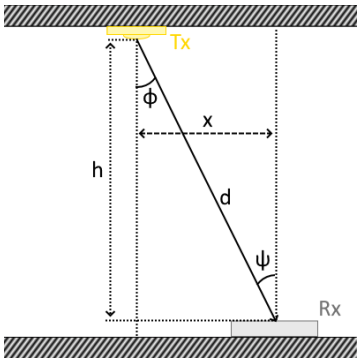

Figure 2.24: VLC LoS transmitter-receiver system.

The AoA technique is particularly useful since it exploits the fact that received power is not only dependent of distance, but a function of the angles of irradiance and incidence. The angles are defined by spatial coordinates of the LEDs and the receiver, which can be determined using trigonometric relations.

For RSS, if the received optical power is proportionally inverse to the square of the distance in LoS between transmitter and receiver, the receiver position can be estimated using the intensities of the received signals.

TDOA technique uses the phase delay information from the received signals, as they are processed such that distance is contained in phase.

2.4.2 Positioning techniques using Image sensors

Although ISs are built with PDs contained in an array, positioning methods using these sensors are different from those using individual PDs. Because the IS produces a two dimensions

(2-D) image, the signal transmitters can be spatially separated as,

$$s \begin{bmatrix} u \\ v \\ 1 \end{bmatrix} = A_{3\times3} \left[R_{3\times3} \, T_{3\times1} \right] \begin{bmatrix} X \\ Y \\ Z \\ 1 \end{bmatrix} \tag{2.24}$$

denotes the projection of a 3-D point in the IS, where s is a scaling factor, (X, Y, Z) are the coordinates of a point in world coordinates, (u, v) the projection of the 3-D point in pixels, A is the camera intrinsic parameters composed by the focal distance length and the optical center, R and T are the rotation and translation matrices. Such feature removes the need for multiplexing/demultiplexing different signals. In IS-based indoor VLP, the coordinates or a unique ID of the luminaries are modulated in light intensity sent over the OCC link and image processing techniques are used to find the central coordinates of the lighting fixtures in the image plane [11], [30]. Using geometrical transformations, the world coordinates of the camera can be estimated. Some systems make use of external sensors included in smart devices, for instance a gyroscope, to improve position estimation error. It is important to remark that to achieve indoor positioning using images sensors, the luminaries should be within the FOV of the image device (See Figure 2.25). The minimum number of LED-based luminaries required to achieve positioning depends on the algorithm used, whether aspects like the camera sensor resolution in pixels, the focal length and the position of light sources, will influence the accuracy of the positioning algorithm results. In order to achieve better results, some related papers make use of ultrawide-FOV lens in order to improve the accuracy of the positioning algorithms. To satisfy customer's photography demands, smart-phone manufacturers attach cameras with a wider FOV, thereby creating better conditions to achieve camera-based IPSs.

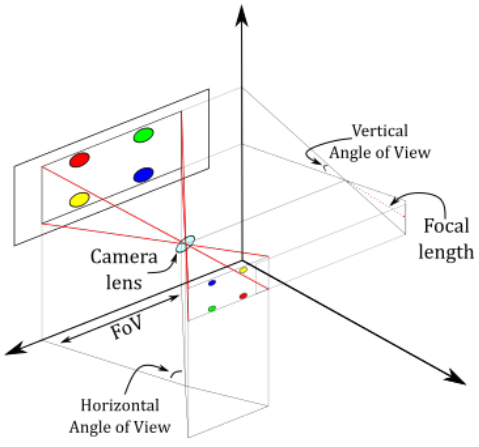

Figure 2.25: Camera pinhole FOV

2.4.3 Related Work

The coverage of the actual State Of The Art (SOTA) related to VLP has revealed that most of the research done so far is mostly simulation experiments. It is necessary to develop physical

platforms that are able to offer the necessary conditions to perform experimental research that can contribute to the actual SOTA. Table 2.3 and 2.4 exhibit experimental works in the field of VLP, where the first is related to works with PDs and the second one is related to research with ISs. A quick analysis to the test-bed size column of these two tables shows that the majority of the works have been conducted in small areas.

System	Positioning Algorithm	Test-bed size (m)	Accuracy (cm)	LEDs	Auxiliary devices
[32]	RSS (Trilateration)	5x8, 2x12, 3.5x6.5	30 (2-D)	4 (10W)	Inertial Sensor
[33]	RSS (Trilateration)	0.6x0.6x0.6	2.4 (3-D)	3	None
[34]	RSS (Trilateration + PDR + Filters)	2.5x2.84x2.5	14 (2-D)	7 (17W)	Inertial sensor
[35]	RSS (Fingerprinting)	1.8x1.2x1	14.84 (2-D)	6	4 extra PDs
[36]	AoA (Triangulation)	5x1x1.5	25 (3-D)	3	Accelerometer

Table 2.3: VLP systems experimental set-ups using PDs

System	Positioning Algorithm	Test-bed size (m)	Accuracy (cm)	LEDs	Auxiliary devices
[37]	AoA (Transformation)	0.6x0.6x2.6	6.1 (3-D)	2 LEDs	Extra camera
[38]	AoA (Transformation)	0.71x0.74x2.46	10 (3-D)	5 LEDs	None
[39]	Transformation	1.4x1.4x1.6	X:3 Y:7	3 LEDs	None
[40]	Transformation	1.8	4.3	3 LEDs (10W)	Inertial sensor

Table 2.4: VLP systems experimental set-ups using ISs

Work [32] demonstrated the implementation of VLP in three typical office environments: a conference room ($5m \times 8m$); a cubicle area ($3.5m \times 6.5m$); a corridor ($2m \times 12m$). In each area, they use five luminaries designed by the authors using small luminaries composed by commercial model Cree T6 LED with 10 W of power and run multiple tests in sixty different points among each areas. The communication packet transferred through VLC has a total of 96 bits that contains a preamble (16 bits), data with the location coordinates of the emitter (64 bits), the duty-cycle (8 bits) and Cyclic Redundancy Check (CRC) to check integrity of the contents (8 bits). The modulation used to transmit data is Binary Frequency Shift Keying (BFSK) with PWM to control dimming of light. The results of the system deployed for VLP, using Trilateration with the support of an inertial sensor, reported a positioning error for the different spaces of 30 cm in average. They have reported that the results of the system shows that center area positions tends to have smaller error when compared to outer positions

because of the small incidence angles which are more robust to measurement noise. They also concluded that the luminaries should be deployed evenly for better accuracy, as a natural rule to deliver even illumination conditions. The system developed by [33] propose an IPS with three LEDs in a triangular configuration with a distance of 60 cm between luminaries. The driving of the LEDs is done with Bias-T circuit, modulated with Phase Shift Modulation (PSK) driving each luminary at different carrier frequencies (2 MHz; 2.5 MHz; 3 MHz). The reception of the signal is accomplished using a PD, a TIA and a low noise amplifier. The technique used for positioning is trilateration to determine the intersection of distances between the transmitters and receivers. The transmitters used are constituted by an array of 2×2 LEDs without any additional information. The results on the project shows an average error for estimated positions of approximately 2.4 cm using adjustment process by normalizing method. Work developed by [34] is about fusion of VLP and inertial navigation on particle filter using Pedestrian Dead Reckoning (PDR) that automates self-positioning based on previous known position, the distance travelled and direction of travel. Particle filter is a technique that implements a recursive Bayesian filter using the Sequential Monte-Carlo method. They use two different modules to estimate position, one collects VLC data process it using RSS algorithm, the other collects inertial measures and uses PDR algorithm. The information is sent to a host computer that compute the fusion algorithm based on particle filter to estimate position. The number of LED light sources is seven, without adding any information about the transmitters. Authors report that the RSS positioning algorithm requires the detection of at least three acpled. In conclusion they reported a positioning system error of 41 cm and 14 cm for maximum and average values respectively on a experimental set-up with the dimensions $2.5 \times 2.84 \times 2.5$ meters. The proposed system by [35] requires multiple LED light source driving a sinusoidal wave at a specific frequency for each transmitter, making the signals distinguishable at the receiver to process and determine its metrics location. The receiver is constructed with PDs to receive the visible light signal and an analog-to-digital converter to convert the signals for further processing in a connected computer. Since they use fingerprinting to estimate positioning, the received power is used as a metric. The set-up size for experimental results is $1.8m \times 1.2m \times 1.0m$ and the total number of acled luminaries is six. The LED panels comprises of nine DomiLED InGaN White LEDs connected in parallel. The obtained results from the localization experiment in free space have an average error of approximately 14.84 cm for positions stepped 10 cm apart from each other.

Table 2.4 report experimental systems for IPS using ISs. The work developed by [37], make use of two Logitech 310 cameras with lenses separated apart by 10 cm. The system is able to receive LED three-dimensional positions from VLC and estimates receiver position as well as azimuth. The proposed system makes use of two adjacent cameras and two LEDs in a experimental area of $0.6m \times 0.6m \times 2.6m$. The luminaries by an array of 5×5 white LEDs. The modulation technique used to broadcast light sources position is OOK using a FPGA. The results obtained for positioning estimation error along the x axis, y axis and z axis from a camera resolution of 1280×960 pixels are 2.26 cm, 5.51 cm, 1.46 cm respectively. For a lower image resolution of 160×120 the positioning error is higher, 5.4 cm, 6.05 cm

and 133 cm for x, y and z axes respectively. They report that the errors in finding the centers of the luminaries images, measurements errors and quantization errors increase the indoor positioning experimental errors. The work developed by [38] use a image sensor of a commercial smart phone Nokia Lumia 1020 with a camera resolution of 7712×5360 pixels to provide positioning using LED beacons. For transmitters they modified commercial LED luminaries by intercepting the wire and wiring it to a control unit, that controls a single FET switch, thus, transmitting its unique ID over VLC with signal frequencies from 2kHz to 4kHz and employing Manchester line coding to maintain light average value stable. The picture provided by the phone using RS is then uploaded to a remote processing unit that estimates positioning using AoA localization algorithm. The area dimension of the experimental set-up is $0.71m \times 0.74m \times 2.46m$ and the number of LEDs used is five. An IS-based VLP system is proposed by [39] by improving the positioning algorithm that speeds up the positioning process and enhances robustness. The experimental set-up consists in three Cool White (5650K) LUXEON rebel ES 40mm LED lamps and a commercial smartphone camera, Nokia Lumia 1020 with a resolution of 7712×4352 pixels. To each luminary, a unique ID related to its location is assigned and transmitted repeatedly through VLC, modulated in light. The camera, using RS, allows signal demodulation of the ID of the different luminaries. For image processing and position estimation, a computer is used. The positioning grid is composed by 35 grid points and the localization algorithm is able to perform results in milliseconds at every test point. The transmitted packet is composed by eleven bits, seven of them are preamble and the remaining 4 are used for LED identification. The experimental results have been conducted in the same area, but at two different heights, 120 cm and 160 cm. The practical experiments report an average 3-D positioning average error of 6 cm and 8.5 cm, for heights of 120 cm and 160 cm respectively. The last entry of the table related to ISs reported the development of a VLP system based on sensor fusion technique that enhances positioning accuracy by fusing the data collected by the IS of a smartphone IS and its embedded motion sensors (accelerometer and gyroscope). The proposed indoor VLP system includes three 10 W Cool White (5650K) LUXEON Rebel ES 40mm LED lamp that broadcasts individually their unique ID through VLC. The receiver is a Nokia 1020 smartphone that uses the rear camera to capture images and decode the LED unique ID using the RS technique. Together with motion sensors, a fusion system is used to estimate position. For image processing errors, the experiment is conducted in 64 different points at a distance of 1.8 m. The authors reported a novel method that reduces the error from 9.7 cm to 4.4 cm representing an improvement of 44 when compared to single camera positioning algorithm. Nevertheless, they report that the error of the image centroids coordinates is affected not only by the characteristics of the image sensor (IS pixel resolution, size and focal length), but also by the experimental settings, LED lamp power, LED HPA and distance between transmitters and receivers.

Despite the fact that theres is already a lot of research associated to VLP, the fact that Tables 2.3 and 2.4 have a considerable low number of articles, the main objective is to refer the lack of information in almost all of the works, relatively to the luminaries used and the set-up information. Most of papers about VLP describes the use of the existing lighting

infrastructure, but a reasonable low number of works implements VLP using the existing one. Some of the works do not report any specification relative to the luminaries.

2.5 Final remarks

This chapter has described the key concepts studied for the development of a test platform for VLP. The evolution of LED lighting is a undeniable phenomena specially because of its power efficiency (lm/W). The actual systems are able to support dimming and color temperature variations for any task required. For the implementation of VLC using LEDs, there are some limitations such as the bandwidth of high power white LEDs and the design of electrical current drivers that are able to regulate a steady value current and perform communication at the same time. IPS are being widely researched to improve indoor location and navigation systems, specially because of its value in market and the attenuation of GPS signals in indoor environments. An alternative to the use of RF signals for IPS is VLP. It makes use of the existent lighting fixtures to estimate position of receivers. The application of VLC allows luminaries to transmit their unique ID, hence, the receiver is able to access the real position of the light fixtures and using positioning algorithms estimate its position relative to the luminaries in the FOV. The devices that allow the reception of light signals are photodetectors, usually PDs and IS.

The related SOTA reported that despite the fact of research in the field suggests the implementation of VLP using existing lighting fixtures, the majority of the VLP experimental set-ups use temporary and small infrastructures with small luminaries, designed by the authors using commercial LEDs, instead of off-the-shelf commercial ones. If VLP is meant to be commercialized, the research needs to approximate the experimental platforms to real world conditions.

CHAPTER 3

Lighting project

This chapter focus on describing the demands of European lighting standards for office or laboratory environments and its importance. It is also described the lighting properties of the chosen luminaries, as well as the results of a lighting system using a professional light planning software. It is also described the adaptation of a dark room to accommodate the planned lighting infrastructure.

3.1 Lighting considerations

Lighting is a very delicate matter and it has common standards for light planning workplaces. Since 2003, the European Union member countries have established the European Lighting Standard EN-12464-1. The document is mandatory for lighting engineering, and the lighting projects must follow the rules defined in the standard in order to be in conformity with EU regulation. The main focus of the document is to create ideal work conditions to perform visual tasks efficiently and accurately. The standard specifies requirements for lighting systems for most indoor work places and their associated areas in terms of quantify and quantity of illumination.

A balanced light distribution is considered an influence in people tasks visibility as it improves visual acuity, contrast sensitivity and efficiency of the ocular functions. However, the rule "the more, the better" should not be the objective of the lighting engineer because there are several constraints that influence visual comfort when illuminance exceeds a certain limit causing increasing glare, contrasts which will cause fatigue, or when it falls beyond a minimum value it will provide a non-stimulating working environment. Useful ranges of reflectance for the major interior surfaces are shown in Table 3.1. The apparent color (chromaticity) of the light emitted is quantified by its CCT, described in Table 3.2.

Type of surface	Normalized value
Ceiling	0.6 to 0.9
Walls	0.3 to 0.8
Working planes	0.2 to 0.6
Floor	0.1 to 0.5

Table 3.1: Reflectance of interior surfaces

Color appearance	Correlated color temperature (K)
Warm	$< 3330\,\mathrm{K}$
Intermediate	$3300\,\mathrm{K}$ to $5300\,\mathrm{K}$
Cool	$> 5300\,\mathrm{K}$

Table 3.2: Correlated Color Temperature

The document also refers that a value inferior to 80 of CRI of an artificial light source should not be used in interiors where people work or stay for longer periods. The lighting requirements for different rooms and activities relative to the working area, are documented from Table 5.1 to 5.8 of European Lighting Standard EN-12464-1, which includes minimum acceptable levels of average illuminance and CRI.

3.2 Description of space and objectives

The ICS laboratory to be equipped with a VLP test platform is a dark room with dimensions of $6.35m \times 4.75m \times 3.00m$ (see Figure 3.1). This room uses four gas-discharge (see Figure 3.2) lighting fixtures that will be replaced with off-the-shelf commercial LED-based luminaries

Figure 3.1: ICS dark room with dimensions of $6.35m \times 4.75m \times 3.00m$

Figure 3.2: Dark room existent luminaries

that are able to perform VLC. For the purpose of designing a lighting project that covers the European Lighting Standard EN-12464-1 and it requirements of an office room to be adapted in the experimental room, the software DIALux Evo 8.1 version 5.8.1.41626 was used. The lighting project should propose an average illuminance superior to 500 lx as stated in reference 6.2.9 for practical rooms and laboratories and a uniformity of light greater or equal than 0.7 for tasks area as stated in section 4.3.2 in EN-12464-1.

3.3 Lighting project

For the design of the architecture of the lighting project, the first aspect to be defined is the chose of the lamps. Commercial LED-based luminaries have several shapes and rated power. For the purpose of VLP receivers have limited FOV, hence, it was defined that having a large number of lighting fixtures with a regular shape (specially important for IS) would be the best implementation considered. If an experiment requests less lighting fixtures but widely separated, the system should be able to turn off the nearest ones.

The selected luminaries for the project are the DLA G2 model, manufactured by Tridonic. These lamps have a CRI equal to 80. The selection of these commercial off-the-shelf luminaries,

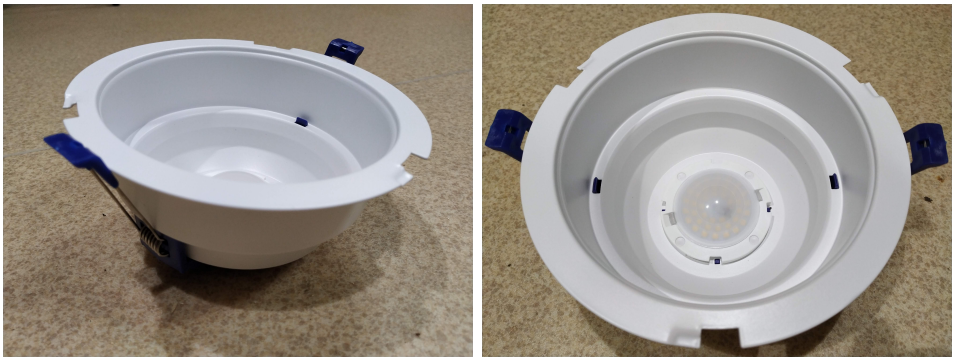

Figure 3.3: Tridonic DLA G2 840 150 mm luminary.

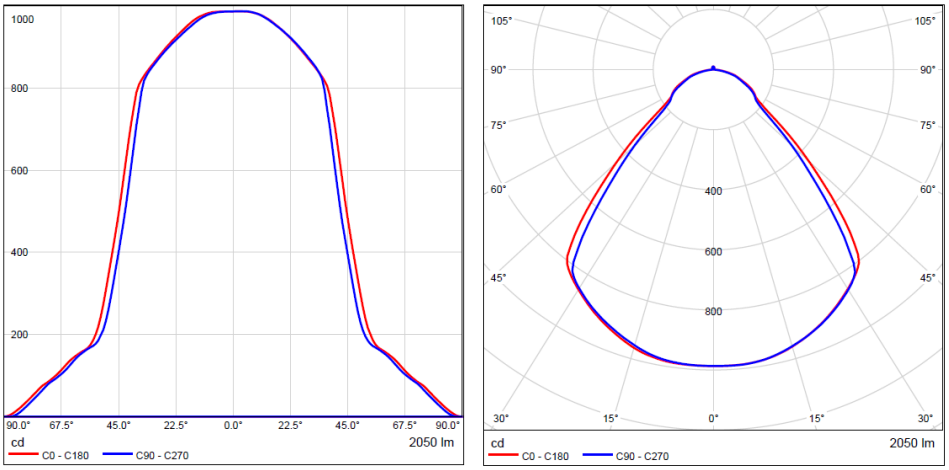

Figure 3.4: Tridonic DLA G2 840 150 mm radiation pattern.

was based on the fact that this specific model has embedded the LEDs with a diffuser in the case. Tridonic offers a three diameters for this specific model, 100 mm, 150 mm and 200 mm, with the possibility of using reflectors that modify the beam angle of the luminary. The radiation pattern of the DLA G2 840 150 mm can be observed in Figure 3.4 where the red and blue lines represent the radiation patterns for two perpendicular planes, hence, the HPA of this lamp is about 43°.

Last, but yet important factor is that these lamps have an easy installation system with springs that forces them to be centered within a hole. The manufacturer offers the possibility to acquire separately the DC driver, the lamp and the reflectors. For the purpose of the work, only the lamps were acquired. Table 3.3 reports the possible configurations for this specific model.

The lighting project uses the Tridonic luminary model 840 that denotes a lamp with a CCT of 4000 K with no reflector and a maximum luminous flux of 2050 lm that accomplishes a luminous efficacy of 20.2 lm/W. The reflection factors considered for the project are 64% for ceiling, 38% for walls and 31% for the floor.

Tridonic provides the photometric file with extension ".IES", that stands for Illumination Engineering Society, compatible with DIAlux software. For a room with the dimensions of the laboratory referred before, the luminaries are mounted in the ceiling at a distance of

Combination DLA G2 150 mm	CCT (K)	Luminous flux (lm)	Input power (W)	Luminous efficacy (lm/W)	Beam angle (°)
840 no reflector	4000	1020	10.1	101	90
840 no reflector	4000	2050	20.2	101	90
840 60° reflector	4000	1120	10.1	111	60
840 60° reflector	4000	2210	20.2	109	60
840 90° reflector	4000	1120	10.1	111	90
840 90° reflector	4000	2210	20.2	109	90

Table 3.3: DLA G2 150mm possible combinations

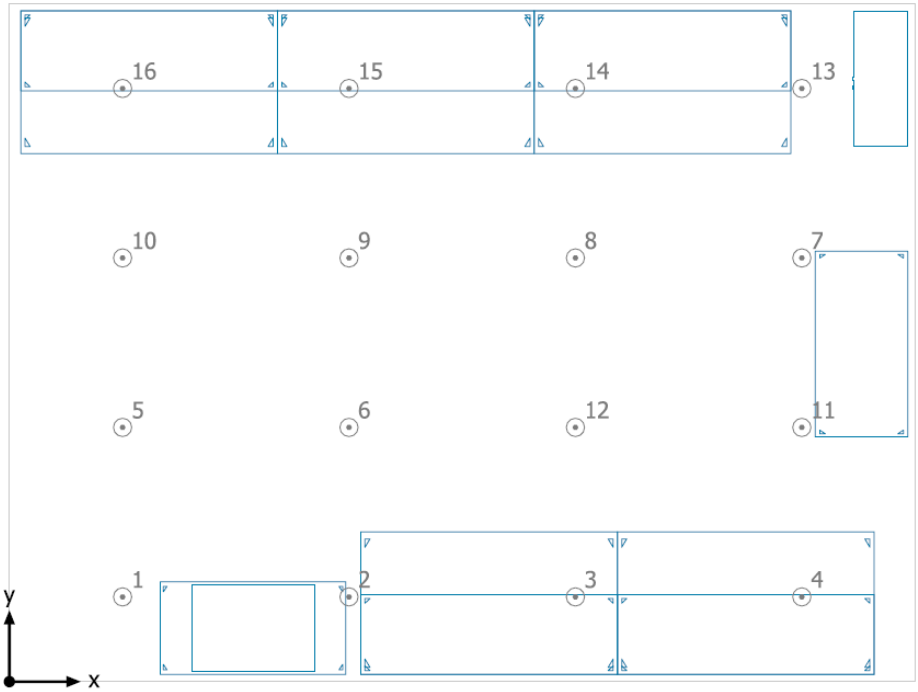

Figure 3.5: Position of luminaries obtained in DIALux for the ICS laboratory.

2.7 m from the floor in a wood support. In order to achieve the necessary requirements for lighting purposes, the necessary number of Tridonic luminaries is sixteen (16) positioned in rectangular shapes (see Figure 3.5). The deviation dx and dy between lamps are 1.587 m and 1.187 m, respectively.

The task areas considered where the conditions of illuminance have a major importance are the laboratory workbenches and the floor (see Figure 3.6).

The results for the average illuminance and the uniformity of light for the considered areas at full and half power are verified in Table 3.4 and 3.5. The dimming of light to half of the rated power, has a direct impact in the average illuminance reducing it to half.

A 3-D simulation view of the laboratory can be observed in Figure 3.7 that includes the workbenches, the luminaries and the wood support.

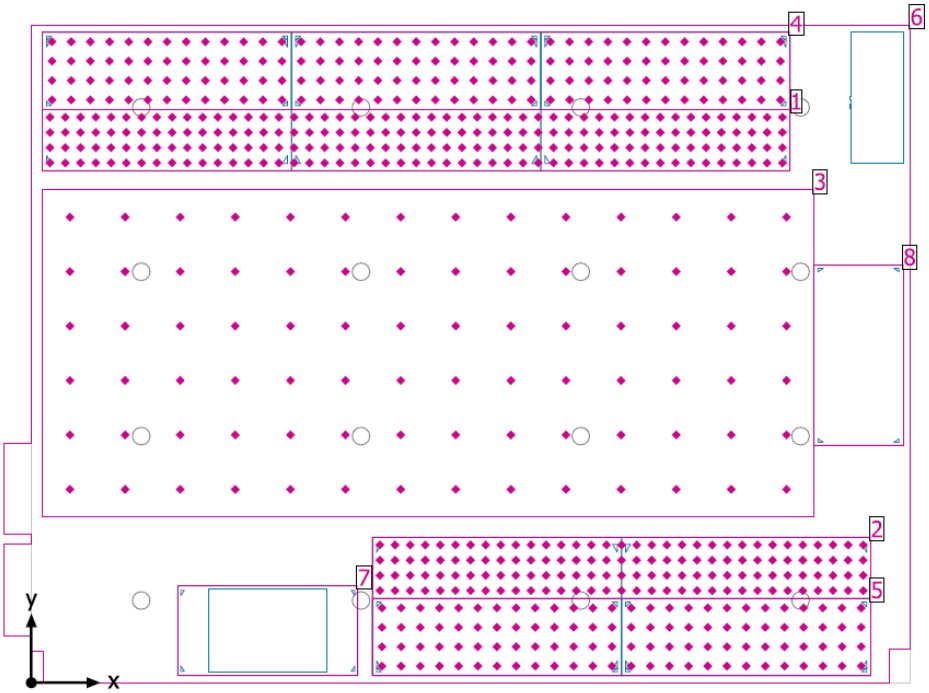

Figure 3.6: Regions of interest for DIALux illuminance calculation.

Figure 3.7: 3-D simulation view of the laboratory with the selected luminaries.

Area number	Height m	Average Illuminance	Uniformity
1	0.82 m	739 lx	0.63
2	0.82 m	748 lx	0.72
3	0 m	739 lx	0.71
4	1.25 m	687 lx	0.61
5	1.25 m	698 lx	0.68

Table 3.4: Average illuminance and uniformity of light obtained in DIALux using 100% of luminous flux.

Area number	Height m	Average Illuminance	Uniformity
1	0.82 m	371 lx	0.63
2	0.82 m	374 lx	0.71
3	0 m	369 lx	0.71
4	1.25 m	344 lx	0.61
5	1.25 m	349 lx	0.68

Table 3.5: Average illuminance and uniformity of light obtained in DIALux using 50% of luminous flux.

3.4 Structure adaptation

The structure that supports the luminaries, is an aggregation of wood panel with dimensions $2.5m \times 1.25m \times 1.2cm$. Since the distance between the floor and the ceiling of the dark room is about 3 m, the distance from floor to the wood boards is kept as in the simulation, 2.7 m. A metal framing system anchored in the concrete ceiling is used to support the weight of the boards to provide safety for users and for long-standing years (see Figure 3.8). The AC switches used for the old luminaries are used to power the newer ones.

Figure 3.8: Metal frame that supports the wood panels.

To assembly the luminaries in the wood support, circular holes with the diameter of 145 mm have been sawn as suggested in the datasheet. The final aspect of the support with

the assembled luminaries can be observed in Figure 3.9.

Figure 3.9: Final result of half room set-up.

3.5 Illumination features

The installation of sixteen luminaries provide the laboratory with a lighting infrastructure suitable to the tasks performed. Since we do not use the compatible current driver from Tridonic, a driver needs to be developed and deployed so the room can be used for other purposes than for VLP. For the function of steady illumination, each driver needs to deliver a constant current flow to the connected luminary. An extra feature that the driver must offer is lighting dimming, using constant or pulsed current.

When VLC is used, the level of illumination will be degraded. Therefore, if an OOK modulation with Manchester code line is used, the optical power of each luminary will suffer a loss of 50%. The use of VPPM modulation scheme to transmit data is meant to improve this loss of power.

CHAPTER 4

Hardware development

The development of drivers for LED-based luminaries for transmission of data through the optical channel is essential for the implementation of a VLP infrastructure that uses VLC. This chapter focus the development of a driver for steady and pulsed electrical current. A memorable quote can also be used.

Most of the related works in VLP make use of small LEDs that emits light with low current supply. The work developed in this section evidence the constraints that should be taken into care to design a driver for commercial off-the-shelf luminaries. Nevertheless, it is important to refer that lighting is nowadays a constant need, by those terms, it is extremely necessary to offer a pleasant environment where some tasks are to be performed. For the purpose of transmitting information using light, a driver that controls the current of the luminary is meant to perform quick variations in light intensity without the perception of the human eye and keep an average value of the illuminance in the room steady. For the purpose of estimating receiver position the luminaries should transmit their unique ID as beams, with the support of VLCs, where the information will directly affect the VLP algorithms.

The proposed driver, should offer the possibility of light dimming by imposing a steady or pulsed current through the LED-based luminaries. This feature offers the possibility of adjusting the brightness of the room to levels required by the users even and maintain it steady even when VLP is being performed.

4.1 System description

The test-bed system proposed to perform positioning experiments uses commercial off-the-shelf luminaries to provide a real-world environment. To create a robust system, several parameters should be possible to adjust such as, the average illuminance of the room, the modulation technique used to transmit the lamps' IDs, the frequency of the modulation, as well as the possibility to turn off selected luminaries. The uC that controls the several functionalities of the individual lamps, implemented in the developed driver, is an ATmega328p chip embedded in a popular open-source electronic platform – The Arduino. This platform is fully equipped with the basic needs for fast embedded systems implementation. The driver remote control is established using an nRF24L01+ transceiver that is able to establish RF communications when applied in a piconet. The driver is powered using the existing 230 VAC from the electrical grid which is converted into DC to feed the luminary and the remaining electronics. An illustration of the overall system can be observed in the Figure 4.1.

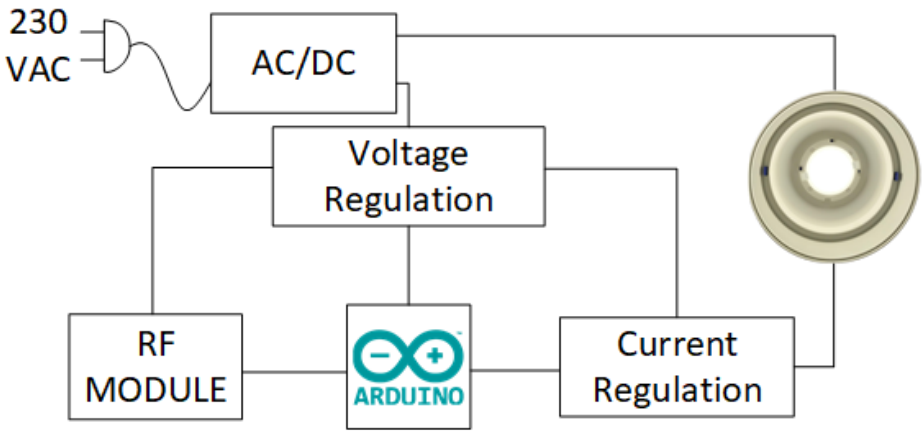

Figure 4.1: Driver system overview.

4.2 Luminary driver description

4.2.1 AC-DC converter

Since this device is powered using the 230 VAC single-phase electrical grid, an AC-DC converter should be used to convert Alternating Current (AC) signal to Direct Current (DC). The developed circuit uses a transformer, a passive electrical device that uses magnet induction to transfer electrical power from one circuit to other, with galvanic isolation, to achieve the down-conversion of the electrical grid voltage. Figure 4.2 illustrates an ideal transformer that transfers power from the primary winding to secondary. The literature formalize an ideal transformer as,

$$\frac{N_1}{N_2} = \frac{E_1}{E_2} = \frac{I_2}{I_1} \tag{4.1}$$

where the ratio between the turns of the primary coil, N_1, and the secondary, N_2, establishes the ratio between the electromotive force of the windings.

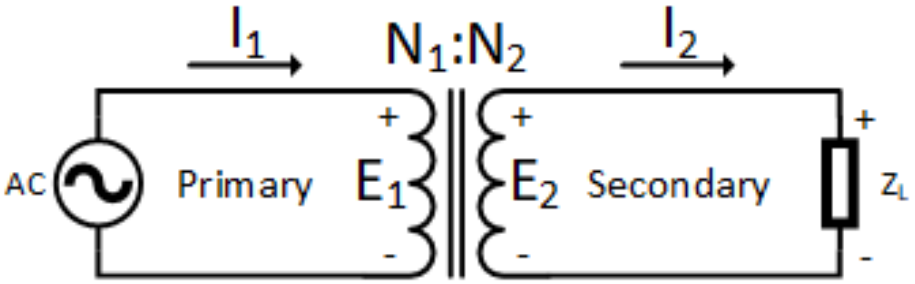

Figure 4.2: Ideal Transformer.

Since the signal in the secondary winding is still a sinusoidal wave, a rectification stage is required to transform AC to DC. This stage can be a half-wave or full-wave configuration depending on the configuration of the diodes rectifiers. A final filtering stage is usually used to improve DC ripple. In accordance with Portuguese Norm NP EN 50160, the effective voltage is 230 V with a maximum tolerance of +10% and -15%.

The AC-DC converter designed makes use of a transformer with center tap as a voltage step-down (see Figure 4.3). This transformer supplies current for two separated conversion stages so it is possible to provide two different DC voltages. The first one uses full winding of the secondary and uses a bridge rectifier, a circuit with four diodes commonly used in rectification stages, and a filtering capacitor $C1$. The second stage only uses half of the secondary winding at each cycle and is composed by one rectifier diode, $D2$, connected to the center tap of the transformer and a filtering capacitor $C2$. The output peak voltages for this circuit can be defined as,

$$\begin{cases} V_{H\,peak}^{+} = (E_{2rms} \times \sqrt{2}) - 2 \times V_{\gamma} \\ V_{L\,peak}^{+} = \left(\frac{E_{2rms} \times \sqrt{2}}{2}\right) - 2 \times V_{\gamma} \end{cases} \tag{4.2}$$

where, E_{2rms} is the root mean square of the voltage induced in the secondary winding of the transformer, and V_{γ} is the forward voltage of the rectification diodes.

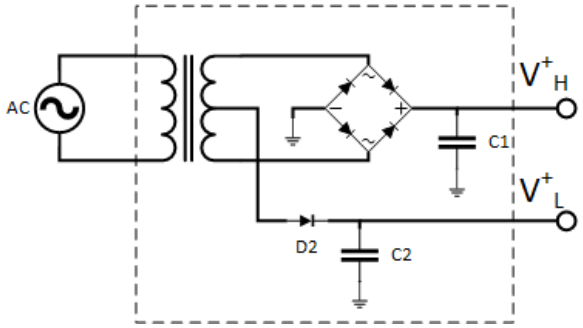

Figure 4.3: AC-DC converter

The LED-based luminary chosen for this project has a voltage drop of 34 V at a rated current of 530 mA providing a luminous flux of 2050 lm. The transformer in the driver circuit

should provide the necessary power to the system having in consideration the tolerance in the electrical grid. The ripple, Δ, in the filtering stage is also a factor to be considered, as its value in a full-wave rectifier is approximately given by,

$$\Delta = \frac{I_{avg}}{2 \times f \times C} \tag{4.3}$$

where I_{avg} is the average current supplied, f is the frequency of the electrical signal, and C is the capacitor used for filtering. The transformer used for this project is a Hammond Manufacturing Power Transformer 183K36 with center tap 115/230V 56 V A. This device is able to provide in the secondary 36 V rms and a current of 1.56 A, satisfying the requirements for the project. The voltage peaks after the rectification stages are given by equation 4.2 where the rectification diodes forward voltage, V_γ, is considered as 1 V for project purposes,

$$\begin{cases} V^+_{H\,peak} = (36 \times \sqrt{2}) - 2 = 48.9V \\ \\ V^+_{L\,peak} = \left(\frac{36 \times \sqrt{2}}{2}\right) - 2 = 23.5V \end{cases}$$

and considering that the voltage in the primary winding is within the legal tolerances , the peak voltages are given by,

$$\begin{cases} V^+_{H\,peak} = 54.0V \\ \\ V^+_{L\,peak} = 26.0V \end{cases} \qquad \begin{cases} V^+_{H\,peak} = 41.3V \\ \\ V^+_{L\,peak} = 19.6V \end{cases}$$

when $E_{1rms} = 230 + 10\%$ when $E_{1rms} = 230 - 15\%$

providing enough slack to power the luminary.

The value of the capacitors is calculated using Equation 4.3, where the frequency f for a full-wave rectifier is the value of the frequency of the electrical grid (50 Hz), I_{avg} is the average current provided by the capacitor when it is not charging, and Δ is the difference between the maximum and the minimum values of the voltage,

$$C1 = \frac{0.530}{2 \times 50 \times 2} = 2.65\,\text{mF} \qquad C2 = \frac{0.150}{2 \times 50 \times 4} = 375\,\mu\text{F}$$

Capacitance of $C1$ Capacitance of $C2$

an average value of the current provided by $C1$ of 530 mA and a ripple of 2 V were considered for calculation of its capacitance. For the capacitor $C2$, an average current of 150 mA and a ripple of 4 V were used.

The AC-DC converter projected should provide two separated non regulated voltages, in the worst conditions ($E_{1rms} = 230 - 15\%$), $V^+_H = 41.2 \pm 1\text{V}$ and $V^+_L = 17.2 \pm 2\text{V}$.

4.2.2 Luminaries driver controller

LED-based luminaries light output are usually controlled with a steady electrical current. To keep a constant luminous flux, the regulation of the current that passes through the LEDs

should provide a low current ripple so human eye cannot percept light intensity variation. The developed driver is a low-side linear current sink that regulates a steady constant current according to the desired values as illustrated in Figure 4.4.

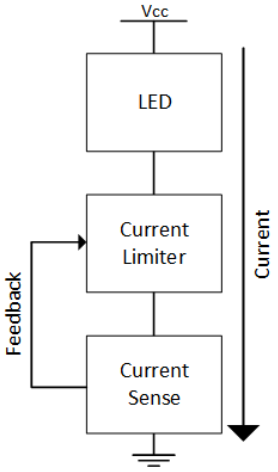

Figure 4.4: Current regulator diagram

The selected circuit to perform the regulation to the current includes an Op-Amp, a MOSFET and a sensing resistor as illustrated in Figure 4.5. The circuit implements a negative feedback configuration that forces the voltage drop in the sensing resistor, V_{R_s}, to be equal to the reference voltage, V_{ref}, by controlling the voltage applied to the gate of a n-channel enhancement MOSFET, $Q1$ independently of the operating region, linear or saturation. One of the disadvantages of using this circuit to regulate current, is that it has low efficiency when the supply voltage is higher than the forward voltage of the LED, introducing heating issues. The use of a heat sinker may be required, which is bulky and moderately expensive.

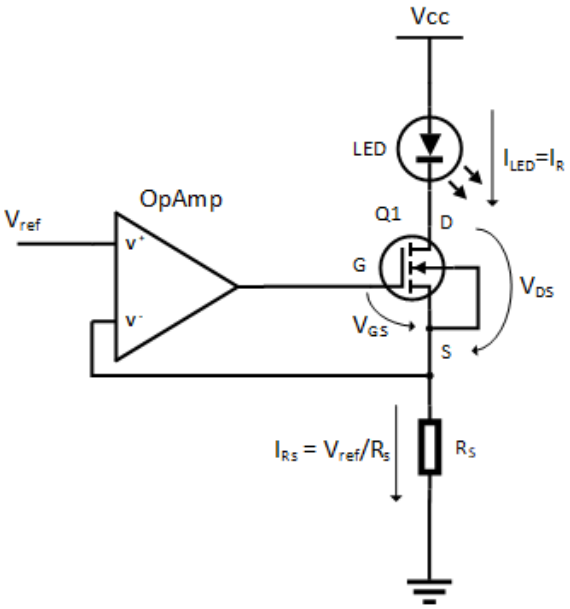

Figure 4.5: Conceptual linear current regulator

Since the MOSFET is a voltage controlled device, the current that passes through the drain-source channel is dependent of the voltage drop from Gate to Source (V_{GS}), thus, this circuit implements a voltage-current converter. To turn-on this device, a sufficient positive V_{GS} should be applied, the minimum V_{GS} is usually indicated in the datasheet of the manufacturer. This MOSFET is applied in a common-drain configuration, which means the signal from gate to source is in phase, and has a unity gain. In order to regulate the current that passes through the LED, the voltage output of the Op-Amp needs to be higher than V_{ref}, hence, if V_{ref} is expected to appear in the source of the MOSFET, the output of the Op-Amp should be equal to $V_{ref} + V_{GS}$. The MOSFET is a device with high input impedance, hence, the current through the LED and the sensing resistor is the same that passes through the MOSFET. Since it handles a considerable amount of power, it should be considered an n-channel power-MOSFET. They are specially meant to handle high levels of power with high switching speed. It is important to keep the MOSFET in the Safe Operating Area (SOA) in order to avoid destruction of the device. To estimate the power dissipated in the MOSFET, the luminary, needs to be characterized in terms of current in function of the forward voltage applied. Figure 4.6 represents the variation of forward current as a function of forward voltage of the luminary chosen with a exponential fitting model, based in Equation 2.10, of the curve given by,

$$I(V_{LED}) = 2.0738 \times 10^{-10} \left(e^{0.8386 \times V_{LED}} - 1\right)$$

which represents a reasonable approximation to the experimental V-I curve with a $r^2 = 0.9970$.

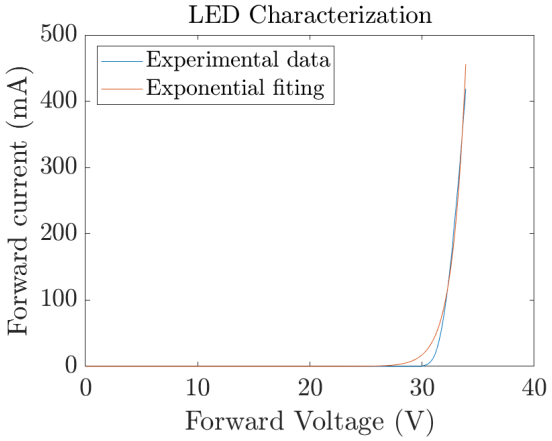

Figure 4.6: Characterization of the Tridonic DLA G2 luminary

For convenience, a third order polynomial fit was considered in the region where the LED is ON, forward current is equal or superior to 1 mA, observable in Figure 4.7, given by,

$$I(V_{LED}) = -1.5343 \times {V_{LED}}^3 + 184.37 \times {V_{LED}}^2 - 6972.6 \times V_{LED} + 84691 \tag{4.4}$$

providing a better approximation to the characteristic curve of the luminary with a $r^2 = 0.9998$.

The average dissipated power by the MOSFET is equal to

$$P_{avg} = V_{rms} \times I_{rms} \tag{4.5}$$

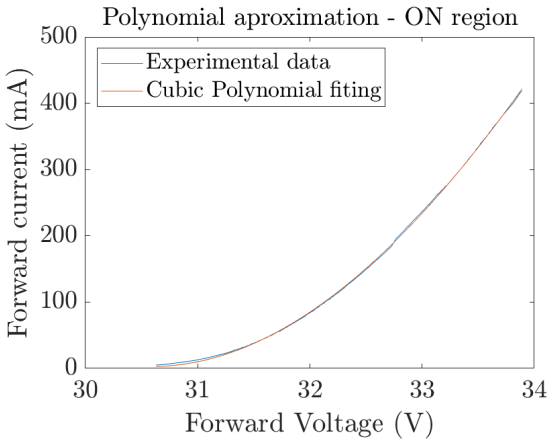

Figure 4.7: Cubic polynomial fit for ON region of the Tridonic DLA G2 luminary

hence, for this circuit, it will be highly dependent of the Vcc rated value and the forward voltage of the LED luminary. According to Kirchhoff's law, we can write the voltage closed loop of this circuit as,

$$Vcc - V_{LED} - V_{DS} - V_{R_s} = 0$$

where Vcc is the supply voltage and V_{LED}, V_{DS}, V_{R_s} are the voltage drops in the luminary, the MOSFET and the sensing resistor, R_s, respectively. It is easy to deduce that the voltage drop between the drain and the source of the MOSFET as a function of the current I_{R_s} is:

$$V_{DS}(I_{R_s}) = Vcc - V_{LED}(I_{R_s}) - R_s \times I_{R_s} \tag{4.6}$$

For a constant current, $I = I_{rms} = I_{avg}$, hence, the average dissipated power in the MOSFET, considering Vcc constant, can be calculated using Equation 4.5. Considering the electrical characteristics of the luminary (34 V at a forward current of 530 mA), a sensing resistor of 2.5 Ω, and a voltage supply of 48.9 V, the average dissipated power in the MOSFET is,

$$P_{avg} = (48.9 - 34 - 2.5 \times 0.530) \times 0.530 = 7.19\,\text{W}$$

The selected MOSFET for the purpose of current regulation is a n-channel IRF510PBF from Vishay, its electrical characteristics can be observable in Table 4.1. It is a power MOSFET with compatible features for the current regulation of the LED.

The junction temperature will increase as a function of the dissipated average power in the MOSFET, hence, the junction temperature, T_J, without the use of a heatsink, is defined as,

$$T_J = T_A + P_{avg} \times R_{JA} \tag{4.7}$$

where, T_A is the ambient temperature, R_{JA} denotes the junction-ambient thermal resistance. If a heatsink is applied to the case of the MOSFET, the junction temperature is described as,

$$T_J = T_A + P_{avg} \times (R_{JC} + R_{CS} + R_{SA}) \tag{4.8}$$

where R_{JC}, R_{CS} and R_{SA} denotes the junction-case, the case-heatsink, and the heatsink-ambient thermal resistances, respectively. Without heatsink applied on the case of the

Characteristic	Value
Package	TO-220 through hole
V_{ds} Breakdown voltage	100 V
Continuous Drain current I_D	5.6 A
$R_{ds}on$ for V_{gs}=10 volt	540 mΩ
V_{gs} Threshold voltage	2 V
Maximum power dissipation	43 W
Maximum junction temperature	175 °C
Maximum junction-ambient thermal resistance	62 °C/W
Maximum junction-case thermal resistance	3.5 °C/W

Table 4.1: Characteristics of IRF510PBF n-channel MOSFET

MOSFET, a T_J of 654 °C is achieved when Vcc is at its peak value, considering the +10% tolerance of the electrical grid (230 + 10%) for a current of 530 mA and a ambient temperature of 40 °C, which will lead to the destruction of the MOSFET, hence, an heatsink applied in the device is required. The thermal resistance of the heatsink should be,

$$\begin{aligned} R_{SA} &\leq \frac{T_J - T_A}{P_{avg}} - R_{JC} - R_{CS} \\ &\leq \frac{175 - 40}{9.90} - 3.5 - 0.5 \\ &\leq 9.64\,^{\circ}\text{C/W} \end{aligned}$$

where, R_{CS} has a typical value of 0.5 °C/W. The elected heatsink is a FA-T220-38E from manufacturer Ohmite, its thermal resistance R_{CA} is 3.8 °C/W without the use of forced air flow.

A thermal analysis using Equations 4.4, 4.6 and 4.8 is performed to evaluate the junction temperature of the MOSFET in the conditions where Vcc is considered stable and equal to $V^{+}_{H\,peak} = 54.0V$. In Figure 4.8, it is verified the difference of the junction temperature with and without heatsink applied to the MOSFET. If a pulsed current, between zero and $I_{máx}$, is applied to control dimming of the LED, eg: PWM, the rms value of the current is defined as,

$$I_{rms} = \sqrt{\frac{1}{T}\int_0^{\delta T} I_{máx}^2 dt} = I_{máx}\sqrt{\delta}$$

where, δ represents the duty cycle of the pulsed current ($0 \leq \delta \leq 1$) and T is the period of the PWM signal. By those terms, the dissipated average power in the MOSFET will be always inferior to the power dissipated in continuous current mode.

The use of a power MOSFET has some limitations in what regards to the maximum frequency that can be applied to a pulsed current, due to the high input capacity in the gate. The output resistance of the Op-Amp and the MOSFET gate capacitance, creates a pole in frequency which can lead the output of the Op-Amp, that follows a negative feedback configuration, to oscillate. This oscillation will affect also the current through the LEDs that will also oscillate. A feedback compensation is meant to improve the response of the feedback control loop, therefore, it is necessary because in transient region, the Op-Amp

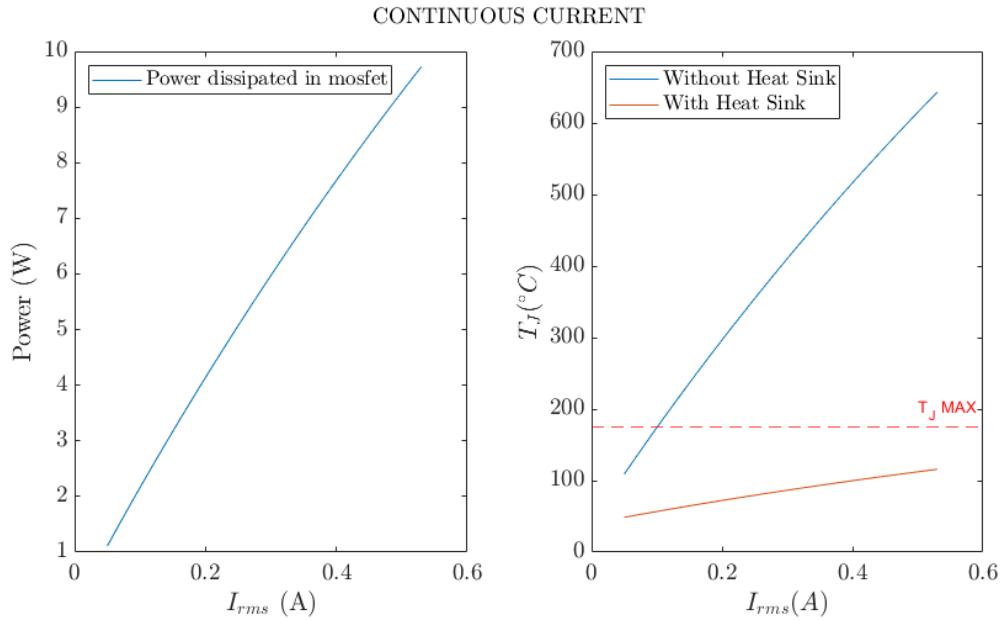

Figure 4.8: Junction temperature of the MOSFET as a function of a continuous current.

is in open-loop with high gain, hence, to reduce the oscillating effect at the output of the Op-Amp the compensation is meant to reduce the possible overshoot in the current that originates a burnout effect on the LEDs. The circuit illustrated in Figure 4.5 is improved with compensation network to reduce the oscillation at the Op-Amp output. The modification is observable in Figure 4.9. The addition of R_2 as an isolation resistor is desirable for steady state regulation, where the addition of R_3 and C_1 improves transient state region. An easy interpretation of the circuit can be assumed as if in the non-inverting input of the Op-Amp, V^+, a step signal is applied, the current in the sensing resistor will be smoothed, reducing the overshoot in the current through the LEDs. The software Tina-TI, a SPICE-based analog simulation program, was used to perform the tuning of the feedback compensation for continuous and pulsed current modes. The value of the components for implementation of the circuit in Figure 4.9 are listed in Table 4.2.

Component	Value
$U1$	TI THS4211D
$Q1$	IRF510PBF
R_s	2.5 Ω
R_2	25.5 Ω
R_3	10 Ω
R_4	470 Ω
C_1	50 pF
LED	Tridonic DLA G2 150 mm

Table 4.2: Selected components to implement circuit 4.9

The selected Op-Amp, THS4211 from Texas Instruments, is a ultra-low distortion, high bandwidth (1 GHz), high slew rate (970 V/µs) device that is able to drive a maximum output

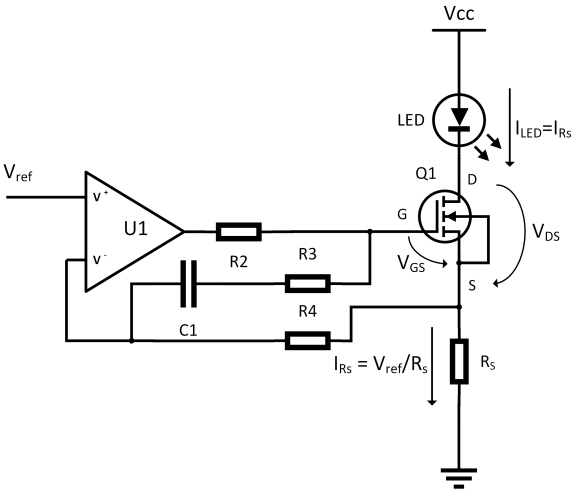

Figure 4.9: Linear current regulator with compensation network

current of 170 mA. This characteristics make the device highly compatible to the regulation circuit since it is driving a power-MOSFET with high input capacitance.

The regulation circuit will force the voltage across R_s to be equal to the non-inverting input of the Op-Amp $U1$, V_{ref}. Considering a control signal generated by a uC, a digital-analog converter stage is required to convert the pinout voltage of the I/O port to the desired reference voltage. Figure 4.10 shows the simplified circuit for signal conditioning for regulation stage, V_{ref}. This stage is composed by a shunt voltage regulator, Z_1, which provides a regulated 2.5 V, a potentiometer, P_1, that enables the adjustment of the voltage at the intermediate pin, an Op-Amp, $U2$, configured as voltage follower, a MOSFET, $Q2$, configured as common-source for pulsed signals and an inverting buffer to drive the MOSFET as well as to maintain the polarity between the signal generated from the uC and V_{ref}. The Table 4.3 points out the selected components for the digital-analog converter stage.

Component	Value
$U2$	TI THS4221D
$U3$	MAX5048CAUT+T
$Q2$	PMGD290XN,115
$Z1$	TL431AIDBZR,215
$P1$	AD5160BRJZ5-RL7
R_5	100 Ω
R_6	470 Ω

Table 4.3: Selected components to implement circuit 4.10

The shunt voltage regulator TL431AIDBZR,215 is a programmable shunt voltage regulator that has an output voltage of 2.5 V when the reference pin is connected to the cathode. This is a temperature compensated device, with 1 % of voltage tolerance. The cathode-anode current should be at least 1 mA and the minimum reference current has a typical value of 0.4 µA when $V_{KA} = V_{ref}$. Resistor R_6 is used to limit the maximum current supplied to the shunt voltage regulator. A digital potentiometer AD5160BRJZ5-RL7, is a device with

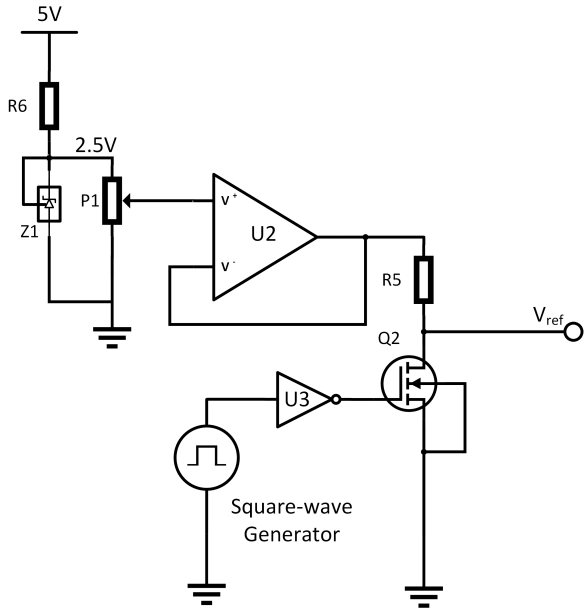

Figure 4.10: Digital-to-Analog signal conditioning for regulation stage

a 5 kΩ resistor between connector A and B is connected between the 2.5 V regulator and ground. It is a 8-bit resolution (256 levels) resistor performing the same electronic adjustment function as a mechanical potentiometer or variable resistor but with enhanced resolution and low temperature coefficient performance and uses Serial Peripheral Interface (SPI) to set the position of the wiper connector (W). Therefore, this model has a resolution of $\Delta R_W = \frac{5000}{2^8-1} = 19.61\,\Omega$, hence, if terminal A is connected to 2.5 V and terminal B is connected to ground, the resolution of the voltage in the wiper is,

$$\Delta V_W = \frac{V_A}{R_{AB}} \times \Delta R_W = \frac{2.5\,\text{V}}{5\,\text{k}\Omega} \times 19.61 = 10\,\text{mV}$$

Since the Op-Amp $U2$, a low-distortion high-speed amplifier with slew-rate of 975 V/µs, is applied in a voltage-follower configuration the resolution of the voltage V_{ref}, when the MOSFET $Q2$ is in cut-off state, is equal to ΔV_W. According to Figure 4.9, the voltage drop in the sensing resistor R_s should be equal to V_{ref}, hence the resolution of the current that flows through R_s when the luminary is ON is equal to,

$$\Delta I_{R_s} = \frac{\Delta V_W}{R_s} = \frac{10\,\text{mV}}{2.5\,\Omega} = 4\,\text{mA}$$

In order to drive the luminary with a PWM signal, the voltage applied to the non-inverting input of the Op-Amp $U1$ should be pulsed. This operation is implemented using a MOSFET ($Q2$) and a MOSFET driver ($U3$). Considering that the component $Q2$ acts as a switch, it should operate in the cut-off region or linear region, the voltage V_{ref} swings between V_W and $\frac{R_{ds}on}{R_{ds}on+R_5} \times V_W$, respectively. The value of the resistor $R_{ds}on$ of the MOSFET has a maximum value of 350 mΩ in the conditions $V_{gs} = 4.5\,\text{V}$ and $I_D = 0.2A$. By those terms, the voltage V_{ref} is meant to be comprised from $8.68 \times 10^{-3}\,\text{V}$ to 2.49 V.

The signal V_{ref} needs to have low rise and fall times, therefore, a MOSFET gate driver ($U3$) is used. It is a high-speed MOSFET driver, capable to sink or source high currents. This

device takes logic input signals and has the signal inverting option, which in this case, will be used to maintain the polarity between the signal generator and V_{ref}. The additional feature that this device offers is TTL logic-level inputs with Hysteresis, with logic low input voltage (V_{IL}) and logic high input voltage (V_{IH}) of 0.8 V and 2.0 V, respectively. It allows the use of different input voltages without affecting rise and fall times of the signal that drives the MOSFET $Q2$.

Circuits from Figures 4.9 and 4.10 have been subjected to simulation using Tina-TI. The simulation conducted, allows to verify the current regulation stage for steady and transient regions when the voltage V_{ref} is subjected to a continuous or pulsed signal, respectively.

If a step input voltage is applied to V_{ref}, the current regulator stage forces the voltage across the sensing resistor, V_{Rs}, to be equal, hence the current that flows through Rs is equal to V_{ref}/Rs. Figure 4.11 shows the response of the current regulator to a step voltage input. The sub-figures 4.11a and 4.11b represents the step response when the wiper connector of the potentiometer is set at 50% and 25% of its maximum value (5 kΩ), respectively.

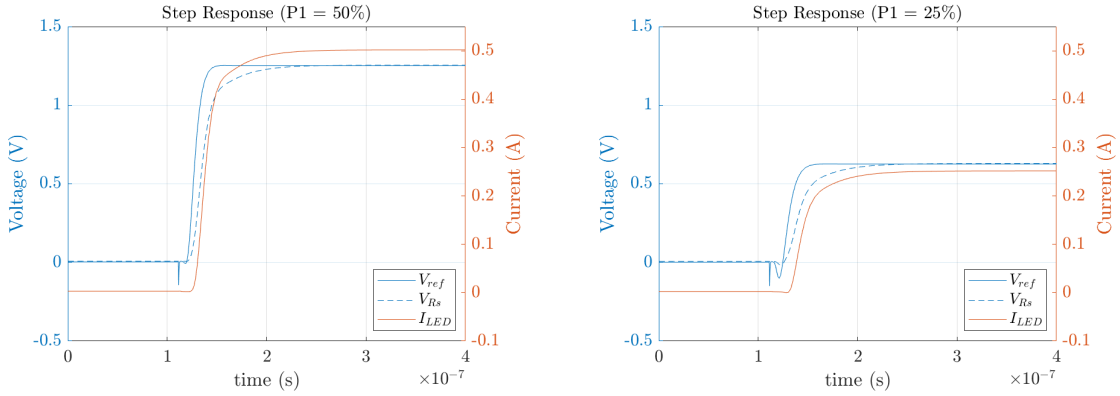

(a) Potentiometer 50%

(b) Potentiometer 25%

Figure 4.11: Step Response

Potentiometer position (%)	V_{ref} rise-time	V_{ref} steady-state	V_{Rs} steady-state	I_{LED} steady-state
50%	14.3 ns	1.2517 V	1.2544 V	501.7 mA
35%	15.3 ns	0.8766 V	0.8799 V	352.0 mA
25%	15.8 ns	0.6258 V	0.6295 V	251.8 mA

Table 4.4: Step response simulation results

The simulation provide essential information relative to the implementation of circuits in Figures 4.9 and 4.10. The extracted data for step input response is detailed in Table 4.4. A first analysis to the rise-time of voltage V_{ref}, evidence its increasing value as the value of the potentiometer position decreases. This behaviour is explained by the fact that the parasitic capacitances of MOSFET Q_2, when the MOSFET transits between regions of operation, will charge at a slower rate since the voltage output of Op-Amp U_2, configured as voltage-follower, is decreasing linearly with the potentiometer wiper. The most pertinent information to extract from the table is the relative error, E_r, relative to the non-inverting voltage of Op-Amp U_1

and the voltage drop on the sensing resistor, which is inferior to 1% for the tested values of the potentiometer position.

A square-wave response analysis is also performed in the simulation for V_{ref} signal frequencies of 100 kHz and 1 MHz, observable in Figure 4.12a and 4.12b respectively. For square-wave analysis, the value of the potentiometer is held at 50 % and the MOSFET Q_2 is acting as a high-speed switch. The source of the signal applied to the input of the MOSFET driver U_3, is a square-wave generator with amplitude equal to 5 V with rise and fall times of 1 ns.

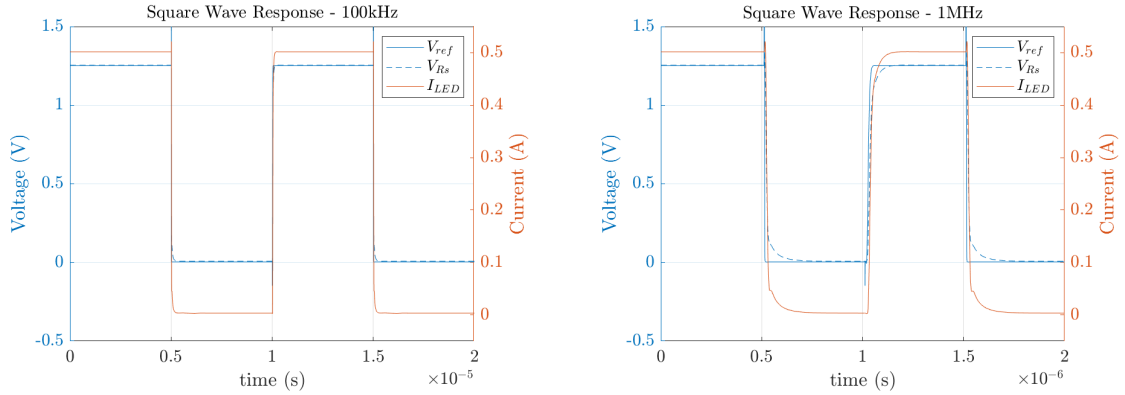

(a) 100 kHz signal frequency **(b)** 1 MHz signal frequency

Figure 4.12: Square-wave Response

Signal	V_{ref}		V_{Rs}		I_{LED}	
frequency	rise-time	fall-time	rise-time	fall-time	rise-time	fall-time
100 kHz	14.4 ns	1.6 ns	32.5 ns	17.2 ns	32.0 ns	15.1 ns
1 MHz	14.5 ns	1.6 ns	33.1 ns	17.6 ns	32.6 ns	15.3 ns

Table 4.5: Square-wave response simulation results

The results in Table 4.5 shows that the rise and fall times of each signal represented in Figure 4.12, are in the order of tens of nanoseconds. Although these results are promising, the simulation does not take in account several aspects such as the inductance in the cables that connect the driver to the luminary, the dynamic resistance in the LEDs, among others factors that may influence the current that flows through the luminary LEDs.

4.2.3 Software description for driver control

The previous described LED current driver requires a control unit to enable all the functionalities that it can perform. Using the open-source electronic board Arduino nano with an embedded uC, ATmega328p from Atmel, the integration of this platform in the driver is fast and low-cost. The ATmega328p chip integrated in the board, uses an external crystal oscilator to run at a clock frequency of 16 MHz. It is a 8-bit AVR RISC-based uC that combines a 32 kB flash memory, a 1024 B EEPROM, 23 General Purpose Input/Output (GPIO), two 8-bit timers, one 16-bit timer, internal and external interrupts, SPI serial port, 6-channel Analog-to-Digital (A/D) converter, among other capabilities.

Figure 4.13 illustrates the main peripheral interfaces used to control the mode of operation of the LED-based luminary driver.

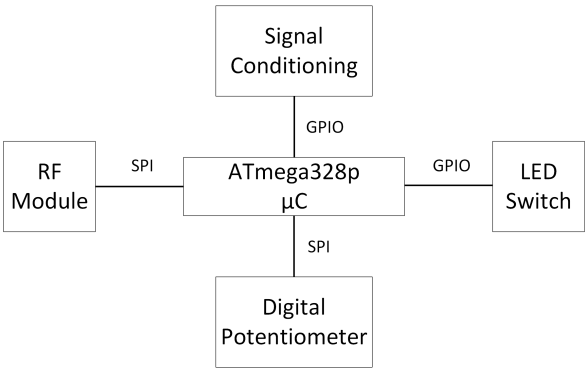

Figure 4.13: Interfaces used by the uC to control the current driver.

The signal to be conditioned is controlled by the 16-bit Timer of the Atmega328p which is used to generate the input signal of the driver for VLC data transmission. The led switch is a module that controls a p-channel MOSFET acting as a master switch located between the luminary voltage supply V_H^+ and the luminary. The digital potentiometer and the RF modules are SPI slave modules, connected to the SPI bus with a dedicated extra slave pin for each of them.

The firmware was developed in Atmel Studio 7 software version 7.0.1931 and programmed in the flash of the uC using the Atmel JTAGICE3 programmer.

The Arduino nano, has a voltage regulator that converts the voltage in the pin V_{in} in 5 V. To program the flash memory of this device, the connector ICSP is used. Table 4.6 lists the pins used and their description.

Pin	Purpose	I/O	Description
PB0	Chip Enable	O	Control the RF module Power functions
PB1	Slave Select	O	Activate the access to the SPI bus to the digital potentiometer
PB2	Slave Select	O	Activate the access to the SPI bus to the RF module
PB3	SPI MOSI	O	Transfer data from Master to Slave
PB4	SPI MISO	I	Transfer data from Slave to Master
PB5	SPI CLK	O	Master output SPI clock signal
PD2	Ext. Interrupt	I	Receive external interruption signals from RF module.
PD6	GPIO	O	Generates a signal for VLC data tansmission.
PD7	GPIO	O	Control the MOSFET p-channel in series with the luminary.

Table 4.6: Description of pins used by the uC

The main routine running in the uC is illustrated in Figure 4.14. It can be described as a routine in loop, that starts by defining the I/O Port directions with method setPinIO(), then the SPI module is set with method spi_begin() that writes in SPI control register SPCR the operation mode of the module, a class object ledInterface instantiated as interface is initiated with interface.init(hwID,MODE) which takes as arguments the hardware ID defined in the pre-processor and the MODE indicates if the firmware is running in a slave or master

controller. The loop in the main routine is repeatedly executed to check if new messages have arrived to the RF module and process them with method interface.checkRF().

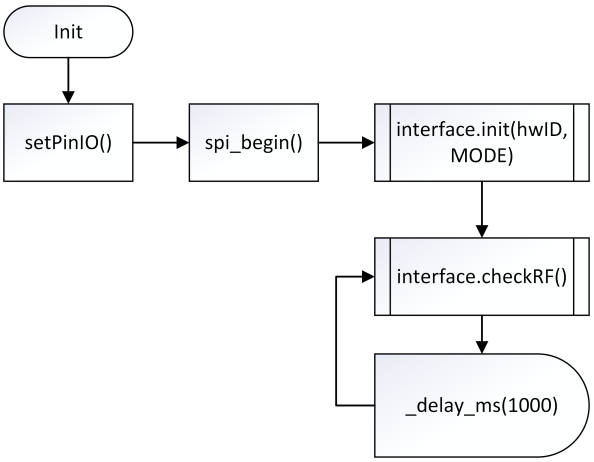

Figure 4.14: Main slave routine running in the uC.

The Classes create for the purpose of controlling the driver are ledCtl and ledInterface. The Class ledCtl encapsulates the access to variables that control the mode of operation of the driver. Public access is given using get and set methods to the private members of a structure. The Class ledInterface is an interface that has methods to interacts with the driver control signals and the uC modules registers (SPI, UART, Timers). Figure 4.15 and 4.16 lists all the methods available in the Class ledCtl and ledInterface respectively.

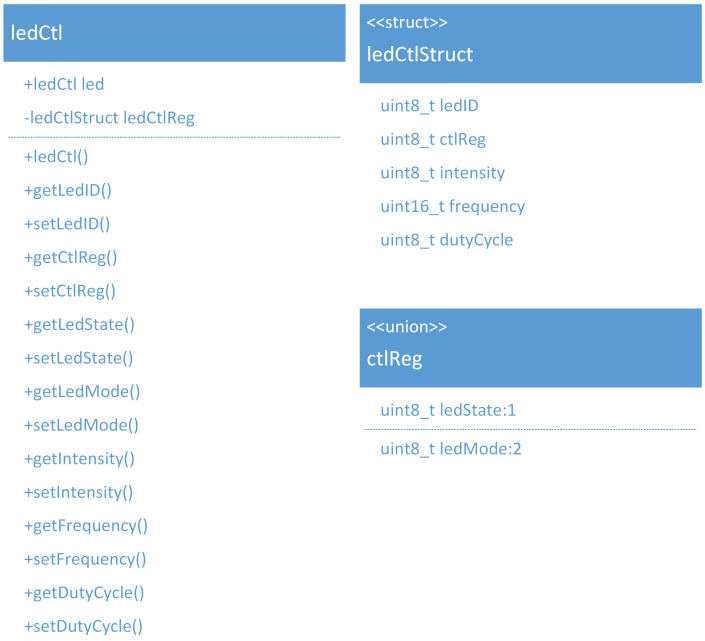

Figure 4.15: Class ledCtl methods.

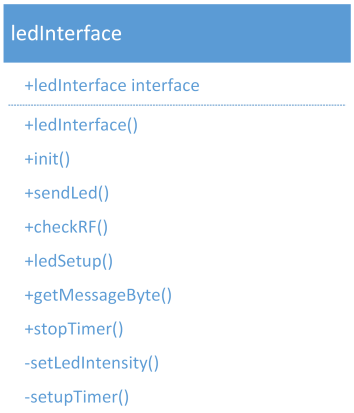

Figure 4.16: Class ledInterface methods.

The Class ledCtl implements a region of memory that contains the desired mode of operation of the driver. This class implements a structure ledCtlReg that can be described as it follows:

- uint8_t ledID: led identification number;
- uint8_t ctlReg: a UNION register that contains the luminary control operation:
  - uint8_t ledState:1 : a one-bit register that defines the state of the luminary (0b1 - ON; 0b0 - OFF);
  - uint8_t ledMode:2 : a two-bits register that defines the operation mode of the luminary (0b00 - DC; 0b01 - OOK+Manchester; 0b10 - VPPM).
- uint8_t intensity: defines the value of current that flows through the luminary when conducting, in percentage (eg: 100 - 530 mA; 50 - 265 mA);
- uint16_t frequency: the signal frequency for pulsed current in Hz (eg: 1000 - 1 kHz).
- uint8_t dutyCycle: is used for VPPM signal modulation to modify the duty-cycle, in percentage (eg: 100 - 100 %; 50 - 50 %).

The Class ledInterface methods can be described as it follows:

- init(uint8_t hardwareID, uint8_t mode): configures the RF module and set the default led driver operation mode;
- uint8_t sendLed(uint8_t hardwareID, ledCtl* ledPtr): method used to send a packet from master to slaves with new configurations;
- void checkRF(void): used by slave drivers to check if the new packets have arrived to the RF module and process them;
- uint8_t* ledSetup(ledCtl* ledPtr): set the driver operation mode accordingly to definitions set passed by the pointer argument;
- uint16_t getMessageByte(uint8_t * data): method used by the timer Interruption Service Routine (ISR).
- void stopTimer(void): method that reset the timer 1.
- void setLedIntensity(ledCtl* ledPtr): sets the value of the potentiometer in function the intensity set in the ledCtl object, ledPtr, passed by argument.
- void setupTimer(ledCtl* ledPtr): used to setup the timer accordingly to the frequency and duty-cycle defined in the ledCtl object, ledPtr, passed by argument.

The method ledInterface::ledSetup() that sets the driver operation mode, performs several operations. The first one is to set the value to transmit over SPI to the digital potentiometer using method ledInterface setLedIntensity(ledCtl* ledPtr). It calls the method digPot digitalPotWrite(float value) where the argument value is equal to the value of the desired voltage to be applied in the wiper connector. The value is equal to the desired voltage drop across the sensing resistor, V_{Rs}, in function of the value of intensity defined in the object 'led', hence, considering a sensing resistor of 2.5 V and a maximum current of 530 mA flowing through the resistor, the value of voltage to be passed should be equal to,

$$value = (ledPtr- > getIntensity() \times 0.01) \times 0.530 \times 2.5$$

according to Ohm's law ($V = R \times I$).

The second operation is to encode the desired ID to be transmitted using VLC. In order to maintain the DC level of illuminance while transmitting, Manchester line coding should be applied. The packet of data to be transmitted is composed by a Start of Frame (SoF) with three bits, followed by four bits of data (representing the ID), and a End of Frame (EoF) composed by two bits. The use of a SoF allows the receiver(s) to recover the data clock rate, where the use of a EoF indicates the end of the transmitted frame. It is important to refer that the use of Manchester line coding, reduces the bandwidth of the signal in half since bits are represented as transition of levels, hence, the data to be transmitted will be doubled as a logical one is represented by a transition from a logical zero to one ($'0' \mapsto' 1'$) and a logical zero is represented by a transition from a logical one to zero ($'1' \mapsto' 0'$). The encoding process can be observed in a simple example where the data to be transmitted is the ID 5 ('0101'),

Original data	Manchester encoded data
111 0101 00	010101 10011001 1010

where the number of logical ones and zeros differs on the original data and in the Manchester this number is equal.

The last operation performed in the method, sets the hardware to the desired operation mode. Hence, if DC operating mode is desired, the method needs to call turnOnLED(true) or turnOffLED() methods. Depending on the value of ledPtr->getLedMode(), it enables or disables the control signal that actuates on the MOSFET switch that is connected in series with the luminary. If transmitting mode is required, the Timer 1 needs to be configured to allow the modification of the logical value in the pin PD6 accordingly to the desired signal frequency set in 'led' object, hence, the method ledInterface::setupTimer(ledCtl* ledPtr) is called.

The method ledInterface::setupTimer(ledCtl* ledPtr) sets the Clear Timer on Compare Match (CTC) mode of Timer 1 with activation of intern interruptions. This mode clears the timer counter register (TCNT1) when its value matches the value in register OCR1A. To produce an OOK+Manchester output signal with the frequency provided in 'led' object, the ISR of the Timer1 output compare A match needs to be triggered at a period of time equal to

the time of a bit. Figure 4.17 illustrates the timing diagram describing this technique using Timer 1 with one compare register.

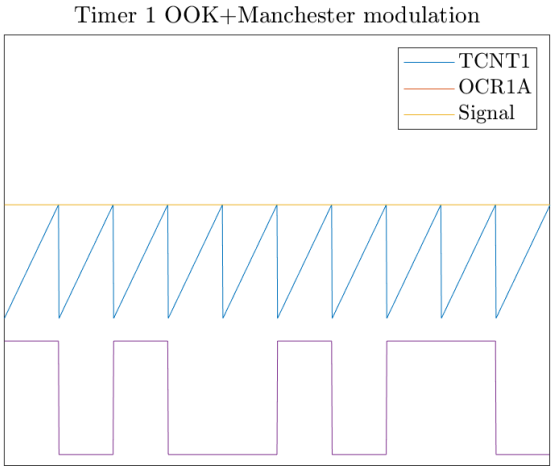

Figure 4.17: OOK+Manchester timing diagram implemented using Timer 1.

To perform VPPM modulation technique, a similar approach is used, with the additional activation of the register OCIE1B (Output Compare B match interrupt enable). In this configuration, the Timer 1 counter register (TCNT1) is cleared at the moment when it is equal to the value loaded in OCR1A, generating an interrupt request for output compare match A but also for output compare match B. By those terms, if the value loaded in register OCR1A is fixed, it defines the signal frequency, and the value of the register OCR1B can be modified to a value between 0 and OCR1A. This is required to maintain the time of a logical one and a logical zero constants, independently of the order of appearance. Figure 4.18 illustrates the technique to implement VPPM using Timer 1 and two compare registers.

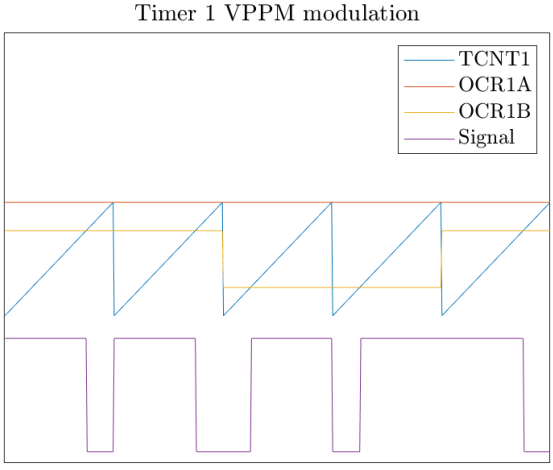

Figure 4.18: VPPM timing diagram implemented using Timer 1.

The slave uC, is kept in the same operating mode until a new operating mode is received

from the RF module.

4.3 Communication interface

In order to allow the remote management of the driver operation, a master controller is required to send messages to the slaves. This feature enables the capability to create a parametrized platform to perform VLP experiments in different conditions of illuminance. Figure 4.19 illustrates the master system overview that is able to connect to a computer and send the LED configuration via RF module.

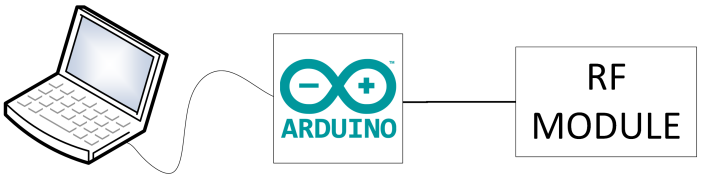

Figure 4.19: Master system overview.

The RF module, a nrf24l01+ transceiver with an antenna is attached to each of the driver luminaries. To control the operation mode of the drivers individually, the Master is capable of converting input data from the computer to the RF channel. Therefore, the information transmitted from the computer should comprise the destination driver ID, the operation mode , the luminary state, the intensity of the illuminance and in case of performing transmission of data through the optical channel, the frequency of the signal and its duty-cycle if required. This information is received in the master uC using Universal Asynchronous Receiver/Transmitter (UART) protocol with the provided serial converter in the Arduino nano board. Using a well defined message to transmit the data, a software that performs reading/writing operations in a serial file descriptor (eg: PuTTy/moserial) is able to configure the platform with the user requirements. Table 4.7 shows the different messages that the master unit is able to process and forward through the RF channel when formatted as "$[Dest. HW ID],[LEDState],[LEDMode],[LEDIntensity (%)],[Signal Frequency(Hz)],[Signal Duty-Cycle (%)],*". The data received trough the UART fills an object ledCtl and when data is ready to be dispatched, the master transmits its data to the recipient(s). It is important to refer that there is a reserved ID (255) which is used to set the operation mode of all slaves listening. The RF module is configured to transmit the data in broadcast to a specific RF channel, hence, the messages are received by all the slaves, being the packet dropped if the ID transported in the packet does not correspond to the receiver. The radio library used for the nrf24l01+ module was created by kehribar can be accessed in GitHub community repository `https://github.com/kehribar/nrf24L01_plus`. The UART library used in the project was created by Peter Fleury can be acessed in Daniel Maierhofer GitHub repository `https://github.com/damadmai/pfleury`.

- Example 1 will inform hardware ID 1 to operate in DC mode at 100 % of power;
- Example 2 will inform hardware ID 2 to turn-off the luminary;

Example	UART String
Example 1	$1,1,0,100,10000,50,*
Example 2	$2,0,0,100,10000,50,*
Example 3	$3,1,1,100,2000,50,*
Example 4	$4,1,2,100,10000,25,*
Example 5	$255,1,0,50,10000,25,*

Table 4.7: Example of messages to be transmitted via UART

- Example 3 will inform hardware ID 3 to transmit ID with OOK-scheme with Manchester code line, at a signal frequency of 2 kHz;
- Example 4 will inform hardware ID 4 to transmit ID with VPPM-scheme, at a frequency of 10 kHz and a duty-cycle of 25 %;
- Example 5 will inform all listening slaves to operate in DC mode at 50 % of power.

4.4 Final remarks

This chapter describes the project of a current driver to power an off-the-shelf luminary. It shows the planning and description of the critical cautions to be taken in account when designing an AC-DC converter, a voltage-current linear regulator and a digital-to-analog signal conditioning.

It is also explained how the driver is controlled by a uC to perform different modes of operation such as DC operation and transmission of data using VLC.

Lastly, it is explained how a user can interact with the framework in order to perform different experiments using a real-world scaled system.

CHAPTER 5

Results

This chapter shows the results obtained along the development of this dissertation.

5.1 DC Luminary results

To test several aspects related to the transmission of data using the chosen luminary, a support was built to perform experimental measures. Figure 5.1 shows the platform built to perform those experiments.

Figure 5.1: Experimental luminary support.

Figure 5.2 shows the relationship between illuminance and distance. In the State Of The Art, it was discussed that in a straight line, the illuminance is inversely proportional to the square of the distance. The fitting of the curve shows that it can be aproximated as

$$E(d) = \frac{659.5}{d^{1.955}}$$

as expected, the experimental values verify the theory.

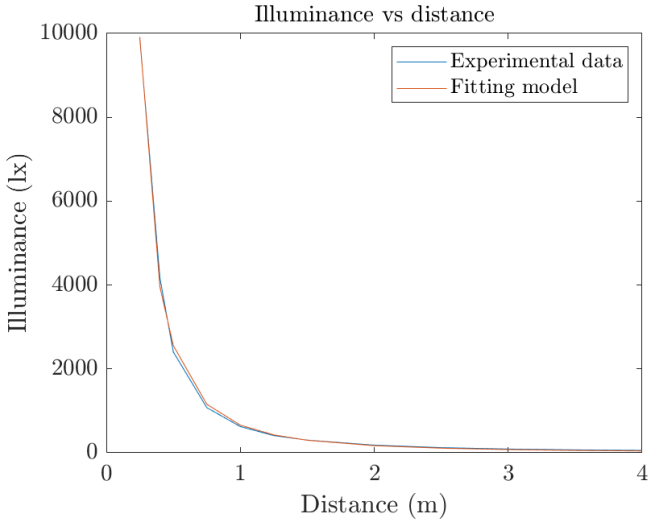

Figure 5.2: Experimental results of illuminance vs distance (r^2=0.9991).

Table 5.1 reflects the defined LED intensity in the software to the received illuminance in a luxmeter. It also compares the voltages V_{ref} and V_{Rs} used to regulated the current that

flows through the luminary when ON. The results shows that the voltage-current converter is correctly regulating the current with low variance. Figure 5.3 represents the linear experimental results of measuring the illuminance at a distance of 3 m for the luminary with the value of intensity set in the software. The linear regression returned a $r^2 = 0.9989$ which describes the linearity between the DC value imposed in the driver, and the received Illuminance. It can be modeled as,

$$E(\%intensity) = 0.9233 \times (\%intensity) + 2.686$$

Knowing the values of the illuminance, E, at a distance of 3 meters, the value of the illuminance in a point contained in the same direction vector, at a different distance can be obtained using,

$$\begin{cases} E_0 = k \times (I/r_0^2) \\ E_1 = k \times (I/r_1^2) \\ r_1 = n \times r_0 \end{cases} \quad \therefore \quad \begin{cases} \frac{E_1}{E_0} = \frac{k \times (I/r_1^2)}{k \times (I/r_0^2)} \\ r_1 = n \times r_0 \end{cases} \equiv \begin{cases} \frac{E_1}{E_0} = \frac{r_0^2}{r_1^2} \\ r_1 = n \times r_0 \end{cases} \equiv \begin{cases} \frac{E_1}{E_0} = \frac{1}{n^2} \\ \hline \end{cases}$$

DC intensity (%)	V_{Rs} (V)	V_{ref} (V)	Illuminance (lx)
10	0.141	0.151	10.6
15	0.201	0.209	15.1
20	0.272	0.280	20.8
25	0.323	0.332	24.7
30	0.393	0.404	30.1
35	0.464	0.476	35.4
40	0.527	0.538	40.2
45	0.598	0.610	45.5
50	0.649	0.662	49.4
55	0.720	0.734	54.5
60	0.783	0.797	59.0
65	0.853	0.868	64.1
70	0.915	0.930	68.2
75	0.982	0.981	72.5
80	1.05	1.054	77.3
85	1.11	1.116	81.4
90	1.19	1.187	86.1
95	1.24	1.239	89.6
100	1.31	1.311	94.1
105	1.38	1.383	98.6
110	1.44	1.444	102.6

Table 5.1: Experimental results of the driver and respective illuminance

It was verified that the ripple in the capacitor of 3.3 mF at a supplying current of 530 mA is approximately of 1.05 V. Figure 5.4 illustrates the ripple verified experimentally. In the voltage supply V_L^+ it was verified a ripple of approximately 2.2 V. The measured value of the voltage provided by the voltage regulators can be observed in 5.2.

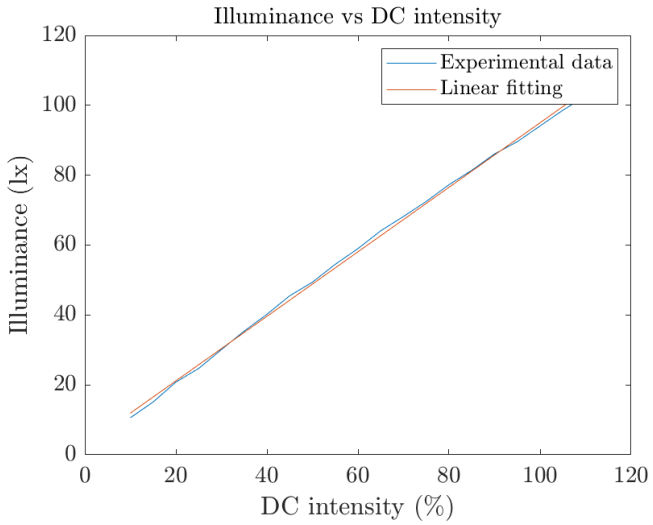

Figure 5.3: Experimental results of driver in DC operating mode (r^2=0.9989).

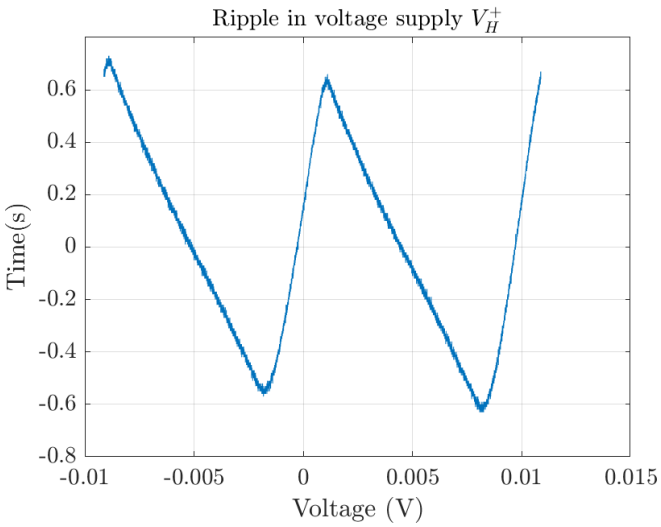

Figure 5.4: Ripple of voltage in V_H^+.

Voltage regulation	Experimental value
-5	-4.9
2.5	2.49
3.3	3.32
5	5.01
9	9.00

Table 5.2: Experimental results of the driver voltage regulators

5.1.1 Comparison with lighting project results

Since the installation of the metal frame was not finished for the whole room, and only four drivers were concluded at the time of experimental measures, the results of the room illuminance are not possible to compare with the project developed in DIALux software. Therefore, experimental results were measured using a luxmeter in a grid of 7×5 points can be observed in Figure 5.5.

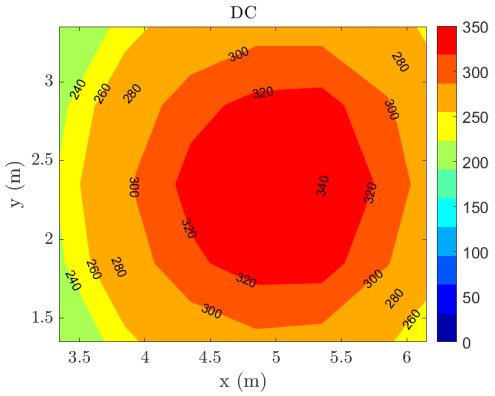

(a) Measured illuminance at maximum power ($I_{LED} = 540\,\text{mA}$).

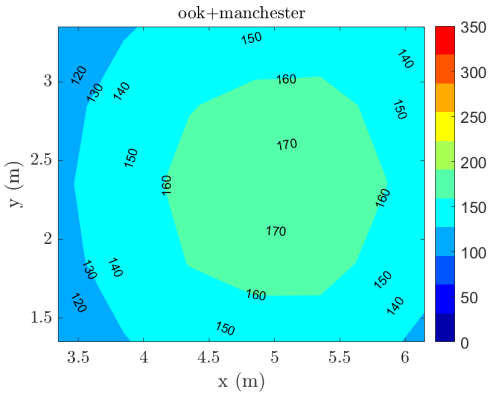

(b) Measured illuminance using OOK+Manchester transmitting mode.

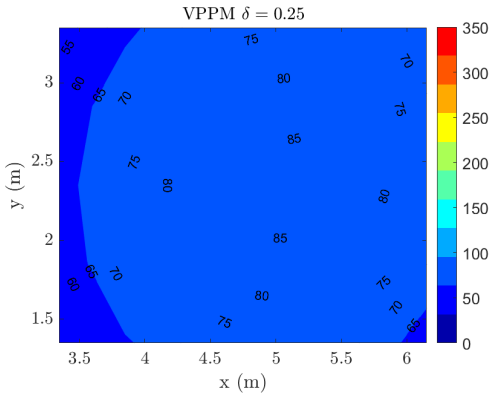

(c) Measured illuminance using VPPM ($\delta = 0.25$) transmitting mode

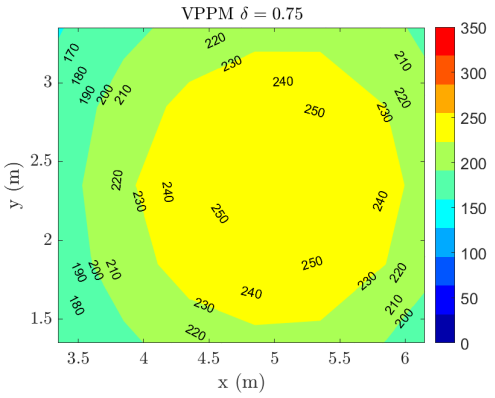

(d) Measured illuminance using VPPM ($\delta = 0.75$) transmitting mode

Figure 5.5: Experimental isolines of the measured illuminance at floor level (heigh=2.7 m)

The average values of illuminance for each mode of operation of the driver, can be observed in Table 5.3. The results shows that the experimental results when transmitting are according with the expected.

Driver mode	Average illuminance compared to max. DC power
OOK+Manchester	50.83 %
VPPM ($\delta = 0.25$)	25.54 %
VPPM ($\delta = 0.75$)	76.22 %

Table 5.3: Experimental results of average illuminance at floor level for different modes of operation

5.2 Transmission results

One of the main important results is the response of the current regulator in transient region observable in Figure 5.6. The comparison of the experimental rise/fall times with the simulated ones can be observed in Table 5.4.

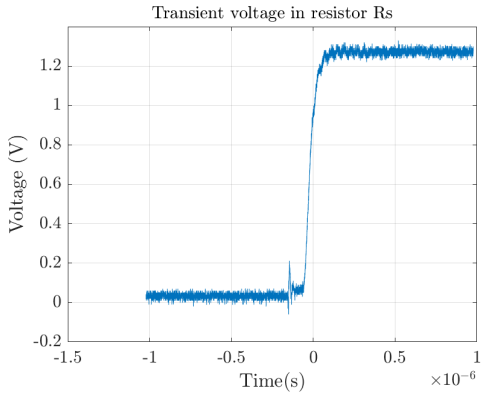

(a) Voltage across the sensing resistor *Rs* in rising-edge.

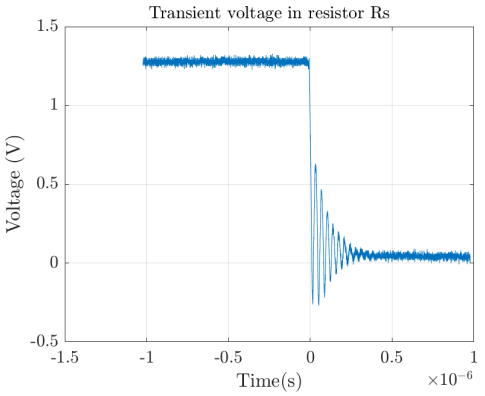

(b) Voltage across the sensing resistor *Rs* in falling-edge.

Figure 5.6: Voltage across the sensing resistor *Rs* in Transient region.

	Simulation result	Experimental result
Rising-time	33.1 ns	73.4 ns
Falling-time	17.6 ns	12.6 ns

Table 5.4: Experimental results for rising/falling times in sensing resistor *Rs*

Experimental results using a photodiode for square and sinusoidal waves can be observed in Figure 5.7. The rising/falling times can be observed in Table 5.5.

	Experimental result
Rising-time	453 ns
Falling-time	439 ns

Table 5.5: Experimental results for rising/falling times in a photodiode

The luminary LED bandwidth can be estimated using Equation 2.15. Therefore,

$$f_{3dB} = \frac{2.2\sqrt{3}}{\pi(453\,\text{ns} + 439\,\text{ns})} = 4.2\,\text{MHz}$$

Using a signal pattern generator HP81130A and some auxiliary circuits to input an OOK+Manchester signal in the driver, the eye diagram for different frequencies is shown in Figure 5.8. It is observable that for higher frequencies the eye is becoming to be smaller and the jitter is very high.

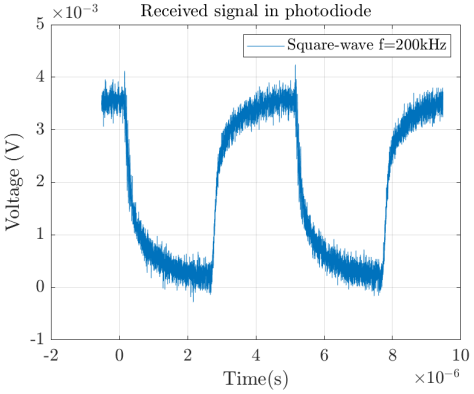

(a) Square-wave with frequency=200 kHz.

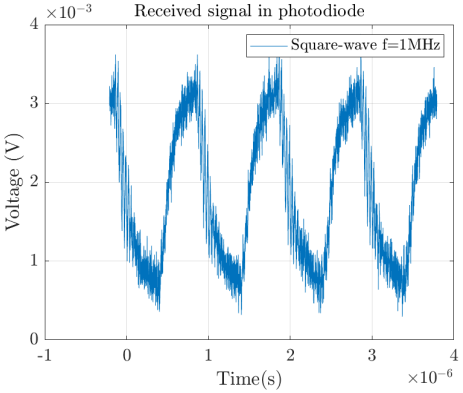

(b) Square-wave with frequency=1 MHz.

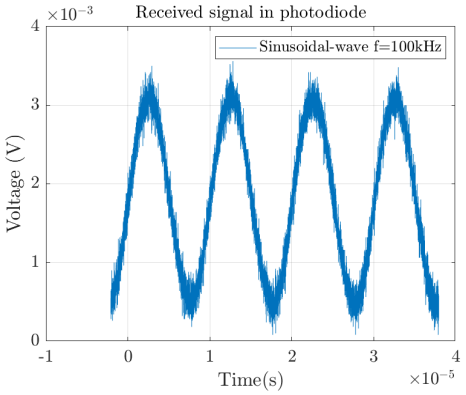

(c) Sinusoidal-wave with frequency=100 kHz.

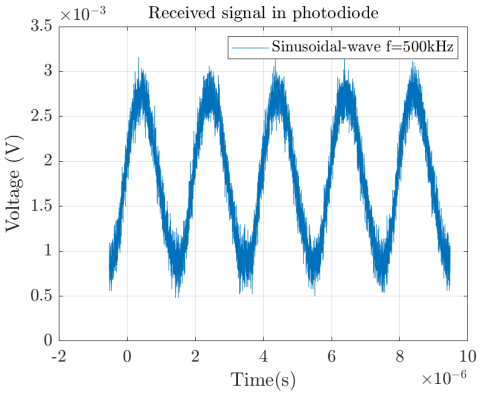

(d) Sinusoidal-wave with frequency=500 kHz.

Figure 5.7: Signal received by a photodiode with no TIA stage.

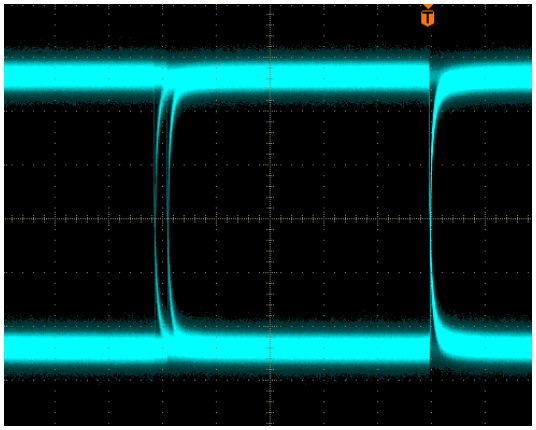

(a) Square-wave with frequency=10 kHz.

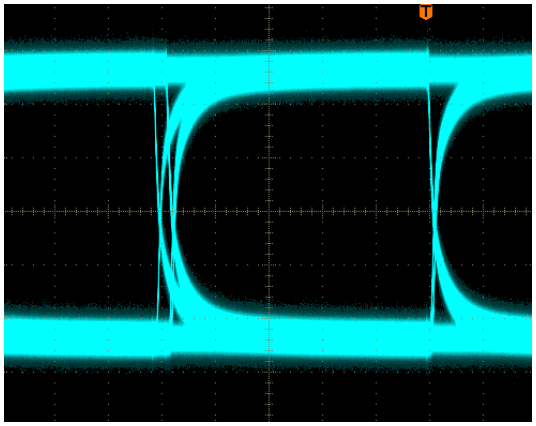

(b) Square-wave with frequency=50 kHz.

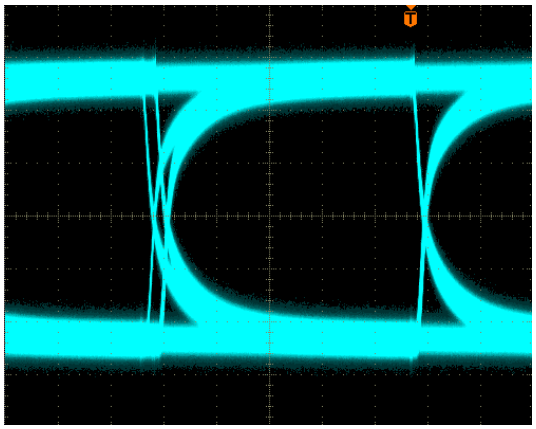

(c) Sinusoidal-wave with frequency=100 kHz.

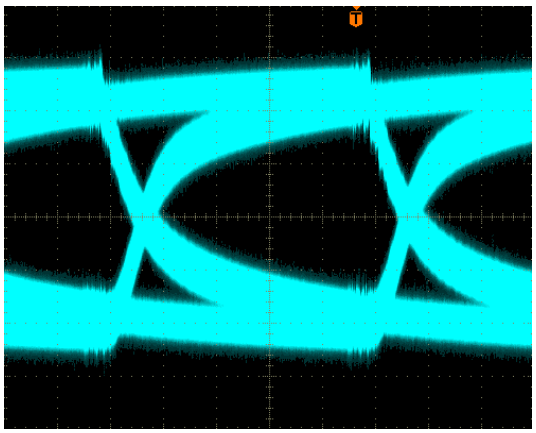

(d) Sinusoidal-wave with frequency=500 kHz.

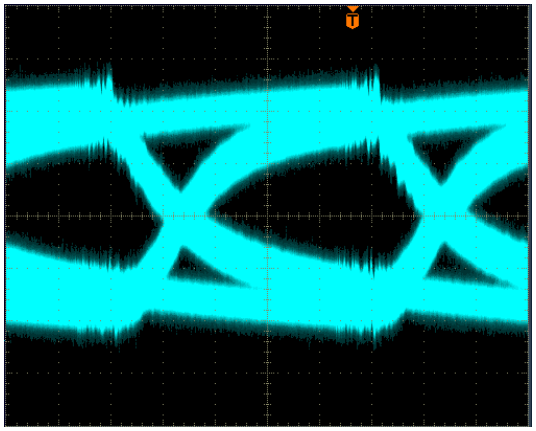

(e) Sinusoidal-wave with frequency=1 MHz.

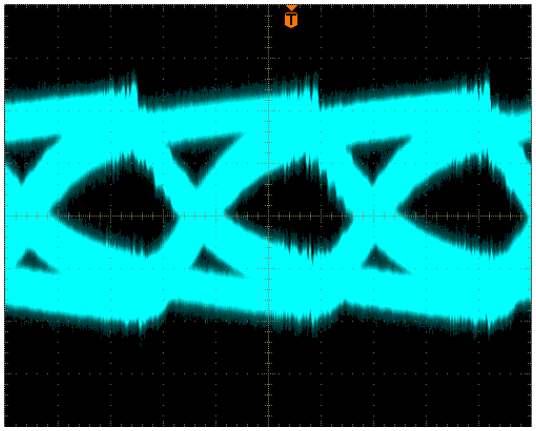

(f) Sinusoidal-wave with frequency=1.5 MHz.

Figure 5.8: Signal received by a photodiode with no TIA stage.

CHAPTER 6

Conclusion

At the end, some conclusions about the work performed in this dissertation and some ideas for the future.

6.1 Final conclusions

The lack of information regarding a real-world scale platform with off-the-shelf luminaries is the base of this work. Since IPSs are becoming more and more important, the need of creating a reliable system is an important aspect in what concerns to the implementation of VLP. This dissertation provides a functional test platform for VLP with a customized driver that has the option to provide constant or pulsed light for transmission of luminaries ID number. The text provides necessary information about how to create a similar environment and what the aspects to be concerned about.

The use of an atmega328p uC is in fact a limitation for the system since it cannot provide high debit data rate. The driver has two inputs, one digital and one analog, that can be used to drive a signal in the driver for VLC purposes.

A colleague, Miguel Rêgo, is already using the platform to estimate positioning using a camera. Hence, it can only be considered a success.

6.2 Future Work

For future work, it is in my opinion that a system that can infer the position of a robot (using a camera for instance) is a must have. The study of the driver for newer versions and more efficient is also a point to be noted. I hope that the lighting system developed will be used in the laboratory for long years.

Bibliography

[1] P. Lanjudkar, *Indoor positioning and indoor navigation (ipin) market by component (software, hardware, and services), technology (ultra-wideband technology, bluetooth low energy, wi-fi, and others), application (asset & personnel tracking, location-based analytics, navigation & maps, and others), and end-use industry (healthcare, retail, manufacturing, travel & hospitality, office spaces, public spaces, logistics & warehouses, and others): Global opportunity analysis and industry forecast, 2018 - 2025*, 2018. [Online]. Available: http://harvestchoice.org/publications/tanzania-national-sample-census-agriculture-20022003-small-holder-agriculture-volume-ii.

[2] G. Adair, *Thomas Alva Edison : inventing the electric age*. New York: Oxford University Press, 1996, ISBN: 9780195087994.

[3] L. U. Khan, "Visible light communication: Applications, architecture, standardization and research challenges", en, *Digital Communications and Networks*, vol. 3, no. 2, pp. 78–88, May 2017, ISSN: 23528648. DOI: 10.1016/j.dcan.2016.07.004. [Online]. Available: https://linkinghub.elsevier.com/retrieve/pii/S2352864816300335.

[4] C. Medina, M. Zambrano, and K. Navarro, "LED BASED VISIBLE LIGHT COMMUNICATION: TECHNOLOGY, APPLICATIONS AND CHALLENGES – A SURVEY", en, vol. 8, no. 4, p. 14,

[5] M. Uysal, C. Capsoni, Z. Ghassemlooy, A. Boucouvalas, and E. Udvary, *Optical Wireless Communications - An Emerging Technology*, 1st ed. 2016. Berlin, Heidelberg: Springer, 2016, ISBN: 978-3-319-30201-0.

[6] F. M. L. Duarte, "Localização em espaços interiores por luz visível para robôs móveis", MsC dissertation, Universidade de Aveiro, 2015.

[7] M. C. M. Vieira, "VLC based position etimation for robotic navigation", MsC dissertation, Universidade de Aveiro, 2016.

[8] A. P. G. Vilas-Boas, "Sistema de iluminação para posicionamento em ambientes interiores de um agente móvel", MsC dissertation, Universidade de Aveiro, 2017.

[9] F. Zafari, A. Gkelias, and K. K. Leung, "A Survey of Indoor Localization Systems and Technologies", en, *IEEE Communications Surveys & Tutorials*, vol. 21, no. 3, pp. 2568–2599, 2019, ISSN: 1553-877X, 2373-745X. DOI: 10.1109/COMST.2019.2911558. [Online]. Available: https://ieeexplore.ieee.org/document/8692423/.

[10] R. F. Brena, J. P. García-Vázquez, C. E. Galván-Tejada, D. Muñoz-Rodriguez, C. Vargas-Rosales, and J. Fangmeyer, "Evolution of Indoor Positioning Technologies: A Survey", en, *Journal of Sensors*, vol. 2017, pp. 1–21, 2017, ISSN: 1687-725X, 1687-7268. DOI: 10.1155/2017/2630413. [Online]. Available: https://www.hindawi.com/journals/js/2017/2630413/.

[11] M. Shahjalal, M. T. Hossan, M. K. Hasan, M. Z. Chowdhury, N. T. Le, and Y. M. Jang, "An Implementation Approach and Performance Analysis of Image Sensor Based Multilateral Indoor Localization and Navigation System", en, *Wireless Communications and Mobile Computing*, vol. 2018, pp. 1–13, Oct. 2018, ISSN: 1530-8669, 1530-8677. DOI: 10.1155/2018/7680780. [Online]. Available: https://www.hindawi.com/journals/wcmc/2018/7680780/.

[12] Zumtobel, *The Lighting Handbook*, 6th edition. Zumtobel Lighting GmbH Schweizer Strasse 30 Postfach 72 6851 Dornbirn, AUSTRIA, Apr. 2018, ISBN: 978-3-902940-72-8. [Online]. Available: https://www.zumtobel.com/PDB/teaser/EN/lichthandbuch.pdf.

[13] D. Schreuder, *Outdoor lighting : physics, vision and perception*. Dordrecht: Springer, 2008, ISBN: 978-1-4020-8601-4.

[14] CGPM, "Comptes rendus des séances de la 16e conférence générale des poids et mesures; paris.", Bureau International des Poids et Mesures, F-92310 Sevres, France, Tech. Rep., 1979, p. 100.

[15] Claude Weisbuch, "Historical perspective on the physics of artificial lighting", *Comptes Rendus Physique*, vol. 19, no. 3, 89 –112, 2018, ISSN: 1631-0705. DOI: {https://doi.org/10.1016/j.crhy.2018.03.001}. [Online]. Available: {http://www.sciencedirect.com/science/article/pii/S1631070518300306}.

[16] Z. Ghassemlooy, *Visible light communications : theory and applications*. Boca Raton: CRC Press, 2017, ISBN: 9781498767538.

[17] H. Li, X. Chen, J. Guo, Z. Gao, and H. Chen, "An analog modulator for 460 MB/S visible light data transmission based on OOK-NRS modulation", en, *IEEE Wireless Communications*, vol. 22, no. 2, pp. 68–73, Apr. 2015, ISSN: 1536-1284. DOI: 10.1109/MWC.2015.7096287. [Online]. Available: http://ieeexplore.ieee.org/document/7096287/.

[18] J. Vučić, C. Kottke, S. Nerreter, K. Habel, A. Buettner, K.-D. Langer, and J. W. Walewski, "230 Mbit/s via a Wireless Visible-Light Link Based on OOK Modulation of Phosphorescent White LEDs", en, in *Optical Fiber Communication Conference*, San Diego, California: OSA, 2010, OThH3, ISBN: 978-1-55752-885-8. DOI: 10.1364/OFC.2010.OThH3. [Online]. Available: https://www.osapublishing.org/abstract.cfm?uri=OFC-2010-OThH3.

[19] I.-S. Jang, J.-D. Jeong, M.-S. Kim, I. Kim, S.-K. Lim, and T.-K. Kang, "Implementation of VLC transmitter using MCU for promotion lighting ID services", en, in *16th International Conference on Advanced Communication Technology*, Pyeongchang, Korea (South): Global IT Research Institute (GIRI), Feb. 2014, pp. 1012–1016, ISBN: 978-89-968650-3-2 978-89-968650-2-5. DOI: 10.1109/ICACT.2014.6779111. [Online]. Available: http://ieeexplore.ieee.org/document/6779111/.

[20] J. Noh, S. Lee, J. Kim, M. Ju, and Y. Park, "A dimming controllable VPPM-based VLC system and its implementation", en, *Optics Communications*, vol. 343, pp. 34–37, May 2015, ISSN: 00304018. DOI: 10.1016/j.optcom.2015.01.008. [Online]. Available: https://linkinghub.elsevier.com/retrieve/pii/S0030401815000139.

[21] A. G. Bell, W. Adams, Tyndall, and W. Preece, "Discussion on "The photophone and the conversion of radiant energy into sound"", en, *Journal of the Society of Telegraph Engineers*, vol. 9, no. 34, pp. 375–383, 1880, ISSN: 2054-0698. DOI: 10.1049/jste-1.1880.0044. [Online]. Available: https://digital-library.theiet.org/content/journals/10.1049/jste-1.1880.0044.

[22] S.-K. Lim, K. Ruling, I. Kim, and I. Jang, "Entertainment lighting control network standardization to support VLC services", en, *IEEE Communications Magazine*, vol. 51, no. 12, pp. 42–48, Dec. 2013, ISSN: 0163-6804. DOI: 10.1109/MCOM.2013.6685756. [Online]. Available: http://ieeexplore.ieee.org/document/6685756/.

[23] R. Kraemer and M. D. Katz, *Short-range wireless communications: emerging technologies and applications*, English. Chichester, U.K.: Wiley, 2009, OCLC: 341591214, ISBN: 978-0-470-74013-2 978-0-470-74012-5. [Online]. Available: http://www.123library.org/book_details/?id=23566.

[24] G. Blinowski and A. Kmieciak, "Modelling and evaluation of a multi-tag LED-ID platform", en, Oct. 2016, pp. 1049–1056. DOI: 10.15439/2016F89. [Online]. Available: https://fedcsis.org/proceedings/2016/drp/89.html.

[25] C. S. Herrmann, "Human EEG responses to 1-100 Hz flicker: Resonance phenomena in visual cortex and their potential correlation to cognitive phenomena", *Experimental Brain Research*, vol. 137, no. 3-4, pp. 346–353, Apr. 2001, ISSN: 0014-4819, 1432-1106. DOI: 10.1007/s002210100682. [Online]. Available: http://link.springer.com/10.1007/s002210100682.

[26] J. Gu, Y. Hitomi, T. Mitsunaga, and S. Nayar, "Coded rolling shutter photography: Flexible space-time sampling", en, in *2010 IEEE International Conference on Computational Photography (ICCP)*, Cambridge, MA, USA: IEEE, Mar. 2010, pp. 1–8, ISBN: 978-1-4244-7022-8. DOI: 10.1109/ICCPHOT.2010.5585094. [Online]. Available: http://ieeexplore.ieee.org/document/5585094/.

[27] Z. Mei, N. Chen, and L.-b. Yao, "Analysis of pixel circuits in CMOS image sensors", en, X. Du, D. Fan, J. Le, Y. Lv, J. Yao, W. Bao, and L. Wang, Eds., China, China, Apr. 2015, p. 952 226. DOI:

10.1117/12.2180432. [Online]. Available: http://proceedings.spiedigitallibrary.org/proceeding.aspx?doi=10.1117/12.2180432.

[28] P. Luo, T. Jiang, P. A. Haigh, Z. Ghassemlooy, and S. Zvanovec, "Undersampled Pulse Width Modulation for Optical Camera Communications", en, in *2018 IEEE International Conference on Communications Workshops (ICC Workshops)*, Kansas City, MO, USA: IEEE, May 2018, pp. 1–6, ISBN: 978-1-5386-4328-0. DOI: 10.1109/ICCW.2018.8403732. [Online]. Available: https://ieeexplore.ieee.org/document/8403732/.

[29] Y. Hu, Y. Xiong, W. Huang, X.-Y. Li, Y. Zhang, X. Mao, P. Yang, and C. Wang, "A Visible Light Based Indoor Positioning System", en, *arXiv:1505.05977 [cs]*, May 2015. [Online]. Available: http://arxiv.org/abs/1505.05977.

[30] C. Lin, B. Lin, X. Tang, Z. Zhou, H. Zhang, S. Chaudhary, and Z. Ghassemlooy, "An Indoor Visible Light Positioning System Using Artificial Neural Network", en, in *2018 Asia Communications and Photonics Conference (ACP)*, Hangzhou: IEEE, Oct. 2018, pp. 1–3, ISBN: 978-1-5386-6158-1. DOI: 10.1109/ACP.2018.8596227. [Online]. Available: https://ieeexplore.ieee.org/document/8596227/.

[31] Y. Zhuang, L. Hua, L. Qi, J. Yang, P. Cao, Y. Cao, Y. Wu, J. Thompson, and H. Haas, "A Survey of Positioning Systems Using Visible LED Lights", en, *IEEE Communications Surveys & Tutorials*, vol. 20, no. 3, pp. 1963–1988, 2018, ISSN: 1553-877X, 2373-745X. DOI: 10.1109/COMST.2018.2806558. [Online]. Available: https://ieeexplore.ieee.org/document/8292854/.

[32] L. Li, P. Hu, C. Peng, G. Shen, and F. Zhao, "Epsilon: A Visible Light Based Positioning System", en, p. 14,

[33] H.-S. Kim, D.-R. Kim, S.-H. Yang, Y.-H. Son, and S.-K. Han, "An Indoor Visible Light Communication Positioning System Using a RF Carrier Allocation Technique", en, *Journal of Lightwave Technology*, vol. 31, no. 1, pp. 134–144, Jan. 2013, ISSN: 0733-8724, 1558-2213. DOI: 10.1109/JLT.2012.2225826. [Online]. Available: http://ieeexplore.ieee.org/document/6336767/.

[34] Z. Li, A. Yang, H. Lv, L. Feng, and W. Song, "Fusion of Visible Light Indoor Positioning and Inertial Navigation Based on Particle Filter", en, *IEEE Photonics Journal*, vol. 9, no. 5, pp. 1–13, Oct. 2017, ISSN: 1943-0655. DOI: 10.1109/JPHOT.2017.2733556. [Online]. Available: http://ieeexplore.ieee.org/document/7997704/.

[35] J. Vongkulbhisal, B. Chantaramolee, Y. Zhao, and W. S. Mohammed, "A fingerprinting-based indoor localization system using intensity modulation of light emitting diodes", en, *Microwave and Optical Technology Letters*, vol. 54, no. 5, pp. 1218–1227, May 2012, ISSN: 08952477. DOI: 10.1002/mop.26763. [Online]. Available: http://doi.wiley.com/10.1002/mop.26763.

[36] M. Yasir, S.-W. Ho, and B. N. Vellambi, "Indoor Positioning System Using Visible Light and Accelerometer", en, *Journal of Lightwave Technology*, vol. 32, no. 19, pp. 3306–3316, Oct. 2014, ISSN: 0733-8724, 1558-2213. DOI: 10.1109/JLT.2014.2344772. [Online]. Available: http://ieeexplore.ieee.org/document/6868970/.

[37] M.-g. Moon, S.-i. Choi, J. Park, and J. Y. Kim, "Indoor Positioning System using LED Lights and a Dual Image Sensor", en, *Journal of the Optical Society of Korea*, vol. 19, no. 6, p. 6, 2015.

[38] Y.-S. Kuo, P. Pannuto, K.-J. Hsiao, and P. Dutta, "Luxapose: Indoor positioning with mobile phones and visible light", en, in *Proceedings of the 20th annual international conference on Mobile computing and networking - MobiCom '14*, Maui, Hawaii, USA: ACM Press, 2014, pp. 447–458, ISBN: 978-1-4503-2783-1. DOI: 10.1145/2639108.2639109. [Online]. Available: http://dl.acm.org/citation.cfm?doid=2639108.2639109.

[39] R. Zhang, W.-D. Zhong, K.-m. Qian, and D.-h. Wu, "Image Sensor Based Visible Light Positioning System with Improved Positioning Algorithm", en, *IEEE Access*, pp. 1–1, 2017, ISSN: 2169-3536. DOI: 10.1109/ACCESS.2017.2693299. [Online]. Available: http://ieeexplore.ieee.org/document/7900356/.

[40] R. Zhang, W.-D. Zhong, D. Wu, and K. Qian, "A Novel Sensor Fusion Based Indoor Visible Light Positioning System", en, in *2016 IEEE Globecom Workshops (GC Wkshps)*, Washington, DC, USA: IEEE, Dec. 2016, pp. 1–6, ISBN: 978-1-5090-2482-7. DOI: 10.1109/GLOCOMW.2016.7848823. [Online]. Available: http://ieeexplore.ieee.org/document/7848823/.

AppendixA

Bill of Materials

Bill of Materials

Bill of Materials For Project [ITLab_LEDProject.PrjPcb] (No PCB Document Selected)

Source Data From: ITLab_LEDProject.PrjPcb
Project: ITLab_LEDProject.PrjPcb
Variant: None

Creation Date: 03/11/2019 22:33:06
Print Date: 03-Nov-19 10:33:27 PM

#Column Nam	#Column Name E	LibRef	Designator	Description	Quantity
		ABS210-13	BR1	Bridge Rectifier	1
		885012207072	C1, C3, C9, C14, C16, C17, C20, C26, C28	Capacitor	9
		THJB106K016HJN	C2, C4, C7, C10, C18, C19, C25, C27, C29	Capacitor Polarised	9
		T58W9105M035C0500	C5	Capacitor Polarised	1
		EMK212B7105MG-T	C6, C23, C24	Capacitor	3
		885012207086	C8	Capacitor	1
		B41231C0338M000	C11	Capacitor Polarised	1
		ECA-1VM471	C12	Capacitor Polarised	1
		1206B334K500CT	C13, C15	Capacitor	2
		CC0603JRNPO9BN500	C21	Capacitor	1
		LMK212BJ225KG-T	C22	Capacitor	1
		VJ1206Y104MXBAT	C30	Capacitor	1
		FM4004W-W	D1, D2, D3	Diode	3
		575002B00000G	HS1	Undefined or Miscellaneous	1
		FA-T220-38E	HS2	Hardware	1
		L7809CV-DG	IC1	Integrated Circuit	1
		AS7805ADTR-G1	IC2	Integrated Circuit	1
		AZ1117IH-3.3TRG1	IC3	Integrated Circuit	1
		THS4221D	IC4	Integrated Circuit	1
		THS4211D	IC5	Integrated Circuit	1
		MAX5048CAUT+T	IC6	Integrated Circuit	1
		PMGD290XN,115	IC7	Integrated Circuit	1
		LM2776DBVT	IC8	Integrated Circuit	1
		VI0221550000G	J1, J2	Connector	2
		SLW-115-01-T-S	J3, J4	Connector	2
		CES-104-01-T-D	J5	Connector	1
		SMA-CONNECTOR	J6, J8	Connector	2
		61300311121	J7, J9	Connector	2
		AD5160BRJZ5-RL7	POT1	Integrated Circuit	1
		FQD8P10TM	Q1	MOSFET (P-Channel)	1
		IRF510PBF	Q2	MOSFET (N-Channel)	1
		BSS64AT116	Q3	Transistor BJT NPN	1
		CR1206-FX-4700ELF	R1, R5	Resistor	2
		ERJ-8ENF1000V	R2	Resistor	1
		ERJ-8ENF25R5V	R3	Resistor	1
		CR1206-FX-10R0ELF	R4	Resistor	1
		CR1206-FX-1002ELF	R6	Resistor	1
		CR1206-JW-432ELF	R7	Resistor	1
		CR1206-FX-49R9ELF	R8	Resistor	1
		CRCW120610R0FKEA	R9, R10, R11, R12	Resistor	4
		183K36	T1	Transformer	1
		TL431AIDBZR,215	Z1	Zener Diode	1
		BZX84C10LT1G	Z2	Zener Diode	1
					72

Approved **Notes**

AppendixB

Simulation circuit

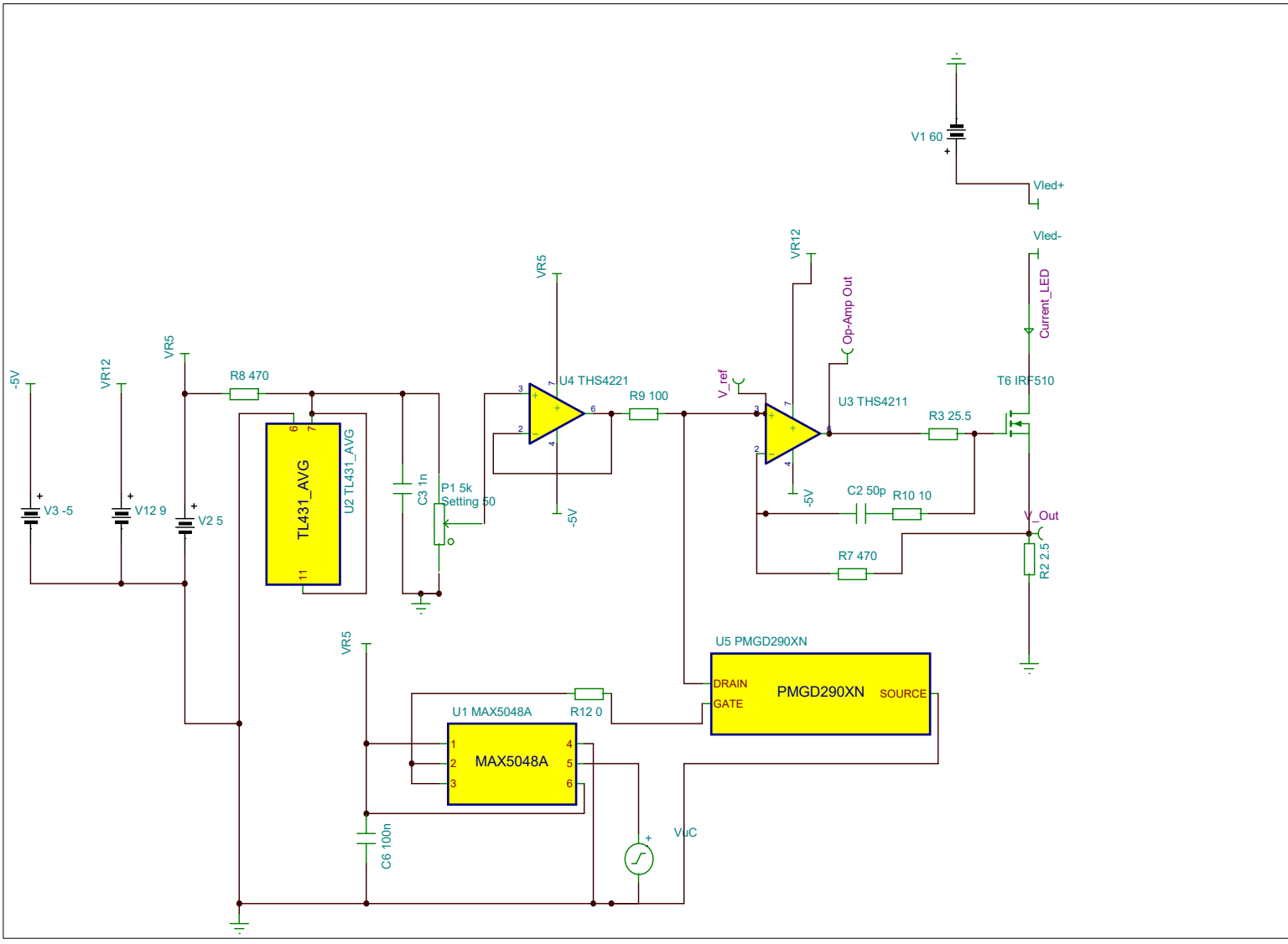
V1 60
Vled+
Vled-
Current_LED
VR12
Op-Amp Out
VR5
U4 THS4221
R9 100
V_ref
U3 THS4211
T6 IRF510
R3 25.5
-5V
VR12
VR5
R8 470
TL431_AVG
U2 TL431_AVG
C3 1n
P1 5k
Setting 50
C2 50p
R10 10
V_Out
R7 470
R2 2.5
V3 -5
V12 9
V2 5
U5 PMGD290XN
DRAIN
GATE
PMGD290XN
SOURCE
U1 MAX5048A
R12 0
MAX5048A
C6 100n
VuC

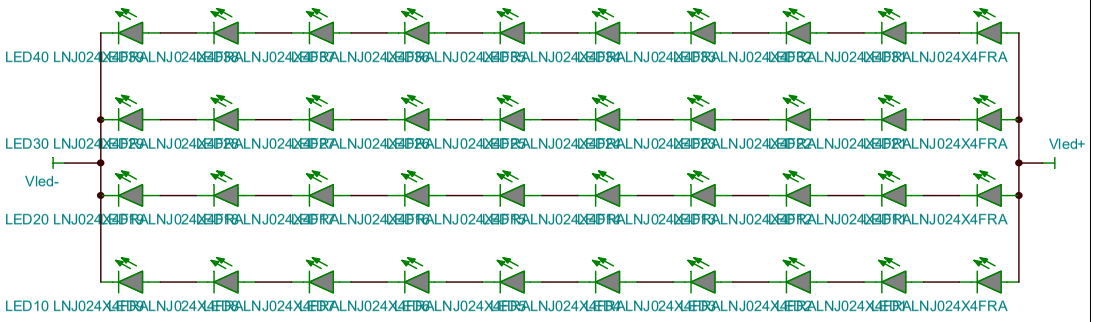
LED40 LNJ024X4FRA
LED30 LNJ024X4FRA
LED20 LNJ024X4FRA
LED10 LNJ024X4FRA
Vled-
Vled+

AppendixC

Driver circuit schemes

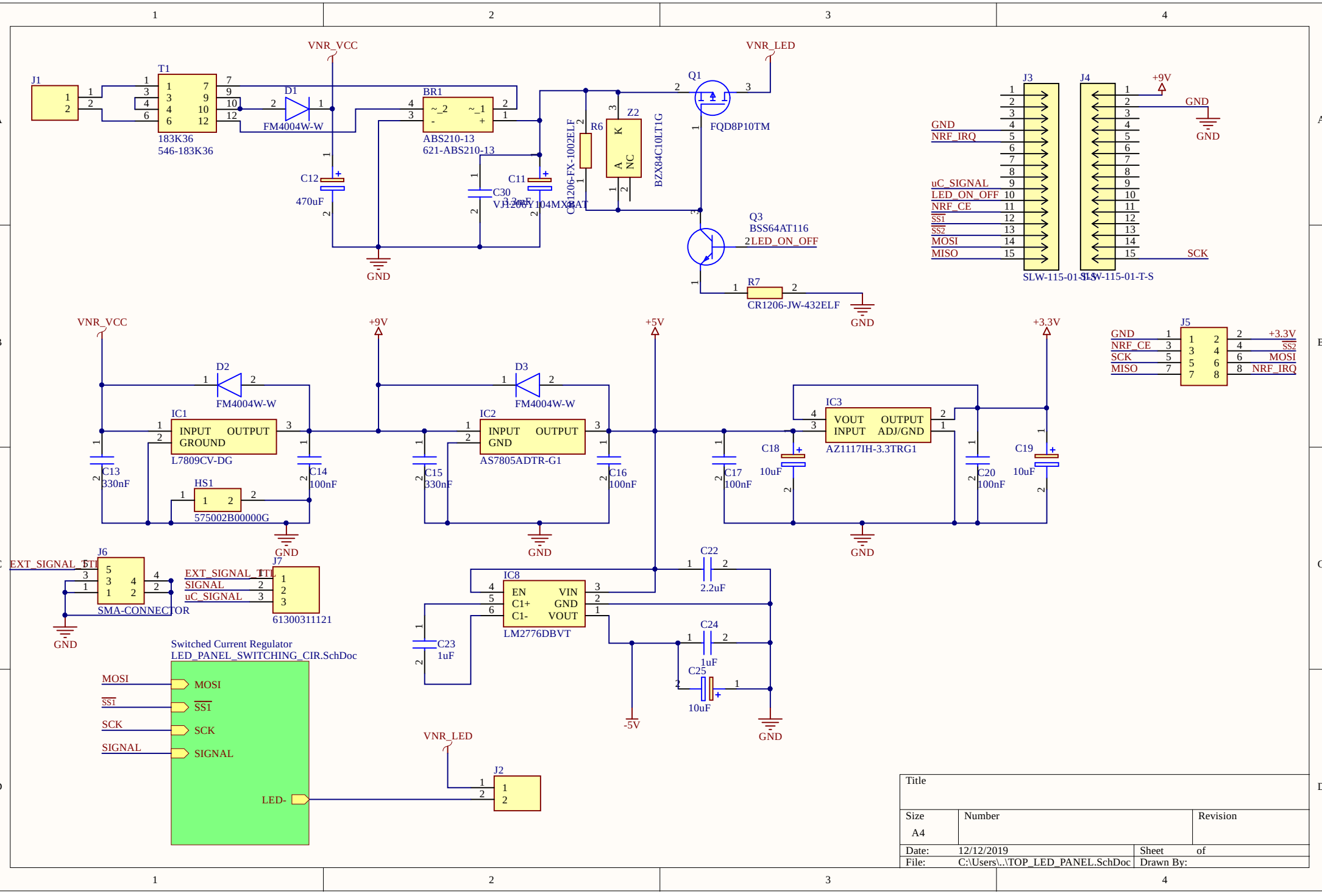
VNR_VCC
VNR_LED
J1
T1
183K36
546-183K36
D1
FM4004W-W
BR1
ABS210-13
621-ABS210-13
C12
470uF
C11
C30
3.3nF
VJ1206Y104MXXAT
CR1206-FX-1002ELF
R6
Z2
BZX84C10LT1G
Q1
FQD8P10TM
Q3
BSS64AT116
2LED_ON_OFF
R7
CR1206-JW-432ELF
GND
J3
J4
+9V
GND
NRF_IRQ
uC_SIGNAL
LED_ON_OFF
NRF_CE
SS1
SS2
MOSI
MISO
SCK
SLW-115-01-T-S
J5
+3.3V
SS2
NRF_CE
SCK
MISO
MOSI
NRF_IRQ
D2
FM4004W-W
D3
FM4004W-W
IC1
INPUT OUTPUT
GROUND
L7809CV-DG
IC2
INPUT OUTPUT
GND
AS7805ADTR-G1
IC3
VOUT OUTPUT
INPUT ADJ/GND
AZ1117IH-3.3TRG1
C13
330nF
C14
100nF
C15
330nF
C16
100nF
C17
100nF
C18
10uF
C19
10uF
C20
100nF
HS1
575002B00000G
J6
SMA-CONNECTOR
EXT_SIGNAL_TTL
J7
SIGNAL
uC_SIGNAL
61300311121
IC8
EN VIN
C1+ GND
C1- VOUT
LM2776DBVT
C22
2.2uF
C23
1uF
C24
1uF
C25
10uF
-5V
Switched Current Regulator
LED_PANEL_SWITCHING_CIR.SchDoc
MOSI
SS1
SCK
SIGNAL
LED-
J2
Title
Size
A4
Number
Revision
Date: 12/12/2019
Sheet of
File: C:\Users\..\TOP_LED_PANEL.SchDoc
Drawn By:

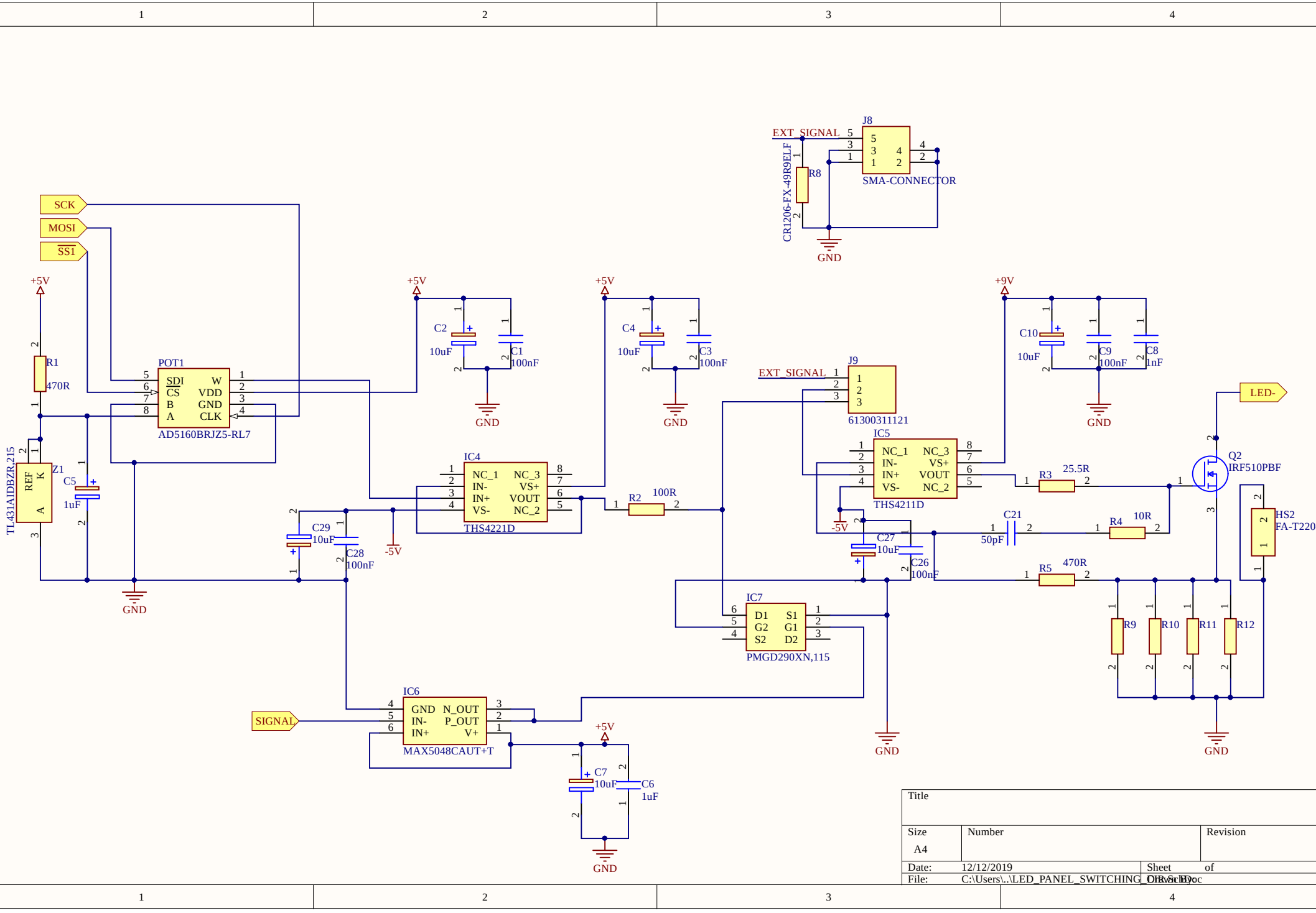
SCK
MOSI
SS1
+5V
R1
470R
POT1
SDI
CS
B
A
W
VDD
GND
CLK
AD5160BRJZ5-RL7
TL431AIDBZR,215
REF
K
A
Z1
C5
1uF
GND
C2
10uF
C1
100nF
GND
C4
10uF
C3
100nF
GND
IC4
NC_1
IN-
IN+
VS-
NC_3
VS+
VOUT
NC_2
THS4221D
C29
10uF
C28
100nF
-5V
R2
100R
EXT_SIGNAL
J8
SMA-CONNECTOR
CR1206-FX-49R9ELF
R8
GND
+9V
C10
10uF
C9
100nF
C8
1nF
GND
EXT_SIGNAL
J9
61300311121
IC5
THS4211D
-5V
C27
10uF
C26
100nF
R3
25.5R
C21
50pF
R4
10R
R5
470R
Q2
IRF510PBF
LED-
HS2
FA-T220-38E
R9
R10
R11
R12
GND
IC7
D1
G2
S2
S1
G1
D2
PMGD290XN,115
GND
SIGNAL
IC6
GND
IN-
IN+
N_OUT
P_OUT
V+
MAX5048CAUT+T
+5V
C7
10uF
C6
1uF
GND
Title
Size
A4
Number
Revision
Date:
12/12/2019
Sheet
of
File:
C:\Users\..\LED_PANEL_SWITCHING_DRIVER.SchDoc
Drawn By:

AppendixD

Driver circuit PCB

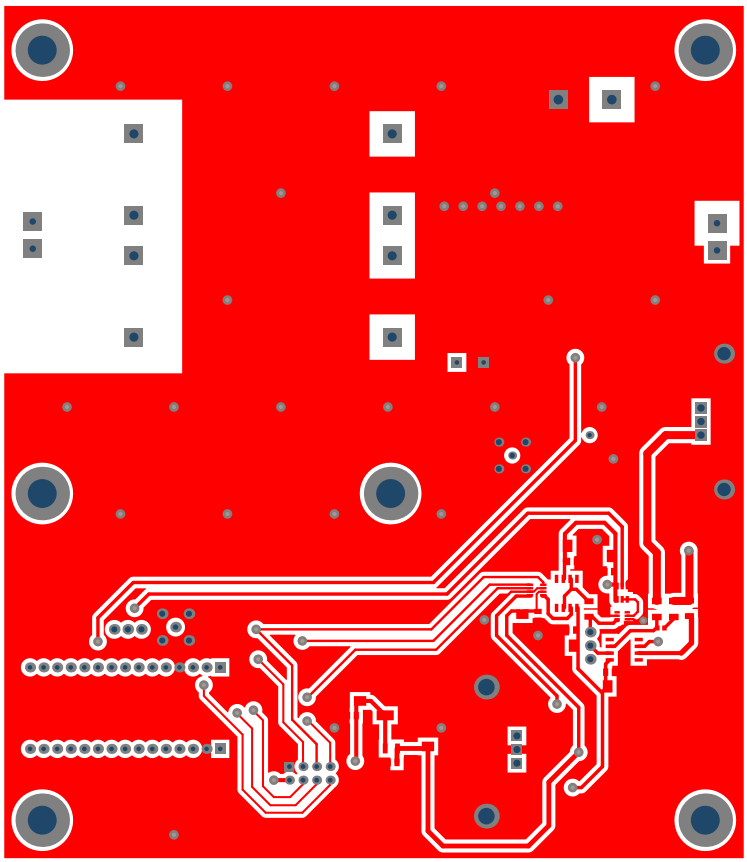

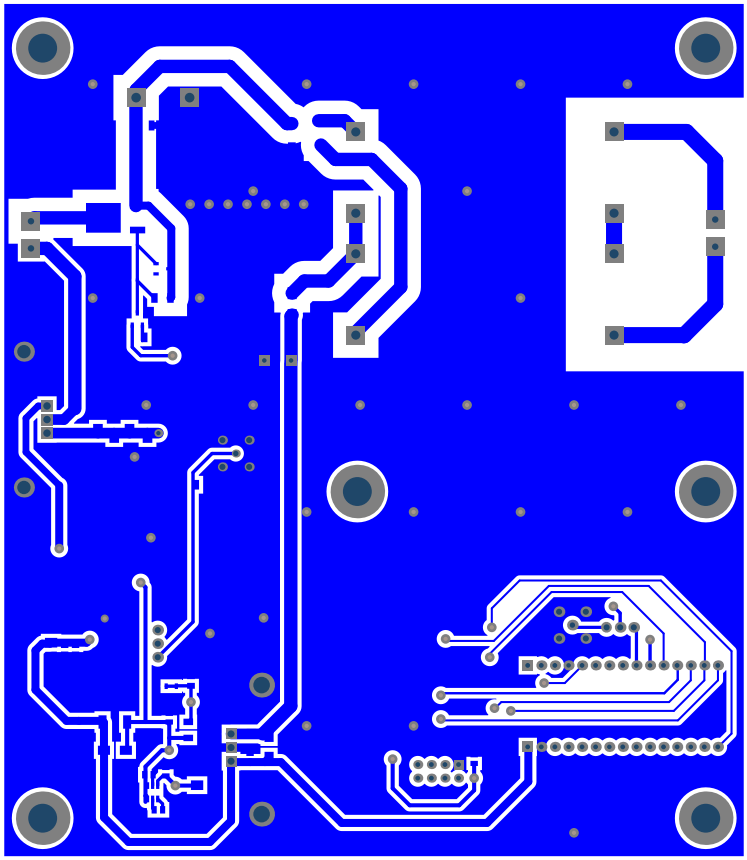

AppendixD

Firmware

MAIN.CPP

```
/*
 * LED_RF.cpp
 *
 * Created: 18/09/2019 14:54:18
 * Author : redeagleye
 */

#define F_CPU 16000000UL

//#define MODE MASTER

#ifndef MODE
        #define MODE SLAVE
#endif
//#define simulator

#include <avr/io.h>


#include <stdlib.h>
#include <avr/interrupt.h>
#include <avr/pgmspace.h>
#include "uart.h"
#define UART_BAUD_RATE      9600



#include <avr/delay.h>
#include <stdint.h>
#include "driverPinout.h"
#include "spi.h"
#include "nrf24.h"
```

```
#include "ledInterface.h"


#define hwID 0



#if (MODE == SLAVE)

        ISR(TIMER1_COMPA_vect)    // Timer1 ISR COMPA
        {
                static uint8_t PortMask;
                OCR1B = interface.getMessageByte(&PortMask);
                LED_PORT ^= PortMask;
        }


        ISR(TIMER1_COMPB_vect)    // Timer1 ISR COMPB
        {
                static uint8_t PortMask;
                interface.getMessageByte(&PortMask);
                LED_PORT ^= PortMask;
        }

#endif



int main(void)
{
        setPinIO();
        spi_begin();

        interface.init(hwID, MODE);


        #if (MODE == MASTER)
                unsigned int c;
                uart_init( UART_BAUD_SELECT(UART_BAUD_RATE,F_CPU) );
                sei();
                uint8_t buffer[255];
                uint8_t *buf_ptr = buffer;
                uint8_t pos = 0;

                static uint8_t ledMode=0;
                static uint8_t ledonOFF=1;
                while(1)
                {
                        c = uart_getc();
                        if ( c & UART_NO_DATA )
```

```
{
        ///*
         //* no data available from UART
         //*/
}
else
{
        /*
         * new data available from UART
         * check for Frame or Overrun error
         */
        if ( c & UART_FRAME_ERROR )
        {
                /* Framing Error detected, i.e no stop bit detected */
                uart_puts_P("UART Frame Error: ");
        }
        if ( c & UART_OVERRUN_ERROR )
        {
                /*
                 * Overrun, a character already present in the UART UDR register was
                 * not read by the interrupt handler before the next character arriv
                 * one or more received characters have been dropped
                 */
                uart_puts_P("UART Overrun Error: ");
        }
        if ( c & UART_BUFFER_OVERFLOW )
        {
                /*
                 * We are not reading the receive buffer fast enough,
                 * one or more received character have been dropped
                 */
                uart_puts_P("Buffer overflow error: ");
        }
        /*
         * send received character back
         */
        uart_putc( (unsigned char)c );

        switch ((unsigned char)c)
        {
        case '$':
                buf_ptr = buffer;
                pos = 0;
                break;
        case ',':
                (*buf_ptr++) = '\0';
                switch (pos)
                {
                        case 0:
                                led.setLedID((uint8_t) atoi((char*)buffer));
```

```
                                        break;
                                case 1:
                                        led.setLedState((uint8_t) atoi((char*)buffer));
                                        break;
                                case 2:
                                        led.setLedMode((uint8_t) atoi((char*)buffer));
                                        break;
                                case 3:
                                        led.setIntensity((uint8_t) atoi((char*)buffer));
                                        break;
                                case 4:
                                        led.setFrequency((uint16_t) atoi((char*)buffer));
                                        break;
                                case 5:
                                        led.setDutyCycle((uint8_t) atoi((char*)buffer))
                                        break;
                                default:
                                        break;
                                }

                                buf_ptr = buffer;
                                pos++;
                                break;
                        case '*':
                                for(int i=0; i<3;i++)
                                        interface.sendLed(led.getLedID(),&led);
                                uart_puts("gone!\r\n");
                                break;
                        default:
                                (*buf_ptr++)=(unsigned char)c;
                        }
                }
        }

#elif (MODE == SLAVE)
        while(1)
        {
                interface.checkRF();
                #ifndef simulator
                        _delay_ms(1000);
                #endif
        }
#else
        while(1);

#endif

        return 0;
}
```

driverPinout.h

```
/*
 * driverPinout.h
 *
 * Created: 27/08/2019 23:36:24
 *  Author: redeagleye
 */

#ifdef __cplusplus
extern "C"
{
#endif
        #ifndef DRIVERPINOUT_H_
        #define DRIVERPINOUT_H_

        #include <avr/io.h>

        #define LED_DDR                DDRD
        #define SPI_DDR                DDRB
        #define NRF24_DDR        DDRB

        #define LED_PORT        PORTD
        #define SPI_PORT        PORTB
        #define NRF24_PORT        PORTB

        #define SPI_PIN                PINB

        #define LED_CTL DDD6
        #define LED_POWERSWITCH DDD7

        #define SPI_SS_DIGPOTSLAVE DDB1
        #define SPI_SS_NRF24L01 DDB2
        #define SPI_MOSI DDB3
        #define SPI_MISO PINB4
        #define SPI_SCK DDB5

        #define NRF24_CE DDB0

        #define set_bit(reg,bit) reg |= _BV(bit)
        #define clr_bit(reg,bit) reg &= ~(_BV(bit))
        #define check_bit(reg,bit) (reg&(_BV(bit)))
        #define xor_bit(reg, bit) reg ^= _BV(bit)

        void setPinIO(void);
        void turnOnLED(uint8_t ledCTLStatus);
        void turnOffLED(void);

        void nrf24_ce_digitalWrite(uint8_t state);
        void nrf24_csn_digitalWrite(uint8_t state);
```

```
        void nrf24_sck_digitalWrite(uint8_t state);
        void nrf24_mosi_digitalWrite(uint8_t state);
        uint8_t nrf24_miso_digitalRead(void);


        #endif /* DRIVERPINOUT_H_ */

#ifdef __cplusplus
} // extern "C"
#endif
```

driverPinout.c

```
/*
 * CFile1.c
 *
 * Created: 27/08/2019 22:29:42
 *  Author: redeagleye
 */

#include "driverPinout.h"

void setPinIO(void)
{
        LED_DDR |= _BV(LED_POWERSWITCH) | _BV(LED_CTL);
        set_bit(SPI_PORT, SPI_SS_DIGPOTSLAVE);
        set_bit(SPI_PORT, SPI_SS_NRF24L01);
        SPI_DDR |= _BV(SPI_SS_NRF24L01) |_BV(SPI_SS_DIGPOTSLAVE) | _BV(SPI_MOSI) |  _BV(SPI_SCK);
        NRF24_DDR |= _BV(NRF24_CE);

}


void turnOnLED(uint8_t ledCTLStatus)
{
        if(ledCTLStatus)
        {
                set_bit(LED_PORT, LED_CTL);
        }
        else
        {
                clr_bit(LED_PORT, LED_CTL);
        }
        set_bit(LED_PORT, LED_POWERSWITCH);
}

void turnOffLED(void)
{
        clr_bit(LED_PORT, LED_POWERSWITCH);
```

```
        set_bit(LED_PORT, LED_CTL);
}

void nrf24_ce_digitalWrite(uint8_t state)
{
        if(state)
        {
                set_bit(NRF24_PORT,NRF24_CE);
        }
        else
        {
                clr_bit(NRF24_PORT,NRF24_CE);
        }
}
/* ------------------------------------------------------------------------ */
void nrf24_csn_digitalWrite(uint8_t state)
{
        if(state)
        {
                set_bit(SPI_PORT,SPI_SS_NRF24L01);
        }
        else
        {
                clr_bit(SPI_PORT,SPI_SS_NRF24L01);
        }
}
/* ------------------------------------------------------------------------ */
void nrf24_sck_digitalWrite(uint8_t state)
{
        if(state)
        {
                set_bit(SPI_PORT,SPI_SCK);
        }
        else
        {
                clr_bit(SPI_PORT,SPI_SCK);
        }
}
/* ------------------------------------------------------------------------ */
void nrf24_mosi_digitalWrite(uint8_t state)
{
        if(state)
        {
                set_bit(SPI_PORT,SPI_MOSI);
        }
        else
        {
                clr_bit(SPI_PORT,SPI_MOSI);
        }
}
```

```
/* ------------------------------------------------------------------------ */
uint8_t nrf24_miso_digitalRead(void)
{
        return check_bit(SPI_PIN,SPI_MISO);
}
/* ------------------------------------------------------------------------ */
```

SPI.H

```
/*
* SPI.h
*
* Created: 26/08/2019 15:26:04
* Author: redeagleye
*/



#ifdef __cplusplus
extern "C"
{
#endif

#ifndef __SPI_H__
#define __SPI_H__

#include <avr/io.h>

#ifndef LSBFIRST
#define LSBFIRST 0
#endif
#ifndef MSBFIRST
#define MSBFIRST 1
#endif

#define SPI_CLOCK_DIV4 0x00
#define SPI_CLOCK_DIV16 0x01
#define SPI_CLOCK_DIV64 0x02
#define SPI_CLOCK_DIV128 0x03
#define SPI_CLOCK_DIV2 0x04
#define SPI_CLOCK_DIV8 0x05
#define SPI_CLOCK_DIV32 0x06

#define SPI_MODE0 0x00
#define SPI_MODE1 0x04
#define SPI_MODE2 0x08
#define SPI_MODE3 0x0C

#define SPI_MODE_MASK 0x0C  // CPOL = bit 3, CPHA = bit 2 on SPCR
```

```
#define SPI_CLOCK_MASK 0x03  // SPR1 = bit 1, SPR0 = bit 0 on SPCR
#define SPI_2XCLOCK_MASK 0x01  // SPI2X = bit 0 on SPSR

inline static uint8_t spi_transfer(uint8_t data)
{
        SPDR = data;

        while (!(SPSR & _BV(SPIF))) ; // wait
        return SPDR;
}

inline static void spi_begin(void)
{
        //SPCR = _BV(SPE) | _BV(DORD) | _BV(MSTR) | (SPI_MODE0 & SPI_MODE_MASK) | (SPI_CLOCK_DIV4 & SPI_CLOCK
        SPCR = _BV(SPE) | 0 | _BV(MSTR) | (SPI_MODE0 & SPI_MODE_MASK) | (SPI_CLOCK_DIV4 & SPI_CLOCK_MASK) ;
}

/*
class SPI
{
//variables
public:
protected:
private:

//functions
public:
        SPI();
        SPI(uint8_t SPI_CLK, uint8_t bitorder, uint8_t SPI_MODE);
        inline static uint8_t transfer(uint8_t data)
        {
                SPDR = data;

                while (!(SPSR & _BV(SPIF))) ; // wait
                return SPDR;

        }

        inline static void begin(void)
        {
                //SPCR = _BV(SPE) | _BV(DORD) | _BV(MSTR) | (SPI_MODE0 & SPI_MODE_MASK) | (SPI_CLOCK_DIV4 &
                SPCR = _BV(SPE) | 0 | _BV(MSTR) | (SPI_MODE0 & SPI_MODE_MASK) | (SPI_CLOCK_DIV4 & SPI_CLOCK_
        }
protected:
private:
        SPI( const SPI &c );
        SPI& operator=( const SPI &c );

}; //SPI
```

```
extern SPI _SPI;
*/
#endif //__SPI_H__
#ifdef __cplusplus
} // extern "C"
#endif
```

ledInterface.h

```
#ifndef __LEDINTERFACE_H_
#define __LEDINTERFACE_H_

#ifndef F_CPU
#define F_CPU 16000000UL
#endif

#include "driverPinout.h"
#include "ledCtl.h"
#include "digPot.h"

#define MASTER        0
#define SLAVE        1

#define nrf24_channel 2
#define nrf24_payLength 7


class ledInterface {
public:
  ledInterface();
  void init(uint8_t hardwareID, uint8_t mode = SLAVE);
  uint8_t sendLed(uint8_t hardwareID, ledCtl* ledPtr);
  void checkRF(void);
  uint8_t* ledSetup(ledCtl* ledPtr);
  bool* getManchesterMessage(void);
  uint16_t getMessageByte(uint8_t * data);
  uint8_t checkMessageByte(void);
  void stopTimer(void);

private:
        void setLedIntensity(ledCtl* ledPtr);
        void setupTimer(ledCtl* ledPtr);


};

extern ledInterface interface;
#endif
```

ledInterface.cpp

```
#include <avr/io.h>
#include <avr/interrupt.h>
#include "nrf24.h"
#include "ledInterface.h"

ledInterface interface;

digPot digPot(DDB1);
static bool manchester_message[18];
static uint8_t message_mask[18];
static uint8_t * p = message_mask;
unsigned int maxIdx;
static uint8_t idx = 1;

uint16_t compB0_1;
uint16_t compB1_0;
uint16_t * array[] = {&compB1_0, &compB0_1};

//uint8_t tx_address[5] = {'M','A','S','T','R'};
//uint8_t rx_address[5] = {'S','L','A','V','E'};


uint8_t data_array[nrf24_payLength];
uint8_t hwID;

uint8_t nrf24_addr[][5] = {
        {'M','A','S','T','R'},
        {'S','L','A','V','E'}
};

ledInterface::ledInterface()
{

}

void ledInterface::init(uint8_t hardwareID, uint8_t mode)
{
        nrf24_init();
        nrf24_config(nrf24_channel,nrf24_payLength);
        if(mode == MASTER)
        {
                nrf24_tx_address(nrf24_addr[MASTER]);
                nrf24_rx_address(nrf24_addr[SLAVE]);
        }
        else if(mode == SLAVE)
        {
                hwID = hardwareID;
                nrf24_tx_address(nrf24_addr[SLAVE]);
```

```
                nrf24_rx_address(nrf24_addr[MASTER]);
                led.setLedID(hwID);
                ledSetup(&led);
        }
}

uint8_t ledInterface::sendLed(uint8_t hardwareID, ledCtl* ledPtr)
{
        data_array[0] = hardwareID;
        data_array[1] = led.getLedID();
        data_array[2] = led.getCtlReg();
        data_array[3] = led.getIntensity();
        uint16_t freq = led.getFrequency();
        data_array[4] = (freq & 0xFF);
        data_array[5] = ((freq & 0xFF00) >> 8);
        data_array[6] = led.getDutyCycle();

        nrf24_send(data_array);
        while(nrf24_isSending());
        uint8_t temp = nrf24_lastMessageStatus();

//        if(temp == NRF24_TRANSMISSON_OK)
//        {
//                xprintf("> Tranmission went OK\r\n");
//        }
//        else if(temp == NRF24_MESSAGE_LOST)
//        {
//                xprintf("> Message is lost ...\r\n");
//        }
//        temp = nrf24_retransmissionCount();
//        xprintf("> Retranmission count: %d\r\n",temp);

        /* Optionally, go back to RX mode ... */
        nrf24_powerUpRx();

        /* Or you might want to power down after TX */
        //                // nrf24_powerDown();

        return temp;

}

void ledInterface::checkRF(void)
{
        if(nrf24_dataReady())
        {
                nrf24_getData(data_array);

                if(data_array[0] == hwID || data_array[0] == 0xFF)
                {
```

```
                        stopTimer();
                        //led.setLedID(data_array[1]);
                        led.setCtlReg(data_array[2]);
                        led.setIntensity(data_array[3]);
                        led.setFrequency((data_array[5] << 8) | data_array[4]);
                        led.setDutyCycle(data_array[6]);
                        ledSetup(&led);
                }
        }
}


void ledInterface::setLedIntensity(ledCtl* ledPtr)
{
  digPot.digitalPotWrite((ledPtr->getIntensity()*0.01)*0.530*2.5);
}

uint8_t* ledInterface::ledSetup(ledCtl* ledPtr)
{
  setLedIntensity(ledPtr);

  unsigned int message = (0b111 << 6) | (ledPtr->getLedID() << 2) | (0b00);
  unsigned int mask = 0x100;
  bool lastBit = 0;
  for(int i = 0, j = 0; i < 9 ; i= i+1 ,j=j+2)
  {
    manchester_message[j] = !((bool)((message & mask) >> (8-i)));
        manchester_message[j+1] = !manchester_message[j];

    message_mask[j] = (manchester_message[j]^lastBit) << LED_CTL;
    message_mask[j+1] = _BV(LED_CTL);

    lastBit = manchester_message[j+1];

    //lastBit = !manchester_bit;
    mask = mask >> 1;
  }
  idx = 1;

  if(ledPtr->getLedMode() != 0)
  {
        turnOnLED(manchester_message[0]);
        setupTimer(ledPtr);
  }
  else
  {
          stopTimer();
          if(ledPtr->getLedState())
          {
                turnOnLED(true);
```

```
          }
          else
          {
                turnOffLED();
          }
  }


  return message_mask;
}

bool* ledInterface::getManchesterMessage(void)
{
  return manchester_message;
}
/*
uint8_t ledInterface::getMessageByte(uint8_t * data)
{
        static uint8_t idx = 1;
        static uint8_t * last;
        const uint8_t * end = message_mask+24;

        last = p;
        p++;

        if (p == end)
        {
                p=message_mask;
        }
        *data=*p;

        return (*p ^ *last);
}*/

uint16_t ledInterface::getMessageByte(uint8_t * data)
{
        *data = message_mask[idx];

        idx++;
        if (idx == 18)
        {
                idx = 0;
        }

        return *array[manchester_message[idx]];
}

uint8_t ledInterface::checkMessageByte(void)
{
        return *p;
```

```
}


void ledInterface::setupTimer(ledCtl* ledPtr)
{
        cli();                          // disable global interrupts
        TCCR1A = 0x00;
        TCCR1B = 0x00;
        TCNT1 = 0;

        if(ledPtr->getLedMode() == 0b01)
        {
                uint16_t compA = ((F_CPU/ledPtr->getFrequency())-1) >> 1;
                OCR1A = compA;                  //Timer1A compare register
                TIMSK1 = (1 << OCIE1A);   // Enable timer1A & timer1B interrupt
        }
        else
        {
                uint8_t DC = ledPtr->getDutyCycle();
                uint16_t compA = (F_CPU/ledPtr->getFrequency())-1;
                compB1_0 = (uint16_t) compA*(DC/100.0);
                compB0_1 = (uint16_t) compA*((100-DC)/100.0);
                OCR1A = compA;                  //Timer1A compare register
                //OCR1B = manchester_message[0];        //Timer1B compare register
                OCR1B = *array[manchester_message[0]];        //Timer1B compare register

                TIMSK1 = (1 << OCIE1A) | (1 << OCIE1B);   // Enable timer1A & timer1B interrupt
        }

        TCCR1B = (1<<WGM12) | (1<<CS10);  // Timer mode with 1 prescaler
        sei();
}

void ledInterface::stopTimer(void)
{
        cli();                          // disable global interrupts
        TCCR1A = 0x00;
        TCCR1B = 0x00;
        TCNT1 = 0;
        sei();
}
```

ledCtl.h

```
#ifndef __LEDCTL_H_
#define __LEDCTL_H_

#include <stdint.h>
```

```
class ledCtl
{
        public:
        static uint8_t sizeofledCtlStruct(void);
        ledCtl();
        uint8_t getLedID(void);
        void setLedID(const uint8_t ledID);

        uint8_t getCtlReg(void);
        void setCtlReg(uint8_t ctlReg);

        uint8_t getLedState(void);
        void  setLedState(uint8_t ledState);

        uint8_t getLedMode(void);
        void  setLedMode(uint8_t ledMode);

        uint8_t getIntensity(void);
        void  setIntensity(uint8_t intensity);

        uint16_t getFrequency(void);
        void setFrequency(uint16_t frequency);

        uint8_t getDutyCycle(void);
        void setDutyCycle(uint8_t dutyCycle);
};

extern ledCtl led;
#endif
```

ledCtl.cpp

```
#include "ledCtl.h"

ledCtl led;

struct ledCtlStruct
{
        uint8_t  ledID;        // LED identifier number
        union{
                uint8_t ctlReg;
                struct{
                        uint8_t ledState:1;
                        uint8_t ledMode:2;        // Mode 0: DC | Mode 1: OOK+MANCHESTER | Mode 2: VPPM
                };
        };
        uint8_t        intensity;        // intensity in percentage (100% = 530mA )
        uint16_t frequency;        // frequency in kHz
        uint8_t        dutyCycle;        // VPPM dutyCycle (t_on/T)
```

```
} ledCtlReg;

uint8_t ledCtl::sizeofledCtlStruct(void)
{
        return sizeof(ledCtlStruct);
}

ledCtl::ledCtl()
{
        setLedID(0);
        //ledCtlReg.ctlReg = 0b100;
        ledCtlReg.ledMode = 0;
        ledCtlReg.ledState = 1;
        ledCtlReg.intensity = 100;
        ledCtlReg.frequency = 10000;
        ledCtlReg.dutyCycle = 50;
}


uint8_t ledCtl::getLedID(void)
{
        return ledCtlReg.ledID;
}

void ledCtl::setLedID(uint8_t ledID)
{
        ledCtlReg.ledID = ledID;
}

uint8_t ledCtl::getCtlReg(void)
{
        return ledCtlReg.ctlReg;
}

void ledCtl::setCtlReg(uint8_t ctlReg)
{
        ledCtlReg.ctlReg = ctlReg;
}

uint8_t ledCtl::getLedState(void)
{
        return ledCtlReg.ledState;
}

void ledCtl::setLedState(uint8_t ledState)
{
        ledCtlReg.ledState = ledState;
}
```

```
uint8_t ledCtl::getLedMode(void)
{
        return ledCtlReg.ledMode;
}

void ledCtl::setLedMode(uint8_t ledMode)
{
        ledCtlReg.ledMode = ledMode;
}

uint8_t ledCtl::getIntensity(void)
{
        return ledCtlReg.intensity;
}

void ledCtl::setIntensity(uint8_t intensity)
{
        ledCtlReg.intensity = intensity;
}


uint16_t ledCtl::getFrequency(void)
{
        return ledCtlReg.frequency;
}

void ledCtl::setFrequency(uint16_t frequency)
{
        ledCtlReg.frequency = frequency;
}

uint8_t ledCtl::getDutyCycle(void)
{
        return ledCtlReg.dutyCycle;
}

void ledCtl::setDutyCycle(uint8_t DutyCycle)
{
        ledCtlReg.dutyCycle = DutyCycle;
}
```

digPot.h

```
#ifndef __DIGPOT_H_
#define __DIGPOT_H_

#ifndef __SPI_H_
#define __SPI_H_
#include "SPI.h"
```

```
#endif


#define SLVADDR 0x2A
#define V_A 2.5f
#define V_B 0.0f
#define R_AB 5000.0f
#define R_WIPER 50.0f



class digPot {
public:
  digPot(unsigned int ss_pin);
  void digitalPotWrite(float value);
  unsigned int getMaxVal(void);
private:
  float getD_WA(float V_WA);
  float getD_WB(float V_WB);
  float R_WA(int D);
  float R_WB(int D);


};

#endif
```

digPot.cpp

```
#include "digPot.h"
#include "driverPinout.h"
#include "SPI.h"
unsigned int SPI_SS_PIN;

digPot::digPot(unsigned int ss_pin)
{
  SPI_SS_PIN = ss_pin;
}

float digPot::R_WA(int D)
{
  return ((256-D)/256.0)*R_AB + R_WIPER;
}

float digPot::R_WB(int D)
{
  return (D/256.0)*R_AB + R_WIPER;
}
```

```
float digPot::getD_WB(float V_WB)
{
        float R_WB = ((V_WB-V_B)/(V_A-V_B))*R_AB;
  return ((R_WB)/R_AB)*256;
}

float digPot::getD_WA(float V_WA)
{
        float R_WB = ((V_WA-V_A)/(V_B-V_A))*R_AB;
  return ((R_WB)/R_AB)*256;
}

unsigned int digPot::getMaxVal(void)
{
  return 1;
}

void digPot::digitalPotWrite(float value)
 {
  float D = getD_WB(value);
  if(D < 0)
  {
    D = 0;
  }
  else if(D > 255)
  {
    D = 255;
  }
  // take the SS pin low to select the chip:
  //digitalWrite(SPI_SS_PIN, LOW);
  clr_bit(SPI_PORT,SPI_SS_DIGPOTSLAVE);
  for( int i = 0; i < 5; i++);
  //  send in the address and value via SPI:
  spi_transfer((uint8_t)D);
  for( int i = 0; i < 5; i++);
  // take the SS pin high to de-select the chip:
  //digitalWrite(SPI_SS_PIN, HIGH);
  set_bit(SPI_PORT,SPI_SS_DIGPOTSLAVE);
}

// for(int i=0; i<8; i++)
//         {
//                 int D = pow(2,i);
//                 float V_WA = (R_WA(D)/R_AB)*(V_B-V_A)+V_A;
//                 float V_WB = (R_WB(D)/R_AB)*(V_A-V_B)+V_B;
//                 printf("D=%d | R_WB = %f | R_WA = %f | V_WA = %f | V_WB= %f\n"
//                 ,D,R_WB(D), R_WA(D), V_WA, V_WB);
//                 printf("D_WA: %f | D_WB: %f\r\n", getD_WA(V_WA),getD_WB(V_WB));
//         }
//
```

```
//          float V_WB = 0.530*2.5;
//          int D = getD_WB(V_WB);
//          float V_WA = (R_WA(D)/R_AB)*(V_B-V_A)+V_A;
//          V_WB = (R_WB(D)/R_AB)*(V_A-V_B)+V_B;
//          printf("D_WA: %f | D_WB: %f\r\n", getD_WA(V_WA),getD_WB(V_WB));
//          printf("D=%d | R_WB = %f | R_WA = %f | V_WA = %f | V_WB= %f\n"
//                  ,D,R_WB(D), R_WA(D), V_WA, V_WB);
```